UNIVERSITAT DE BARCELONA

Response of simple-metal systems with plane symmetry to local one-body operators

Jordi Sellarès González

Response of simple-metal systems with plane symmetry to local one-body operators

Jordi Sellarès González

Departament d'Estructura i Constituents de la Matèria

UNIVERSITAT DE BARCELONA

Contents

Chapter 1

Introduction

Normal modes have proven to be a very fruitful concept within the framework of mechanics and field theory. The understanding of the phenomena that occurs in many-body systems relies deeply on the knowledge of the properties of these modes. Normal modes are characterized by well-defined quantum numbers (or, classically, by conserved quantities). The number of normal modes is related with the number of degrees of freedom of the system. They evolve as quasi-particles and provide a manageable way of solving the interaction of many-body systems with external probes. Any possible state of the system can be expressed as a superposition of normal modes. This is the reason why they are so useful. Normal modes are not only found in many-body systems. Systems with few degrees of freedom can also display them. A textbook example consists in two pendulums coupled by a spring (see Fig. 1.1). This system has only two degrees of freedom since we can specify completely its state using two generalized coordinates. For this purpose we will use the angles that form each rod with the vertical direction. If the system is in a normal mode there will be no exchange of energy between degrees of freedom. Hence, the oscillation amplitude of both pendulums will be constant. Two normal modes can be found and are represented in Fig. 1.2. The existence of normal modes in an electron gas can be discussed within Classical Electrodynamics. One of the most simple models that contains normal modes is the following one. Lets consider a non-magnetic, infinite and isotropic medium, made up of an homogeneous electron gas embedded in a neutralizing positive background, that is also homogeneous.

In this system the normal modes will be traveling waves with a well-defined wave-vector

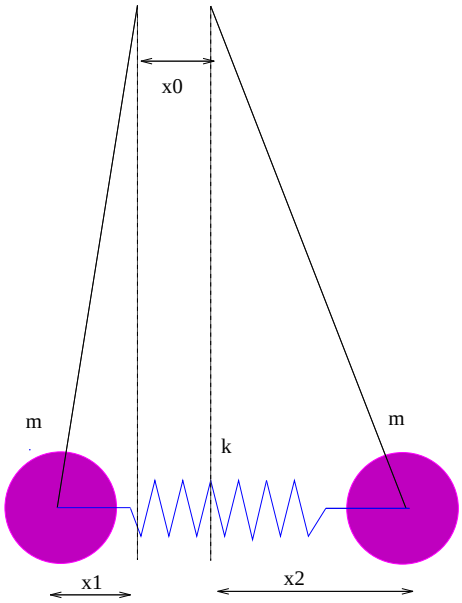

Figure 1.1: Pendulums coupled by a spring.

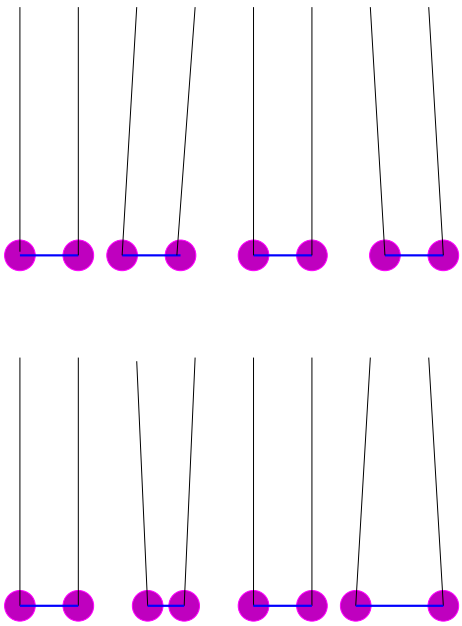

Figure 1.2: Normal modes of a system made up of two coupled pendulums.

$\vec{k}$ and frequency ω. These traveling waves have associated fields $\vec{E}$, $\vec{D}$, $\vec{P}$, ρ_{ind}, $\cdots$, with the same time and spatial dependence. The response of the medium to an external field can be taken into account through a dielectric function. Since the dielectric function will relate the fields $\vec{E}$ and $\vec{D}$ associated to the same wave, the dielectric function will also depend on $\vec{k}$ and ω.

This system presents two types of normal modes. A type corresponds to transverse electro-magnetic waves that propagate through the medium. Their wave-vector is perpendicular to the electric field and their dispersion relation is given by the equation

$$\frac{\omega^2}{c^2}\epsilon(\omega,\vec{k}) - k^2 = 0. \tag{1.1}$$

The other type are longitudinal polarization waves. Their wave-vector is parallel to the electric field and their dispersion relation can be obtained from

$$\epsilon(\omega,\vec{k}) = 0. \tag{1.2}$$

It is well known that transverse electro-magnetic waves can propagate even in vacuum. On the other hand, polarization waves can only exist in material media. So, we consider that these are the normal modes of the electron gas. Microscopically, a polarization wave is an oscillation in which all the electrons of the gas participate. For this reason such a wave is also called a collective mode.

The most simple dielectric function that contains this phenomena is the Drude dielectric function

$$\epsilon(\omega) = 1 - \frac{4\pi n e^2}{m\omega^2}, \tag{1.3}$$

that implies a free-electron approximation. It can be useful to study the normal modes of simple-metals in the large wavelength limit. It is the appropriate limit for any dielectric function at $k = 0$. Anyway, even for simple-metals the interaction of the electrons with themselves and with the ions must be taken into account to obtain good results for shorter wavelengths. In this equation n stands for the electronic particle density, e is the electron charge and m is the electron mass. It is a local dielectric function because it has no dependence on the wave-vector $\vec{k}$.

If we apply Eq. 1.2 then the frequency of normal modes is

$$\omega_p^2 = \frac{4\pi n e^2}{m}. \tag{1.4}$$

The Drude dielectric function can be expressed in terms of ω_p

$$\epsilon(\omega) = 1 - \frac{\omega_p^2}{\omega^2}. \tag{1.5}$$

Quantum mechanics plays a key role in the study of the normal modes of the electron gas. The valence electron density in solids ranges from 10^{22} to $10^{24}\, cm^{-3}$. For these values of n, ω_p lies in the region of optical frequencies. As a consequence, the discretization of the energy due to Quantum Mechanics will be easily observable using energetic probes. Taking this fact into account, we define plasmon [1] as the quantum associated with a normal mode of the electron gas.

Until now we have considered bulk modes, that is, three-dimensional polarization waves. If, instead of infinite, the medium is semi-infinite we also have surface modes. The number of modes is reduced because now traveling waves have to fulfill a matching condition at the surface. Some of the missing bulk plasmons are replaced by surface plasmons, but anyway the number of modes is reduced.

It will be supposed that the charge density of the electron gas, when there are no plasmon modes, is the same as the one of the positive background, although this is a rather crude approximation. Within Classical Electrodynamics, the polarization related to surface modes is found mainly in the surface plane and their dispersion relation comes from the equation

$$\epsilon(\omega, \vec{k}) = -1, \tag{1.6}$$

that follows from the continuity at the surface of the normal component of the field $\vec{D}$ and of the parallel component of the field $\vec{E}$. Also, the normal component of the charge current $\vec{j}$ must be 0. If the Drude dielectric function represents the material we obtain the frequency of the surface plasmon

$$\omega_{sp} = \frac{\omega_p}{\sqrt{2}}. \tag{1.7}$$

These dispersion relations have no dependence on $\vec{k}$. As mentioned earlier, we can only trust these results in the long- wavelength limit. A dependence on $\vec{k}$ can appear in several ways. Sometimes the geometry of the system produces a dependence on the wavelength even if a local dielectric function is used. This is what happens in the case of the surface modes of a slab. Using the Drude dielectric function the dispersion relations for the two

possible solutions for longitudinal waves are

$$\omega_{\pm}^2 = \frac{\omega_p^2}{2}[1 \pm e^{-kz}]. \tag{1.8}$$

More frequently, the dependence on $\vec{k}$ comes from the use of a non-local dielectric function such as the RPA or the Linhard-Mermin dielectric functions.

In the previous lines we presented the most simple model that includes normal modes. This has lead us to suppose that, if there are not plasmon modes, everywhere the electron gas has the same charge density as the neutralizing positive background, even at a surface. In practice, at a surface there exists a selvedge region where the electronic density decreases smoothly. Instead the positive background finishes in an abrupt way. In many calculations additional modes are found when the selvedge region is modelized properly. These modes are called multipole plasmon modes and its frequency for small $\vec{k}$ lies between $0.8\omega_p$ and ω_p.

In spite of its simplicity, this model follows the same general procedure as the majority of calculations that have been done. A response function must be available. From it, the properties of plasmon modes can be deduced: dispersion relation, lifetime, cross section for production of a plasmon and in which conditions it will be a well-defined collective mode.

To have a good knowledge about plasmon modes is important because there are several areas where this concept plays an important role. Without being exhaustive, we can mention some ones: photo-emission yield [2, 3] (See Ref. [4] for experimental data of aluminium), non-local corrections to Fresnel equation [2, 3], influence of roughness on reflectance [5] (See Ref. [6] for experimental data of aluminium), light emission from rough surfaces [7], light emission from STM [8], transmittance of thin films [9] and dynamic image potential of a charged particle [10, 11, 12].

An historical overview can be found in Chapter 3 and in Section 6.1. Also, a summary of the main publications on the subject can be found in Ref. [13]. We will just mention here a few works that had a decisive influence on the development of the subject. The concept of surface plasmon is introduced by Ritchie in 1957 [14]. He used the hydrodynamical approximation to predict certain energy losses that fast electrons suffered when they crossed thin metal films. This losses where observed experimentally by Powell and Swan in 1959 [15].

Two major advances took place at the early seventies. Bennett shows how important is

to use a realistic model of the selvedge region [16]. In that case, the dispersion relation of the surface plasmon modes in the large wavelength limit turns out to have a negative slope. Moreover, additional plasmon modes appear with higher order multipolarity (the density fluctuation of surface plasmons is monopolar). For this reason they are called multipole plasmons. On the other hand, Feibelman introduces an important function that will be used later in a greater number of calculations [17]. It is the centroid of the density fluctuation and he is able to relate it with many physical observable, like the surface photo-electric yield, the linear coefficient of the surface plasmon dispersion, the electronic lifetime of adsorbate vibrations or non-local corrections to the Fresnel equation [2]. After several unsuccessful attempts, Bennett's result about the dispersion relation of surface plasmons was confirmed experimentally in 1989 [18] and a year later the existence of multipole plasmons was detected [19].

Nowadays the most common technique used in theoretical calculations is the time dependent local density approximation (TDLDA). It has been used to obtain information about plasmon modes in clusters [20], surfaces [19], slabs [21], parabolic quantum wells [22] and overlayers [23]. In these references the jellium model is used for the ionic background. For this reason, results are restricted to simple-metals or materials which have a similar electronic structure. Some theoretical efforts have been made recently to incorporate the more relevant effects due to the ionic structure [24, 25]. This would allow to treat also d-metals.

On the experimental side, conclusive results have been obtained for simple-metal surfaces [19], except for aluminium [26]. In these last metal EELS experiments show no sign of the multipole plasmon, unlike other simple-metals. Now the interest of experimentalists is focused on systems with a reduced dimensionality, such as overlayers [27] and chains [28], and on the properties of surface plasmons at d-metal surfaces [29].

RPA sum rules [30] were used at the beginning to study nuclear giant resonances. Later, they were applied successfully to investigate plasmons in simple-metal clusters [31, 32, 33, 34, 35]. Another technique based in the RPA, the Local RPA [36], was used to study this system [37]. Sum rules provide a method to obtain an average response of the system to a given external perturbing operator. If this operator is local, as it usually happens, the calculations that have to be performed are very similar to the ones of the Local RPA

method. Moreover, Local RPA can be considered as a method to find a local operator that can be used successfully as external operator in a sum rule calculation. More recently, the sum rule method was employed also for an infinite system: a simple-metal surface [38]. It was shown that a careful treatment of the Coulomb energy in the calculations was the key step that allowed to extend the formalism to infinite systems. The work contained in this thesis can be considered as the logical continuation of these studies.

The objective of this work is to perform an alternative study of plasmon modes in systems with plane symmetry. There are still some aspects of this problem to which no conclusive answers have been given. The sum rule approach has some advantages over more sophisticated methods. This allows to address us some questions that are not easily answered using other methods. Limit cases, such as low momentum or step density profile, can be worked out often because results are analytical in many cases. Also, the observability of the modes can be discussed since the different contributions to the total energy can be analyzed on their own. Moreover, we will see that the numerical results obtained show an agreement with experimental data comparable to that of more involved methods, like TDLDA. This is due to the fact that realistic models for the density profile, the kinetic energy functional or the exchange and correlation functional can be employed. Therefore, the main motivation of this work is to exploit all these advantages to accomplish our goal.

The contents are organized in the following way. In Chapter 2 we expose the sum rule formalism in a general way and some previous findings are commented in Chapter 3. This formalism is applied to study plasmon modes of simple-metal surfaces in Chapters 4 and 5. The Local RPA formalism is discussed and its application to simple-metal slabs is presented in Chapter 6. Finally, the main conclusions are summarized in Chapter 7. The relationship between atomic units and other systems is discussed in Appendix A and the expressions of the sum rules of the operators employed are given in Appendix B and C.

Chapter 2

The sum-rule formalism

The spectrum of a many-body system gives detailed information about the response of that system. It can be obtained using formalisms like the RPA or the TDLDA, that involve heavy numerical calculations and whose results are not always easy to interpret. Moreover, a detailed knowledge of the ground state is needed for the calculation to be done. This means that one-particle wave functions should be found previously, preferably in a self-consistent way.

Instead, valuable information can be obtained evaluating only some sum rules. In this way, it is not necessary to calculate the spectrum. This approach has been successfully applied to different systems such as nuclei [30], clusters [32, 34, 37], surfaces [38, 39, 40, 41] and thin films [42]. In many cases sum rules allow a calculation of the global properties of the response of a system to an external excitation operator, like the centroid or the width of the spectrum, with RPA precision. In fact, sum rules should not be regarded as a formalism on its own. They are just useful quantities that can be calculated in the framework of any many-body formalism (usually RPA).

Average results can be very useful if they are obtained from an operator such that it produces a unique and well-defined peak on the spectrum. In this case mainly one collective mode is excited and many properties of this mode can be found from this operator. Often the results are analytical and connections with macroscopic or hydrodynamical models can be easily made. Another advantage is that semi-classical approximations can be used easily to describe the ground state or some terms of the Hamiltonian. As a consequence, a sum-rule calculation is very economical in a computational sense.

In this Chapter the main features of the sum rule approach will be exposed in Section 2.1. Section 2.2 will treat on how to evaluate the main sum rules. Some interesting quantities involved on this evaluation will be analyzed in Section 2.3. Finally, some simplifying approximations will be discussed in Section 2.4.

2.1 General equations

Excitation spectra of many-body systems can be analyzed in terms of the moments $m_k(Q)$ of the strength function $S_Q(E)$ for a given external excitation operator Q:

$$S_Q(E) \equiv \sum_{n\neq 0} \delta(E - \hbar\omega_n) \left|\langle n|Q|0\rangle\right|^2, \tag{2.1}$$

$$m_k(Q) \equiv \int_0^\infty E^k S_Q(E) dE = \sum_{n\neq 0} (\hbar\omega_n)^k \left|\langle n|Q|0\rangle\right|^2, \tag{2.2}$$

where $|n\rangle$ stands for the n-th excited state, ω_n is its energy and the ground state is represented by $|0\rangle$. Although no particular requirements can be deduced from these definitions, we can restrict ourselves to certain kind of operators. In first place, if sum rules are going to be evaluated with RPA precision, we only need to consider one-body operators. The states of the RPA spectrum are excited by these type of operators. As a consequence, we can try only one-body operators for Q if our goal is to obtain RPA precision.

$$Q = \sum q_{pq} a_p^\dagger a_q. \tag{2.3}$$

The Q operator usually represents a physical process and so it must be an observable. Nevertheless, sometimes a non-hermitian operator can be chosen for mathematical convenience. This can be done when, due to the particularities of the problem that we are trying to solve, results are the same with a non-observable operator than with the observable built from this operator by adding its conjugate. Later on, we will see that this is what happens in systems with plane symmetry. In these cases we can take the operator that yields simpler calculations.

Finally, when all the forces between particles are velocity-independent we can take Q to be a local operator, that is, an operator of the form

$$Q = \sum_{i=1}^{A} q(\vec{R}_i), \tag{2.4}$$

where the subindex i runs over all the particles of the system and $\vec{R}_i$ stands for the position operator of each particle. The whole system has A particles. The key part of the sum-rule approach is finding a function q in such a way that the operator Q built from it excites mainly one collective mode. In this case the average spectral properties of the response to the operator Q given by

$$\bar{E} = \frac{m_1}{m_0}, \tag{2.5}$$

$$\sigma^2 = \frac{m_2}{m_0} - \left(\frac{m_1}{m_0}\right)^2, \tag{2.6}$$

can give useful information about that mode.

The odd moments (with $k > 0$) can be expressed by multiple commutators of Q with the Hamiltonian H [30]. Using the completeness of the states $|n\rangle$, a simple manipulation of Eq. 2.2 leads to

$$m_1(Q) = \frac{1}{2}\langle\phi|[Q^\dagger,[H,Q]]|\phi\rangle, \tag{2.7}$$

$$m_3(Q) = \frac{1}{2}\langle\phi|[[Q^\dagger,H],[H,[H,Q]]]|\phi\rangle. \tag{2.8}$$

In these expressions the uncorrelated HF ground state $|\phi\rangle$ is used instead of the correlated RPA ground state. There is an equivalence theorem by Thouless [43] that states that the result is exactly the same for both ground states when there are not density-dependent forces in the Hamiltonian H. If there are density-dependent forces in the Hamiltonian, the theorem must be generalized. It can be shown that the theorem can also be applied when the density- dependent parts of the Hamiltonian do commute with Q. If this condition is fulfilled, it is safe to use a HF ground state when density-dependent forces are present. In fact, the expectation value of double commutators is not very sensible to the details of the ground state and further approximations can be done in this direction.

No equivalence theorems exist for the even k moments because these are very sensitive to ground state correlations. This is the reason why rather than evaluate m_0 and m_2 and substitute the values in Eqs. 2.5 and 2.6 it is better to define the following energies

$$E_k(Q) = \sqrt{\frac{m_k(Q)}{m_{k-2}(Q)}} \tag{2.9}$$

that can be used to set bounds to the values of $\bar{E}$ and σ^2 [30] using the 1

$$E_1 \leq \bar{E} \leq E_3, \tag{2.10}$$

$$0 \leq \sigma^2 \leq \frac{1}{4}(E_3^2 - E_1^2). \tag{2.11}$$

The m_{-1} sum-rule is calculated in a different way because, unlike m_1 and m_3, it can not be expressed as the expectation value of a set of commutators. It can be seen [44] that this sum-rule is closely related to the static polarizability

$$m_{-1}(Q) = \frac{1}{2}\alpha(Q) \tag{2.12}$$

This allows to evaluate the m_{-1} sum-rule using the result of a constrained HF calculation with RPA precision.

If we want to know the energy of a collective mode we have to find an operator that, ideally, excites only that mode. In this case the Eqs. 2.10 and 2.11 are satisfied with equal sign and we can take either E_3 or E_1 as the energy of the mode. In practice, E_3 and E_1 will not coincide and we will have to use σ^2 as a test on how appropriate is our operator. It is not essential to calculate E_1 if comparison with previous results (experimental or theoretical) indicates that the operator does not mix different modes although then E_3 would be, strictly speaking, just an upper bound to the energy of the centroid.

2.2 Evaluation of sum rules

From now on we will assume that our system is an electron gas placed in a positive ionic background whose geometry we do not specify yet. Also, atomic units will be used throughout. The Hamiltonian of this system is

$$H = H_k + H_c + H_{xc} + H_I, \tag{2.13}$$

where

$$H_k = \frac{1}{2}\int \hat{\tau}(\vec{r})d^3r, \tag{2.14}$$

$$H_c = \int \left\{ \hat{n}(\vec{r})v_I(\vec{r}) + \frac{1}{2}\hat{n}(\vec{r}) \left[\int \frac{\hat{n}(\vec{r}')}{|\vec{r} - \vec{r}'|} d^3r' \right] \right\} d^3r, \tag{2.15}$$

$$H_{xc} = \int \epsilon_{xc}[\hat{n}(\vec{r})]d^3r. \tag{2.16}$$

In metal systems, the term H_I, the Hamiltonian of the ionic background, can be omitted because it commutes with the external excitation operator. In the case of simple-metals, the valence electrons are so delocalized that even such a simple model for the ionic background as

the jellium model can be employed successfully. The function $v_I(\vec{r})$ represents the potential created by this background. The one-body operators $\hat{n}(\vec{r})$ and $\hat{\tau}(\vec{r})$ are, respectively, the particle density operator and the kinetic energy density operator and are defined by

$$\hat{n}(\vec{r}) \equiv \sum_{i=1}^{A} \delta(\vec{r} - \vec{R}_i) \tag{2.17}$$

$$\hat{\tau}(\vec{r}) \equiv \sum_{i=1}^{A} \overleftarrow{P}_i \, \delta(\vec{r} - \vec{R}_i) \vec{P}_i \tag{2.18}$$

The HF ground state $|\phi\rangle$ is a slater determinant of plane waves. Its one-particle wave functions will be noted as ϕ_i. Taking this into account directly in Eq. 2.7 allows to find m_1 in a straightforward way. Only the kinetic part of the Hamiltonian contributes to the sum-rule. The result, for a local one-body operator Q, is

$$m_1 = \frac{1}{2} \int |\vec{u}(\vec{r})|^2 n(\vec{r}) d^3r, \tag{2.19}$$

where $\vec{u}$ stands for the velocity field

$$\vec{u} \equiv \vec{\nabla} q(\vec{r}) \tag{2.20}$$

and the ground state particle density

$$n(\vec{r}) \equiv \langle \phi | \hat{n}(\vec{r}) | \phi \rangle = \sum_{i=1}^{A} |\phi_i(\vec{r})|^2. \tag{2.21}$$

In an analogous way, we can define the ground state kinetic energy density as

$$\tau(\vec{r}) \equiv \langle \phi | \hat{\tau}(\vec{r}) | \phi \rangle = \sum_{i=1}^{A} |\vec{\nabla} \phi_i(\vec{r})|^2. \tag{2.22}$$

To calculate m_3 from Eq. 2.8 is a formidable task. It is simpler to define the following scaled state

$$|\eta\rangle \equiv e^{\eta [H,Q]} |\phi\rangle, \tag{2.23}$$

where η is the scaling parameter. It can be seen, by a simple substitution, that the following equation is fulfilled

$$m_3 = \frac{1}{2} \frac{\partial^2}{\partial \eta^2} \langle \eta | H | \eta \rangle |_{\eta=0}. \tag{2.24}$$

The expectation value $\langle \eta | H | \eta \rangle$ can be put in terms of $\langle \eta | \hat{\tau}(\vec{r}) | \eta \rangle$ and $\langle \eta | \hat{n}(\vec{r}) | \eta \rangle$. On the other hand, these two brackets can be expanded on η around the ground state value.

$$\langle \eta | \hat{n}(\vec{r}) | \eta \rangle = n + \eta n_1(\vec{r}) + \eta^2 n_2(\vec{r}) + \cdots, \tag{2.25}$$

$$\langle\eta|\hat{\tau}(\vec{r})|\eta\rangle = \tau + \eta\tau_1(\vec{r}) + \eta^2\tau_2(\vec{r}) + \cdots. \tag{2.26}$$

Using now Eq. 2.24, m_3 can be given in function of just the coefficients n_1, n_2 and τ_2

$$\begin{aligned} m_3 &= \int \{\tau_2(\vec{r}) + n_2(\vec{r})[v_I(\vec{r}) + \int \frac{n(\vec{r}')}{|\vec{r}-\vec{r}'|}d^3r'] + \\ &\frac{1}{2}n_1(\vec{r})\int \frac{n_1(\vec{r}')}{|\vec{r}-\vec{r}'|}d^3r' - \frac{1}{2}n(\vec{r})n_1(\vec{r})\frac{\delta^2\epsilon_{xc}}{\delta n^2}\nabla\vec{u}(\vec{r})\}d^3r. \end{aligned} \tag{2.27}$$

In the next section the physical meaning of the quantities $n_1(\vec{r})$ and $\vec{u}(\vec{r})$ will be discussed. Substituting Eq. 2.23 in Eqs. 2.25 and 2.26 the following expressions are found

$$n_1 = \langle\phi|\left[\hat{n},[H,Q]\right]|\phi\rangle, \tag{2.28}$$

$$n_2 = \frac{1}{2}\langle\phi|\left[[\hat{n},[H,Q]],[H,Q]\right]|\phi\rangle, \tag{2.29}$$

$$\tau_2 = \langle\phi|\left[[\hat{\tau},[H,Q]],[H,Q]\right]|\phi\rangle. \tag{2.30}$$

Their evaluation leads to [45]

$$n_1 = -\nabla_i(nu_i), \tag{2.31}$$

$$n_2 = -\frac{1}{2}\nabla_i(n_1u_i), \tag{2.32}$$

$$\begin{aligned} \tau_2 &= \frac{1}{3}\tau\{-u_k(\nabla_k\nabla_iu_i) + (\nabla_ju_i)[\nabla_iu_j + \nabla_ju_i]\} + \\ &\frac{1}{4}(\nabla_i\nabla_ju_j)[\nabla_i\nabla_k(nu_k)] + \\ &\frac{1}{4}(\nabla_in)(\nabla_j\nabla_ku_k)[\nabla_iu_j + \nabla_ju_i]. \end{aligned} \tag{2.33}$$

In these expressions, ∇_i means the Cartesian i-coordinate derivative and a sum over repeated indices is understood. The expression for τ_2 is complete only if τ comes from the Thomas-Fermi approximation. If τ is obtained from the one-particle wave functions then an additional term should be included to take into account the centrifugal kinetic energy [34]. Inserting these results in Eq. 2.27 one obtains at last the m_3 sum-rule.

As the m_{-1} sum-rule is proportional to the static polarizability, it can be calculated with RPA precision from a constrained HF calculation similar to that used to find the one-particle wave functions. The difference is that now the Hamiltonian has an additional term representing a small disturbance produced by the excitation operator Q

$$H' = H - \lambda Q. \tag{2.34}$$

The constrained ground-state, that depends on the small parameter λ, is labeled as $|\lambda\rangle$. The m_{-1} is then obtained using a similar expression to that of Eq. 2.24

$$m_{-1} = \frac{1}{2}\frac{\partial^2}{\partial\lambda^2}\langle\lambda|H|\lambda\rangle|_{\lambda=0}. \tag{2.35}$$

This equation, unlike Eq. 2.24, is not very usable by itself because the coefficients of the series involved in its calculation do not have explicit expressions and therefore have to be calculated in the frame of the same formalism as the ground-state.

2.3 Transition density and velocity field of a collective mode

Some quantities involved in the calculation of m_3 have an interesting physical meaning that allows to compare sum-rule results with those of hydrodynamical or macroscopic models [44]. The transition density, defined by

$$n^{(1)k} \equiv \langle k|\hat{n}(\vec{r})|\phi\rangle, \tag{2.36}$$

plays a key role in the description of vibrations in quantum mechanics. Any wave-packet can be described as a superposition of the ground-state $|\phi\rangle$ and some excited states $|k\rangle$. The time dependence of this state is

$$|\Phi(t)\rangle = |\phi\rangle + \sum_k c_k|k\rangle e^{-iE_k t/\hbar}. \tag{2.37}$$

If we assume that the coefficients c_k are small, the expectation value of the operator $\hat{n}(\vec{r})$ is, up to first order,

$$\langle\Phi(t)|\hat{n}(\vec{r})|\Phi(t)\rangle = n(\vec{r}) + \sum_k c_k\langle\phi|\hat{n}(\vec{r})|k\rangle e^{-iE_k t/\hbar}. \tag{2.38}$$

The time dependent term represents the density fluctuation of the wave-packet. Lets assume that an external excitation operator has excited only one state. For this case, the equation reveals that the profile of the density fluctuation produced by an excited state is proportional to its transition density.

Now we will consider the coefficient n_1 that can be obtained from Eq. 2.31. It is clear, from Eq. 2.25, that it is the first-order approximation to the density fluctuation of the scaled state $|\eta\rangle$ in relation to the ground state but, moreover, can provide an approximation to

the transition density as it can be seen taking a close look at the following sum-rule

$$m_\rho(\vec{r}) = \sum_{k\neq 0} \hbar\omega_k \langle\phi|\hat{n}(\vec{r})|k\rangle\langle k|Q|\phi\rangle. \tag{2.39}$$

Taking advantage of the completeness relation the following equation is deduced from Eq. 2.39

$$m_\rho(\vec{r}) = \frac{1}{2} n_1(\vec{r}). \tag{2.40}$$

If the operator Q excites only the collective mode $|k\rangle$, m_ρ is proportional to the transition density defined by Eq. 2.36, showing that n_1 is also proportional to the transition density if Q is a proper operator. Another magnitude with a well-defined physical meaning is the velocity field $\vec{u}$, previously defined in Eq. 2.20. To see the reason for this name, the current density operator must be defined as

$$\hat{\vec{j}}(\vec{r}) = \frac{1}{2}\sum_{i=1}^{A}\left[\hat{\overleftarrow{P}}_i\delta(\vec{r}-\hat{\vec{R}}_i) + \delta(\vec{r}-\hat{\vec{R}}_i)\hat{\vec{P}}_i\right]. \tag{2.41}$$

From this operator, the sum-rule

$$m_{\vec{j}}(\vec{r}) = \sum_{k\neq 0}\langle\phi|\hat{\vec{j}}(\vec{r})|k\rangle\langle k|Q|\phi\rangle \tag{2.42}$$

can be build. Again, when Q excites just one mode, only one term contributes to the sum and this is found to be proportional to the transition current density

$$\vec{j}^{(1)k} \equiv \langle k|\hat{\vec{j}}(\vec{r})|\phi\rangle. \tag{2.43}$$

Using once more the completeness relation one can obtain from Eq. 2.42

$$m_{\vec{j}}(\vec{r}) \propto n(\vec{r})\vec{u}(\vec{r}). \tag{2.44}$$

Because this sum-rule is proportional to the current density, this last expression means that $\vec{u}$ is the equivalent of the velocity field of the hydrodynamical models.

2.4 Semi-classical approximations for the evaluation of sum-rules

The most accurate application of the method consists in the use of self-consistent one-particle wave functions in Eq. 2.21 to calculate the particle density and in Eq. 2.22 for

the kinetic energy density. Nevertheless, the particle density obtained from semi-classical calculations does not differ greatly from self-consistent results although all the shell effects will be averaged. It is even possible to use an analytical approximation for this density, allowing to express the sum-rules in analytical form. In any case the sensitivity of the results on the choice of the ground-state is very low.

Once an appropriate particle density is fixed, a kinetic-energy density can be obtained using a local density approximation like the improved Thomas-Fermi-von Weisäker functional given by

$$\tau = \frac{3}{10}(3\pi^2)^{2/3} n^{5/3} + \frac{\beta}{8}\frac{n'^2}{n}. \tag{2.45}$$

β is taken to be 0.5. With this value the functional works best in the limit of rapid density oscillations while $\beta = 1/6$ would be valid for slowly varying oscillations. For the exchange and correlation, Slater- and Wigner-type LDA expressions will be used

$$\epsilon_{ex} = -\frac{3}{4}\left(\frac{3}{\pi}\right)^{1/3} n^{4/3} \tag{2.46}$$

and Wigner

$$\epsilon_{cor} = -\frac{a(4\pi n/3)^{1/3} n}{b(4\pi n/3)^{1/3} + 1}, \tag{2.47}$$

where $a = 0.44$ and $b = 7.8$. It should be stressed that although the exchange and correlation interaction is treated in a purely local way, non-locality is included in the kinetic energy because the local density functional is used only through the exact expression given by Eq. 2.33. A completely local τ_2 could be calculated taking Eq. 2.45 as the definition of $\hat{\tau}$ for Eq. 2.30 but this would be a poorer approximation.

Until this point neither the geometry of the system nor the structure of the positive background have been settled. In the following chapters it is assumed that the system has plane symmetry and, as a consequence, the electronic density n will only depend on the z coordinate. The jellium model will be used to describe the ionic background. In this model the positive charge of the ions is smeared over the whole volume of the system with constant density. This description is appropriate in the case of simple-metal systems, where the band effects are small and can be taken into account just introducing an effective mass for the electrons. Improvements to the jellium model can be made [41] and give essentially the same results for simple-metal surfaces.

Chapter 3

Review of previous results

In the following, the main concepts that have been worked out in the past are presented briefly. Our historical outline only includes the main milestones in the subject and more detailed reviews can be found elsewhere [2, 13, 26, 29].

Ritchie [14] was the first to point out, in 1957, the existence of the surface plasmon mode in a work about the energy loss of fast electrons passing through a metal slab. Although this prediction was made within the hydrodynamical approximation, three years later Stern and Ferrell [46] also found this mode. A little earlier, in 1959, Powell and Swan [15] could verify experimentally the existence of this mode, using an electron energy loss spectroscopy (EELS) study of aluminium and magnesium surfaces.

Some major theoretical advances were made at the beginning of the seventies. Bennett [16] implemented an electronic profile that, although it was not completely realistic, included surface diffuseness, in an hydrodynamical model. The density fluctuation of the surface plasmon was known to be monopolar but he discovered two unsuspected features: the existence of higher multipolarity surface excitations, later called multipole plasmon modes, and the negative slope of the dispersion relation for low values of the transfered momentum (in the case of the monopolar surface plasmon). In this way, the importance of a correct description of the ground state became clear.

On the other hand, Feibelman [47], also using a diffuse density profile, performed a microscopic RPA calculation of the excited states of a metallic surface. He was the first to

recognize the importance of the following function

$$d(\omega) = \frac{\int z\delta n(z,\omega)dz}{\int \delta n(z,\omega)dz}, \tag{3.1}$$

that represents the centroid of the density fluctuation associated with a plasmon mode. Feibelman was able to relate this function to many surface properties [2] like the surface photo-electric effect, the image plane of a charge, the energy transfer of excited adsorbate, the Van der Waals force, the inelastic scattering of electrons, non-local corrections to the Fresnel equations or the dispersion of surface plasmons. In other words, the function $d(\omega)$ characterizes the dynamical response of the system.

The response function of a semi-infinite system $\alpha_k(\omega)$ can be defined in terms of the potential induced by an external field. Lets consider that the metal is placed at the $z < 0$ zone. If the external field creates a potential given by

$$\phi_{ext}(\vec{r},t) = A_{k,\omega}e^{i\vec{k}\vec{\rho}}e^{kz}, \tag{3.2}$$

then the induced potential takes the form, far away from the surface,

$$\phi_{ind}(\vec{r},t) = -A_{k,\omega}e^{i\vec{k}\vec{\rho}}\alpha_k(\omega)e^{-kz}. \tag{3.3}$$

This response function can be expressed in terms of the centroid in the following way. First, we express it in an alternative form [26, 48]

$$\alpha_k(\omega) = \int e^{kz}\delta n(z,k,\omega)dz. \tag{3.4}$$

Expanding Eq. 3.4 in the small k limit the relation that we were looking for is obtained

$$\alpha_k(\omega) = \frac{\epsilon(\omega)-1}{\epsilon(\omega)+1}\left(1 + \frac{2\epsilon(\omega)}{\epsilon(\omega)+1}kd(\omega)\right). \tag{3.5}$$

This formula was also stated by Harris and Griffin [49] and Flores and Garcia-Moliner [50].

The response function given by Eq. 3.3 is sometimes called the image charge and plays a key role in more than one approach [26, 39] to the problem of the collective modes of a surface. A plasmon mode is defined by the poles of the response function, so that an infinitesimally small field will be enough to excite a mode. A close look at Eq. 3.5 allows to see two different possibilities for the existence of a collective mode. The most obvious pole corresponds to the surface plasmon and is given by the equation $\epsilon(\omega) + 1 = 0$. In the

particular case in which we consider a Drude response of the electron gas, the well-known dielectric function

$$\epsilon(\omega) = 1 - \frac{\omega_p^2}{\omega^2}, \tag{3.6}$$

can be used to find the frequency of the surface plasmon. It leads to the result $\omega_{sp}^2 = \omega_p^2/2$. Taking this reasoning a little further and assuming that the variation of the centroid with ω is slow at the frequency $\omega_p/\sqrt{2}$, the dispersion relation

$$\omega(k) = \omega_{sp}\left[1 - d(\omega_{sp})\frac{k}{2}\right] \tag{3.7}$$

can be deduced. Another possibility for a pole structure in the response function is a pole in the real part of the function $d(\omega)$. In this case we have a multipole plasmon. In general $d(\omega)$ has also an imaginary part, due to the presence of dissipative forces.

Hydrodynamic models are not sufficiently reliable for predictive purposes [16] and further work was done, using microscopical methods, in order to fix the sign of the slope of the dispersion relation and the existence of multipole plasmon modes, but the results were inconclusive. An RPA calculation [51], that used a step potential to obtain a diffuse density profile, confirmed Bennett's result, while others, also within the RPA, using the infinite barrier method (IBM) indicated a positive slope [52, 53]. This is not surprising because the IBM model is not very trustworthy in the long wavelength limit due to the unphysical condition that it imposes on the metal-vacuum interface.

The experiments that were being done at that time did not throw much light on the subject. The experimental study of surface electronic excitations is based either on optical methods or on the inelastic scattering of electrons. The first method has the drawback that, as surface plasmons are not optically active, a coupling with the electro-magnetic field has to be generated. For this purpose, a grating coupler or the attenuated total reflection method can be employed. However these methods are limited to large wavelengths, where retardation effects are important. Shorter wavelengths can only be achieved by inelastic scattering of electrons. Therefore, the first experiments used high energy EELS (the energy of each electron was of the order of 50 KeV) and were performed over thin films [54, 55]. This technique has the advantage that also bulk excitations can be probed, allowing for a complete investigation of the system. Unfortunately, the equipment used was oriented towards the study of bulk modes and had no facilities to check the cleanliness and order of

the surface. Different signs for the slope of the Mg surface plasmon were obtained and this discrepancy was ascribed to the roughness of the surfaces and to the possible presence of contaminants [56, 57]. Other experiments were done, by first time, over well-defined single-crystal surfaces [58]. The metal chosen was Al and the technique used was the inelastic low energy electron diffraction. These experiments were more surface-oriented because the lower energies (100 eV) of the electrons that makes them interact mainly with this part of the metal. The Al(001) face showed a negative slope, not like the Al(111) face that presented a positive slope. Nevertheless these results were far from conclusive because very different curves could be adjusted to the experimental data, allowing for other interpretations, and little credit was given to them.

In 1974 Feibelman [59] presents an RPA calculation based on a self-consistent calculated ground state that gives a negative slope of the dispersion relation. In Eq. 3.7 it can be seen that the sign of the slope depends mainly on the position of the centroid $d(\omega)$. A hand-waving argument can be given to explain it. The electric potential associated with the density fluctuation of the surface plasmon is peaked at the centroid position and decreases more sharply for large momentum. The surface diffuseness creates a dipole electric field at the surface region with the negative charge facing outside the metal. In ordinary surface plasmon modes, the centroid is placed outside the metal surface. In this case, the penetration of the electric potential in the surface region is larger for smaller momenta, giving a negative slope of the dispersion relation. This happens because the negative face of the dipole is oriented towards the (negative) potential created by the density fluctuation.

The experimental confirmation [60, 61] comes more that ten years later from the study of surfaces and thin films of Ag, using low energy angle-resolved EELS. These are the first works in which the form of the dispersion relation is investigated. In these experiments a monochromatic beam of electrons of energy E_i, incident on a flat surface at an angle θ_i is reflected inelastically and detected by an angle resolved energy analyzer, positioned at an angle θ_s from the normal direction. If the incident electron excites a surface plasmon with energy $\hbar\omega$ his energy will become $E_s = E_i - \hbar\omega$. When an electron with this loss of energy arrives at the detector it is sure that it has transmitted to the plasmon a momentum

$$\hbar k = \sqrt{2m}(\sqrt{E_i}\sin(\theta_i) - \sqrt{E_s}\sin(\theta_s)). \tag{3.8}$$

For a given combination of the beam-detector geometry and an initial energy of the incoming

electrons, the energy of a plasmon is determined looking at the position of its peak in the plot of the number of detections in front of the energy loss, and its momentum is obtained from Eq. 3.8. Varying the configuration of the experiment, the whole dispersion relation can be found.

By the same time, TDLDA calculations [62] are done, showing an excellent agreement with experimental data [18].

Now a few words about the multipole surface plasmon mode are in order. Some indirect experimental signs were found in photo-yield data from alkali metals [63] and in surface photo-emission experiments [4] but it is not until 1990 that direct experimental evidence is found using low energy EELS [19] of alkali metals. In the same experiment, no signs of the multipole mode were found on Al, although previously an enhancement of the surface photo-emission from this metal had been found at $0.8\omega_p$ [4].

From the first works [16, 49, 64, 65] it was understood that, within the hydrodynamical approximation, additional modes were found if a surface electronic structure, which mimicked the electronic-surface diffuseness, was assumed. Nevertheless, there were some doubts about the reliability of this model. It was even thought that multipole plasmon modes could be just an artifact of the hydrodynamical model but Dobson and Harris [66] confirmed the existence of multipole modes on a bare jellium surface within a microscopic calculation. They emphasized the use of a correct self-consistent electronic density profile. Feibelman [2] and, later, Liebsch [62] obtained $d(\omega)$ for time-dependent external fields and found a resonant structure at $\omega = 0.8\omega_p$ which is due to the multipole mode. In these calculations the real part of $d(\omega)$ swings from large positive to large negative values in a small range of frequency and the imaginary part has a sharp peak. This behavior is more pronounced as the electron density decreases.

More recently, a good agreement has been found between TDLDA calculations and experimental results [19, 26]. In these experiments, data about the damping of surface modes has also been obtained. The lifetime of the surface plasmon is limited by its decay into single-particle excitations. This is the so-called Landau mechanism. An intuitive picture can help to understand when it is likely to find this kind of decay. We can consider that the energy of a plasmon mode is due to different reasons. The kinetic part will come from the kinetic energy of the electrons that form the electron gas and the Coulomb part is

caused by the interaction of the electrons between them. The total energy of the plasmon mode is the sum of all the contributions. A fast particle can excite a collective mode when its kinetic energy is close to the energy of the mode. In the same way, a collective mode will have a large probability to decay into a particle-hole excitation when the kinetic energy of the electrons is comparable to the total energy of the mode. In other words, the Landau mechanism will probably occur when the kinetic contribution is the larger one.

The jellium model only includes the Landau mechanism and can not take into account any contribution to the damping due to the ionic structure, like the Drude mechanism. If the jellium model is used, plasmons appear to have an infinite lifetime at $k = 0$ and a linear growth of the loss line with k, corresponding to the growing phase space into which the surface plasmon can decay. However, in physical systems, the Drude mechanism causes a finite line width even at $k = 0$. Also, multipole plasmons have a finite lifetime for any momentum, even if only the Landau mechanism is considered. This is related to the fact that the total energy of a multipole plasmon mode has a significant kinetic contribution even at $k = 0$. This is characteristic of multipole plasmons, because the kinetic contribution of volume plasmons and ordinary surface plasmons vanishes at $k = 0$.

Nowadays, the main properties of surface and multipole plasmons are well established. The density fluctuation of the surface plasmon has essentially monopole character perpendicular to the surface. A negative dispersion of the surface plasmon should be expected because the electronic profile is diffuse at the surface. Instead, multipole plasmons are associated with electronic density fluctuations that are peaked at the surface region and have decreasing oscillating amplitude towards the interior of the metal. These modes have been referred to as multipole surface plasmons because their density fluctuation integrates to 0 in the direction normal to the surface. They carry momentum both in the normal as well as in the parallel direction, making them optically active in contrast to surface plasmons. The origin of their dispersion relation is placed at $\omega = 0.8\omega_p$, between the bulk and the surface values. For small k values the slope of the dispersion relation is positive in contrast to the case of surface modes, which have negative slope.

The reason why multipole modes in aluminium do not appear in EELS experiments but can be detected through photo-yield data is also understood. Multipole plasmons are severely damped on aluminium and will be hardly seen by any excitation mechanism that

can also excite ordinary surface plasmons because they will contribute much more to the response of the system that multipole modes. Only when surface plasmons are not present in the response of the system, like in photo-yield, multipole plasmons will not be masked. In metals where multipole plasmon modes are not so damped, like sodium, EELS data can reflect the existence of these modes.

Chapter 4

Response of simple-metal plane surfaces

The response of a plane surface to a q- and ω-dependent excitation within a model valid for general non-local dielectric functions, representing the electronic surface diffuseness by a double step density has been obtained. The surface plasmon dispersion relation obtained in this model is compared with a sum-rule calculation which assumes a jellium positive background for the ionic part of the metal and uses an analytical approach to a Lang-Kohn calculation for the electronic density profile at the surface. The role played by the different physical assumptions made for each model is stressed. Finally, a comparison of the results with experimental data and some previous theoretical calculations is made.

4.1 Introduction

Much attention has been devoted to the study of the interaction of external probes with metal surfaces as it provides useful information about the electronic [67] and optical [3, 68] properties of solids. Grazing incident probes parallel to the surface as well as probes crossing the interface may induce surface and volume excitations in the medium that characterize its response function. Recent high resolution experiments on angle-resolved reflection inelastic electron scattering [18, 19] allow for a detailed comparison between different approximations and clear up previous controversies. It is now clear that the surface plasmon dispersion relation at small transfer momentum parallel to the surface is negative for metals like Na,

K or Al [18, 19, 69], as was previously predicted [16, 17, 51, 70]. The simplest theories assume local dielectric functions for the bulk and abrupt electronic density profiles at the surface. More realistic models including non-locality are necessary to produce a much richer absorption spectrum comparable with experiments [2, 3, 71]. A non-local dielectric function couples the surface and bulk plasmon modes and may provide an additional interaction mechanism through the creation of electron-hole pairs. In addition to these contributions, the smooth decrease of the electronic density at the surface must be somehow incorporated in the calculations to reproduce experiments (this has been extensively discussed in the literature, see for example Refs. [3, 72]. A compromise must be reached between the simplicity and transparency of the expressions used and the ability to include the most important physical aspects to describe the electron gas surface response.

The aim of this Chapter is to make an analysis of different approaches (some of them extensively used in the literature) that model the response of the metallic surface. We first study the response through a semi-classical approximation to the amplitude coefficient $\alpha_q(\omega)$ of the potential outside the surface induced by a q- and ω-dependent perturbation, using dielectric functions of different complexity. Next, a comparison between the surface plasmon dispersion relation obtained from the poles of the $\alpha_q(\omega)$ coefficient and that obtained from the sum rule (SR) technique used previously in metal clusters [34] is made. Special attention is paid to the different physical contributions of each approximation.

Results are given for the $\alpha_q(\omega)$ coefficient using a random phase approximation (RPA) [73] and the Lindhard-Mermin (LM) [74] dielectric functions modeling the electronic profile by a double step density. The use of an RPA dielectric function makes it possible to study, within a plasmon-pole approximation, the changes in the absorption spectrum when plasmon dispersion or the electron-hole contribution is removed. Besides these contributions, in the case of interaction with low energetic probes, a plasmon-pole dielectric approximation is not reliable. In this case both low energy and momentum transfers are the main inelastic processes and one would expect that the inclusion of absorption within the electron-hole band in the response function would become necessary. This effect is examined using the LM dielectric function.

The sum rule approach has been used previously to calculate the dispersion relation of collective excitations of metallic systems of different geometries [34, 38, 75, 76, 77]. One

of the advantages of this method is that it can easily incorporate electronic exchange and correlation interactions and realistic electronic density profiles. In this paper, within this approximation, the jellium model is used for the ionic background and a parameterized electronic density function is employed to reproduce a Lang-Kohn calculation of the electronic structure to study the role played by the surface diffuseness. Taking advantage of the simplicity and transparency of the method, the different contributions to the energy of the surface modes are analyzed.

This chapter is organized as follows: In section 4.2 the $\alpha_q(\omega)$ coefficient is calculated using the semi-classical infinite barrier method (SCIB) [78, 79] and results are given for different dielectric functions. In section 4.3 a SR calculation is carried out and the surface plasmon dispersion relation is obtained. In section 4.4 results are compared with experimental data and with previous calculations and conclusions can be found in section 4.5.

4.2 The $\alpha_q(\omega)$ coefficient: a dielectric formalism

The response of a plain metallic surface to an arbitrary exterior electric field is studied through the amplitude $\alpha_q(\omega)$ (relative to that of the external electric field) of the induced potential, which gives the reaction to the q-component of the multipolar expansion of the field. $\vec{q}$ is a two-dimensional wave vector parallel to the metallic surface which is assumed to be perpendicular to the z-axis. To simulate the smooth decrease of the electronic density at the surface, a double step model is used: the material characterized by the metallic dielectric function $\epsilon_1(\vec{k},\omega)$ extends from $z = -\infty$ to $z = 0$, a layer of thickness t and dielectric function $\epsilon_2(\vec{k},\omega)$ occupies the region $0 \leq z \leq t$ and the exterior is assumed to have a dielectric constant ϵ_0 which extends from $z = t$ to $z = \infty$. The thickness and the bulk electronic density n_0 of the layer is adjusted for each material as explained in the next section. $\vec{k} = (\vec{q}, k_z)$ is a three-dimensional wave vector.

In this section, the method used by Rojas et al. [80] is closely followed in the calculation of the polarizability of coated metallic spheres. The SCIB enables the use of general non-local dielectric functions for the material and the overlayer.

If a q-dependent external potential of the type

$$V_{ex}(\vec{r}) = A_q e^{i\vec{q}\vec{\rho}} e^{qz} \tag{4.1}$$

is assumed, where $\vec{r} = (\vec{\rho}, z)$ and A_q is a frequency- dependent function, then the total potential for $z > t$ is given by

$$V(\vec{r}) = A_q e^{\vec{q}\vec{\rho}} \left(e^{q(z-t)} - \alpha_q e^{-q(z-t)} \right) ; z > t, \tag{4.2}$$

where a non-divergent solution of the Laplace equation has been added to the external potential. This α_q-dependent term is the induced potential.

The α_q coefficient plays a role similar to that of a surface polarizability in the sense that the dispersion relation of the surface modes of the system is obtained from the condition [80]

$$Re\left(1/\alpha_q\left(\omega\right)\right) = 0 \tag{4.3}$$

which reduces to the well-known expression $\epsilon + 1 = 0$ for the local dielectric function and a single step surface (see Eq. 4.14). Moreover, the variation of α_q with ω and q (see Figs. 4.1 to 4.12) is similar to that of the polarizability of a metal sphere, as obtained by Rojas et al. [80]. Sometimes the product $\alpha_q e$ (where e is the charge of the electron) is called "the image charge" [81].

The α_q coefficient is determined as follows. Due to the local nature of the dielectric constant for $z > t$, the z-component of the displacement vector $\vec{D}$ can be directly deduced from $\vec{D} = -\epsilon_0 \vec{\nabla} V$, yielding:

$$D_z(\vec{r}) = -\epsilon_0 A_q e^{i\vec{q}\vec{\rho}} q \left(e^{q(z-t)} + \alpha_q e^{-q(z-t)} \right) \tag{4.4}$$

for $z \geq t$.

Within the SCIB model, similar expressions for V and D_z in the bulk and the overlayer can be deduced. One first assumes the dielectric medium (ϵ_1 or ϵ_2 in each case) to fill the whole space and the solves the Poisson equation in this unbounded medium for a surface charge distribution that replaced the real boundaries. Inside the overlayer the potential is found using

$$\nabla^2 V_{D_2}(\vec{r}) = \left(F_q \delta(z) + B_q \delta(z-t)\right) e^{i\vec{q}\vec{\rho}} \tag{4.5}$$

while inside the bulk material

$$\nabla^2 V_{D_1}(\vec{r}) = C_q \delta(z) e^{i\vec{q}\vec{\rho}} \tag{4.6}$$

is used. The calculated V_{D_i} yield the displacement vector $\vec{D_i}$ using the relation

$$-\vec{\nabla} V_{D_i}(\vec{r}) = \vec{D}_i(\vec{r}) \; ; \; i = 1, 2 \tag{4.7}$$

inside each dielectric. The i-index labels the bulk and overlayer ($i = 1$, the bulk, $i = 2$, the overlayer). It is assumed that the dielectric properties of the material are unchanged up to the boundary.

Using Eq. 4.7 and the relation between the total potential and V_{D_i} given by

$$V_{D_i}(\vec{k}) = \epsilon_i(\vec{k}, \omega) V_i(\vec{k}) \; ; \; i = 1, 2 \tag{4.8}$$

and imposing the two standard boundary conditions (continuity of the potential and the z-component of the displacement vector) at the interfaces, the problem of determining the fields is reduced to solving a four-equation system which provides the four unknowns, α_q, F_q, B_q and C_q. For the α_q coefficient, we obtain (atomic units are used from now on):

$$\begin{aligned} \alpha_q(\omega) = \quad & [(\beta_1 + \beta_2)(\pi - \epsilon_0 q \beta_2) - (\beta_1 e^{-tq} - \beta_3) \\ & \times (\pi e^{-qt} + \epsilon_0 q \beta_3)] \\ & [(\beta_1 + \beta_2)(\pi + \epsilon_0 q \beta_2) \\ & - (\beta_1 e^{-tq} - \beta_3)(\pi e^{-qt} - \epsilon_0 q \beta_3)]^{-1}, \end{aligned} \tag{4.9}$$

where

$$\beta_1 = \int_{-\infty}^{\infty} \frac{e^{ik_z 0^-} dk_z}{(q^2 + k_z^2)\epsilon_1(q, k_z, \omega)}, \tag{4.10}$$

$$\beta_2 = \int_{-\infty}^{\infty} \frac{e^{ik_z 0^+} dk_z}{(q^2 + k_z^2)\epsilon_2(q, k_z, \omega)}, \tag{4.11}$$

$$\beta_3 = \int_{-\infty}^{\infty} \frac{e^{ik_z t} dk_z}{(q^2 + k_z^2)\epsilon_2(q, k_z, \omega)}. \tag{4.12}$$

The validity of the method used, employing the fields V and $\vec{D}$ and the boundary conditions deduced from the macroscopic Maxwell equations even for large q-values is justified by the high similarity of the results obtained in the calculation of the z-component of the screened fields inside a metal from a macroscopic (hydrodynamical (HD)) [82] and a full microscopic approach performed by Feibelman [83] (see Ref. [3] for discussion). The similarity between the two approaches should be pointed out especially in the range of frequencies dealt with in this section, $\omega > \omega_p$. Feibelman's calculation was performed for small q-values, but the increase of the momentum parallel to the surface does not modify the spatial resolution of the field in the z-direction.

For a single step surface ($t = 0$, $\epsilon_1 = \epsilon_2 = \epsilon$), α_q reduces to:

$$\alpha_q(\omega) = \frac{\pi - \epsilon_0 q \beta}{\pi + \epsilon_0 q \beta}, \tag{4.13}$$

where $\beta = \beta_1 = \beta_2 = \beta_3$. The substitution of Eq. 4.13 into Eq. 4.3 reproduces the expression given by Ritchie and Marusak [84] in the derivation of the dispersion relation for surface plasmons using non-local dielectric functions.

For a local dielectric medium $\beta = \pi/q\epsilon$, and the well-known expression [81] is obtained

$$\alpha(\omega) = \frac{\epsilon - \epsilon_0}{\epsilon + \epsilon_0}. \tag{4.14}$$

The full solution of the electro-magnetic field (with transverse and longitudinal components) at the metal-vacuum and metal-metal interfaces needs three and four boundary conditions, respectively. The two boundary conditions deduced from the Maxwell equations have been applied in the previous expressions but the SCIB model implies two more.

In order to establish a connection between this calculation and the HD model [85], some thought is given to the two additional boundary conditions (ABC) implicit in the SCIB model. Consider the vacuum-metal interface without an overlayer (the surface is assumed to be at $z = 0$). The continuity of the z-component of the polarization vector

$$P_z = \frac{1}{4\pi}(D_z - E_z) \tag{4.15}$$

implies that the dielectric function must satisfy

$$\int_{-\infty}^{\infty} \frac{k_z e^{ik_z 0^-} dk_z}{(q^2 + k_z^2)\epsilon(q, k_z, \omega)} = -\frac{i\pi}{\epsilon(\infty)}. \tag{4.16}$$

Johnson and Rimbey [86] have shown that this condition is fulfilled by very general dielectric functions. They must be even functions in k_z and finite for $k_z \to \infty$; these conditions are satisfied by the dielectric functions used in the calculations presented here.

When a layer of thickness t is considered, the continuity of P_z at $z = t$ (metal-vacuum interface) gives the relation:

$$\int_{-\infty}^{\infty} \frac{k_z e^{ik_z t} dk_z}{(q^2 + k_z^2)\epsilon(q, k_z, \omega)} = \frac{i\pi e^{-qt}}{\epsilon(\infty)}, \tag{4.17}$$

which ensures the continuity of P_z at the metal-metal boundary at $z = 0$. Actually, the continuity of P_z (or the induced current $\partial P_z/\partial t = j_z$) is satisfied because no charge can pass through the boundary, as a consequence of a model that involves an infinite barrier potential at the interfaces. Finally as Forstmann and Stenschke have shown [85], if $j_z = 0$ at the boundary, the continuity of the energy flow is guaranteed, which is the fourth boundary condition in the SCIB model.

Dielectric functions of different complexity are now used in Eq. 4.9. The imaginary part of $\alpha_q(\omega)$ is shown for Al in Figs. 4.1 to 4.4 (directly related to the absorption spectrum of the material) versus momentum q for four different frequencies. The α_q coefficient was obtained from Eq. 4.9 using the dielectric function

$$\epsilon(k,\omega) = 1 - \frac{\omega_p^2}{\omega(\omega + i\gamma) - \beta_F^2 k^2 - k^4/4}, \tag{4.18}$$

which reproduces for $\gamma = 0$ the RPA bulk-plasmon dispersion relation of Lundqvist [87]

$$\omega^2 = \omega_p^2 + \beta_F^2 k^2 + k^4/4, \tag{4.19}$$

where $\beta_F = \sqrt{3/5} v_F$, (v_F is the Fermi velocity) and $\omega_p^2 = 4\pi n_0$. Numerical results have been obtained using $r_s = 2.07$ a.u. ($r_s = (3/4\pi n_0)^{1/3}$) for the bulk, $r_s = 2.61$ a.u. for the overlayer and $t = 2.9$ a.u. The constant damping parameter γ used is $\gamma = \omega_p/50$ or $\gamma_1 = 0.0116$ a.u. for the bulk and $\gamma_2 = 0.008$ a.u. for the overlayer. The $\alpha_q(\omega)$ values are quite insensitive to γ variations, $\alpha_q(\omega)$ varies by less than 1% for variations of γ from 0.001 to 0.02 a.u. The solid line corresponds to the full expression in Eq. 4.18, the dashed-dotted line is obtained by removing the electron-hole pair term $k^4/4$ and the dashed line is obtained by also removing the dispersion term $\beta_F^2 k^2$ (or equivalently, using the Drude dielectric function). α_q becomes a constant for large values of q in the Drude model [80, 88], an unphysical result that requires the use of a q cut-off value in any calculation that involves all the q-components of the response function. This problem is avoided if a q-dependent dielectric function is used. It is also apparent from Figs. 4.1 to 4.4 that the structure of α_q is washed out in the Drude model. The structure of the α_q curves consists of two peaks. The peak shown at higher momentum is produced by the overlayer, as can be seen from Fig. 4.5 where a comparison between the double and single step cases is shown. The peak at lower momentum corresponds to the surface plasmon excitation that shows up at $\omega = 0.98\omega_p/\sqrt{2}$ and disperses to larger momenta as the energy increases. The electron-hole type contribution is more important for large energies and in general, it reduces the excitation momentum.

In Figs. 4.6 to 4.9 the imaginary part of $\alpha_q(\omega)$ as a function of energy for four different q-values is shown. The prescription for each type of line is the same as that adopted in Fig. 4.1. The main peak (at $\omega = 0.46$ a.u. for $q = 0.1$ a.u., solid line) is due to the surface plasmon excitation, and is the result of the overlapping of two peaks, one for each 1. When

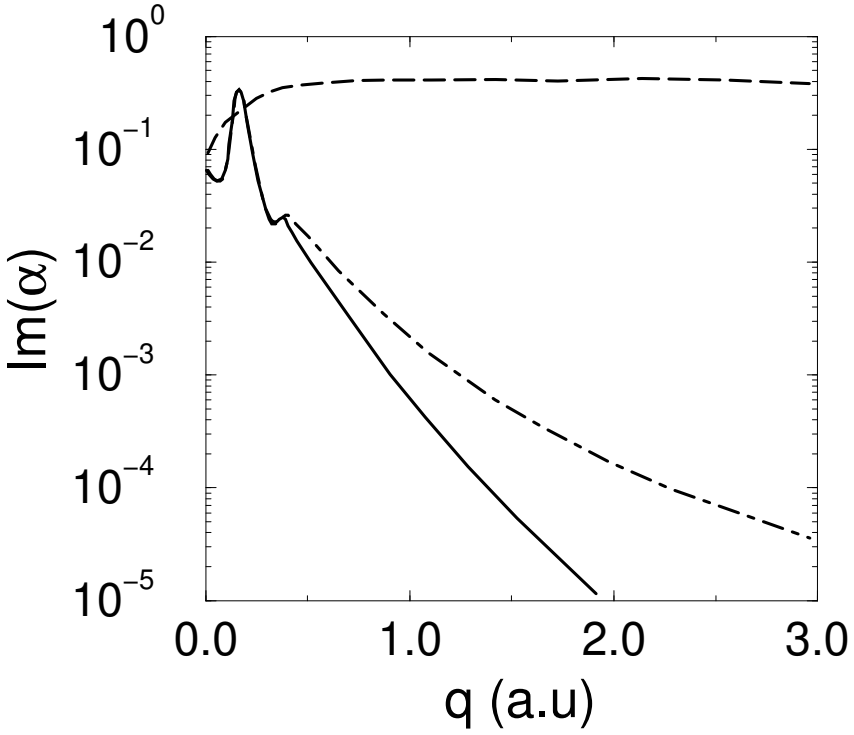

Figure 4.1: q-dependence of the imaginary part of the α_q coefficient for Al for $\omega = 0.5(\omega_p/\sqrt{2})$. Numerical values are obtained by substitution of Eq. 4.18 into Eq. 4.9 (full line), removing the $k^4/4$ term (dashed-dotted line) and also removing the β_F-dependent term (dashed line). $r_s = 2.07$ a.u. for the bulk, $r_s = 2.61$ a.u. and $t = 2.9$ a.u. for the overlayer and $\gamma = \omega_p/50$ for the damping parameter.

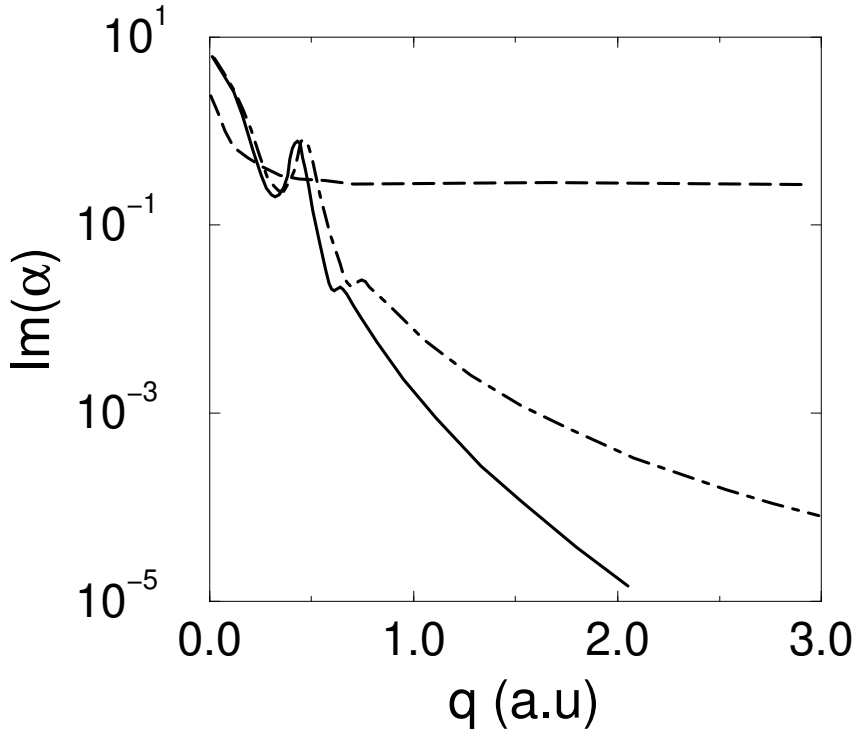

Figure 4.2: same as Fig. 4.1 with $\omega = 0.98(\omega_p/\sqrt{2})$.

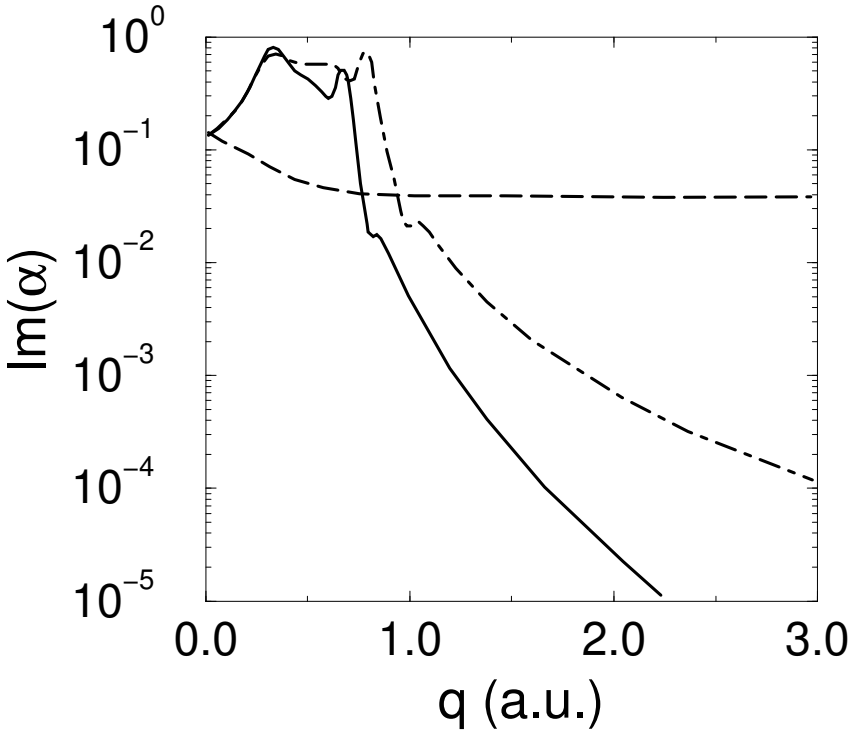

Figure 4.3: same as Fig. 4.1 with $\omega = 0.98\omega_p$.

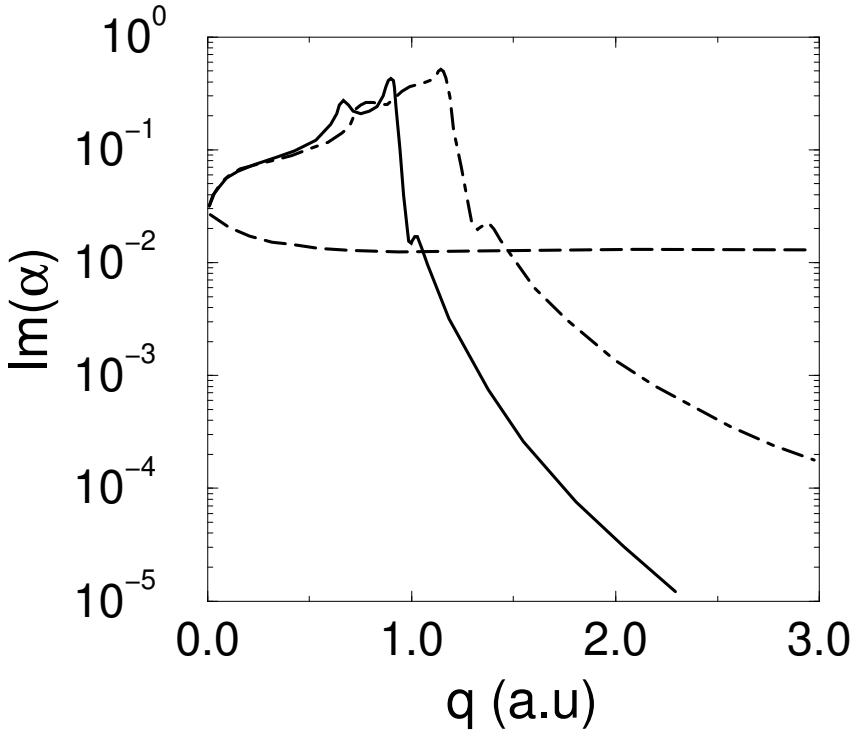

Figure 4.4: same as Fig. 4.1 with $\omega = 1.3\omega_p$.

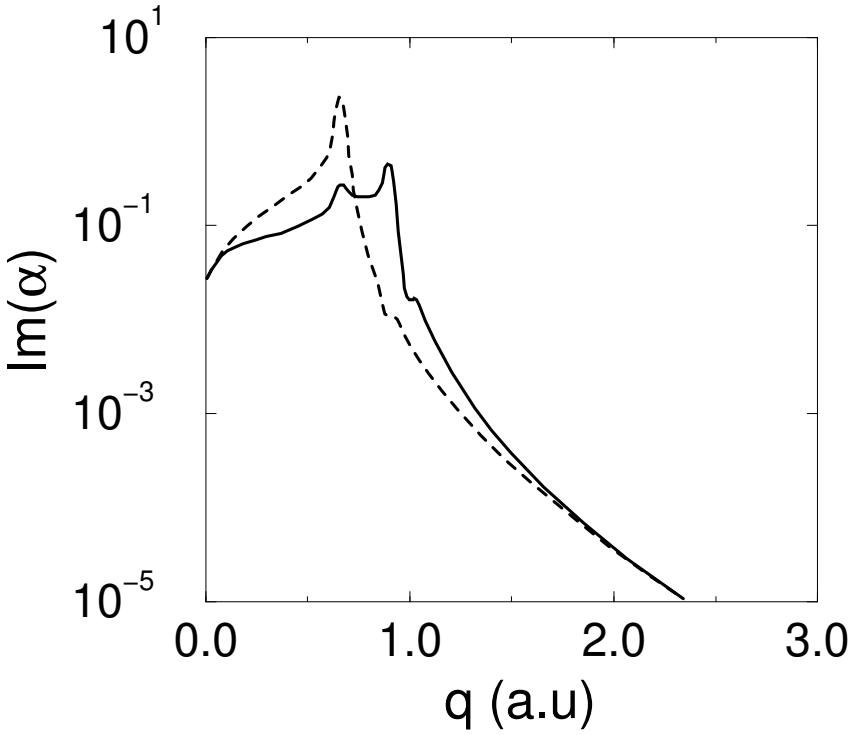

Figure 4.5: q-dependence of $Im(\alpha_q(\omega))$ obtained with the same parameters as in Fig. 4.4 (full line) and with a different step width $t = 0$ a.u. (dashed line).

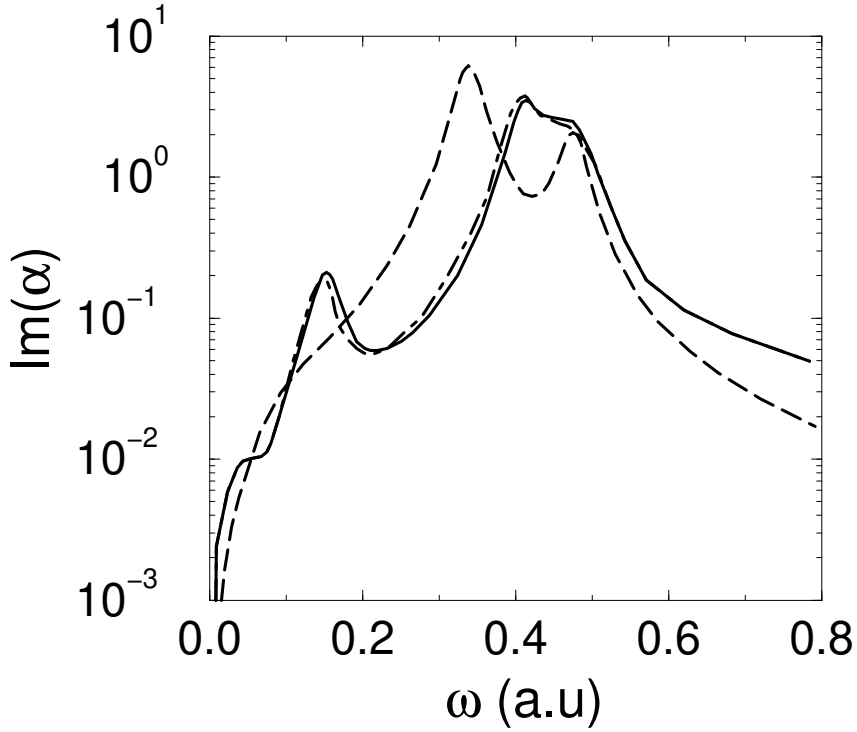

Figure 4.6: Same as Fig. 4.1 for the imaginary part of the α_q coefficient as a function of ω for $q = 0.1$ a.u. The prescription for each type of line is the same as that adopted in Fig. 4.1.

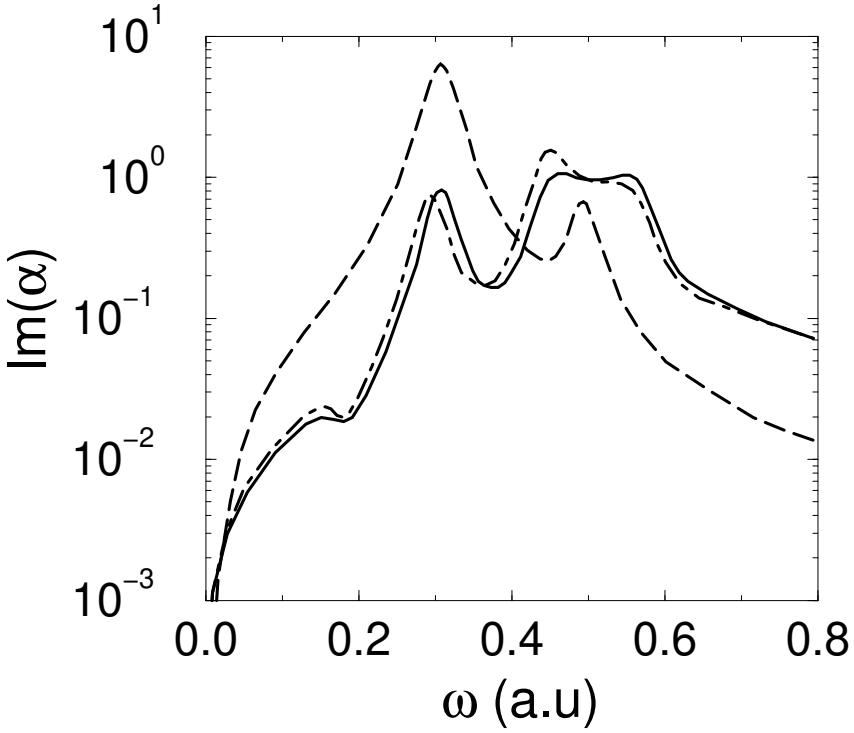

Figure 4.7: Same as Fig. 4.6 for $q = 0.3$ a.u.

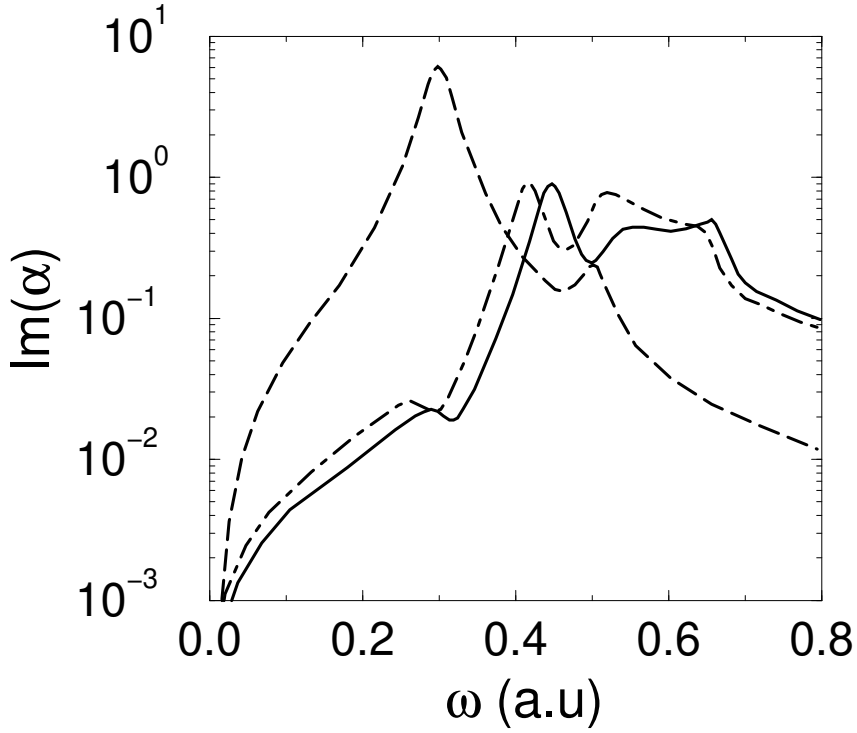

Figure 4.8: Same as Fig. 4.6 for $q = 0.5$ a.u.

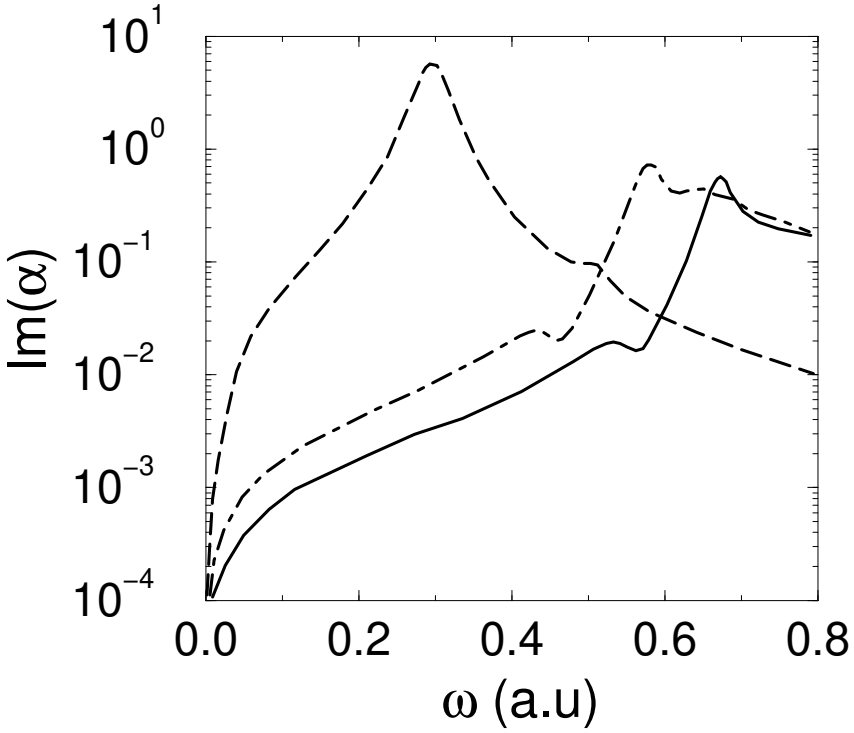

Figure 4.9: Same as Fig. 4.6 for $q = 0.8$ a.u.

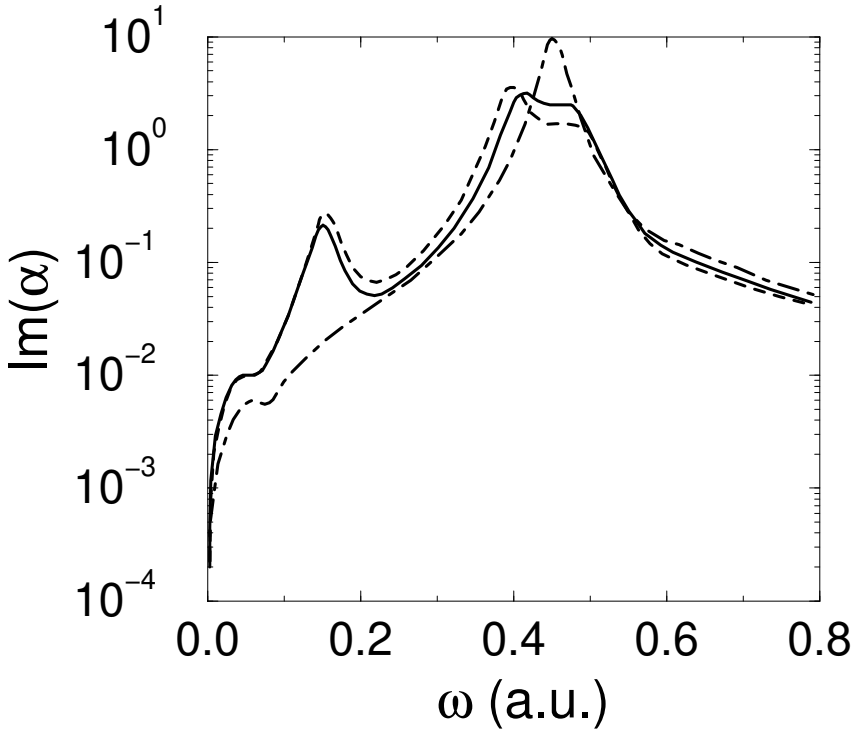

Figure 4.10: Same parameters as Fig. 4.6 (full line) and two other different step widths: $t = 0$ a.u. (dot-dashed line) and $t = 4$ a.u. (dashed line).

the width of the step is increased, the peak splits up into the two components (see fig. 4.10 for $t = 4.0$ a.u.). A similar effect is obtained by increasing the q-momentum. This is so because the shape of the peak is determined by the ratio between the wavelength of the probe and the size of the step. The same splitting into two surface modes was obtained by Rojas et al. [80] for the absorption cross section of a tin-coated Al_2O_3 sphere.

The shift of the dashed-dotted line relative to the solid line indicates that the inclusion of electron-hole type excitations increases the energy of the surface modes. This effect is more important for larger momenta. The peak at low energy ($\omega = 0.14$ a.u. for $q = 0.1$ a.u., solid line) is produced by the double step, since it disappears for $t = 0$ (see Fig. 4.10). Its amplitude becomes comparable to that of surface plasmons for large q-values.

This is due to the fact that as the wavelength of the probe decreases, the structure of the interface becomes more important. For large wavelengths, the Drude model is insensitive to the electronic profile and the low energy peak disappears. In Figs. 4.11 and 4.12 similar results are obtained using the LM dielectric function. The main differences are, on the one hand, the bump that appears in Fig. 4.11 for large momenta, indicating a much richer absorption spectrum. On the other hand, the absorption structure disappears for values of q above a critical value, as is the case of $q = 0.8$ a.u. shown in Fig. 4.12. This is due to the fact that for these momenta the mode is well inside the electron-hole band in the $\omega - q$ plane, an effect which was not included in the previous model.

The numerical calculation of Eq. 4.9 with the Linhard- Mermin dielectric function entails some difficulties. To avoid them, the β_i integrals (Eqs. 4.11 and 4.12) were separated into the real and imaginary parts, so that only real numerical calculations were performed. Convergence and accuracy of the results were improved by dividing the integrals into several parts, so that numerical integration errors could be carefully monitored.

4.3 The surface plasmon dispersion relation: a sum-rule approach

Sum rules provide a useful and instructive method to obtain an average response of the system to a given external perturbing operator. If the external operator has the appropriate symmetry, it may couple to the eigenexcitations, and the response saturates by a single mode. Within this condition, a good approximation of the dispersion relation of collective modes can be obtained.

SR are energy moments of the strength function defined as

$$S(E) = \sum_l \delta(E - E_l) |\langle l|Q|\phi\rangle|^2, \tag{4.20}$$

where the sum extends over all excited states of the system. Q is the perturbing external operator, E_l, $|l\rangle$ and $|\phi\rangle$ are the excitation energies, excited states and the ground state (GS) of the system, respectively. If, by definition, the p-sum rule reads

$$m_p = \int E^p S(E) dE = \sum_l E_l^p |\langle l|Q|\phi\rangle|^2, \tag{4.21}$$

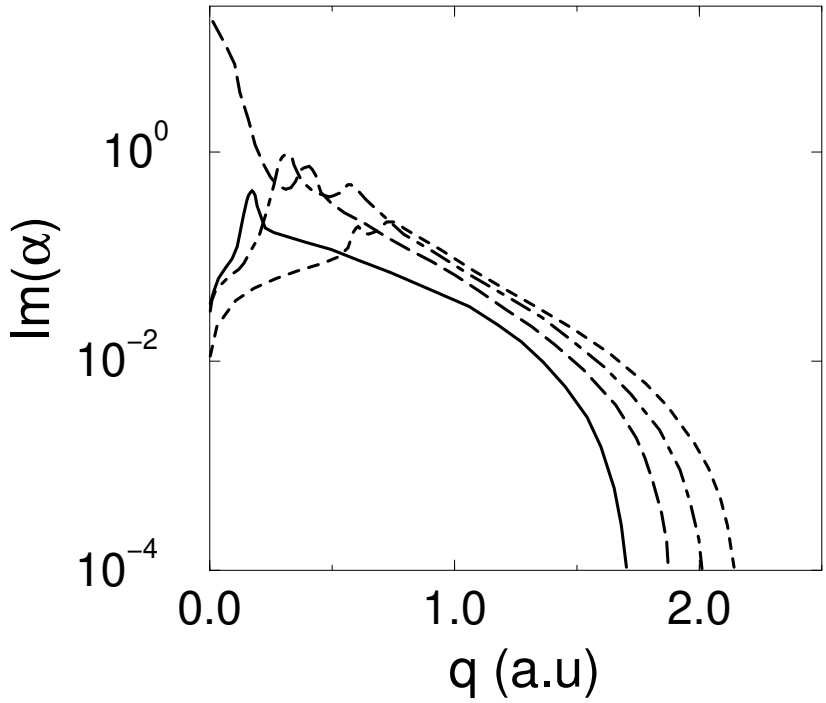

Figure 4.11: q dependence of the imaginary part of the α_q coefficient for Al for four different frequencies: $0.5(\omega_p/\sqrt{2})$ (solid line), $0.98(\omega_p/\sqrt{2})$ (dashed line), $0.98\omega_p$ (dot-dashed line) and $1.3\omega_p$ (short-dashed line). Numerical values are obtained using the Lindhard-Mermin dielectric function in Eq. 4.9.

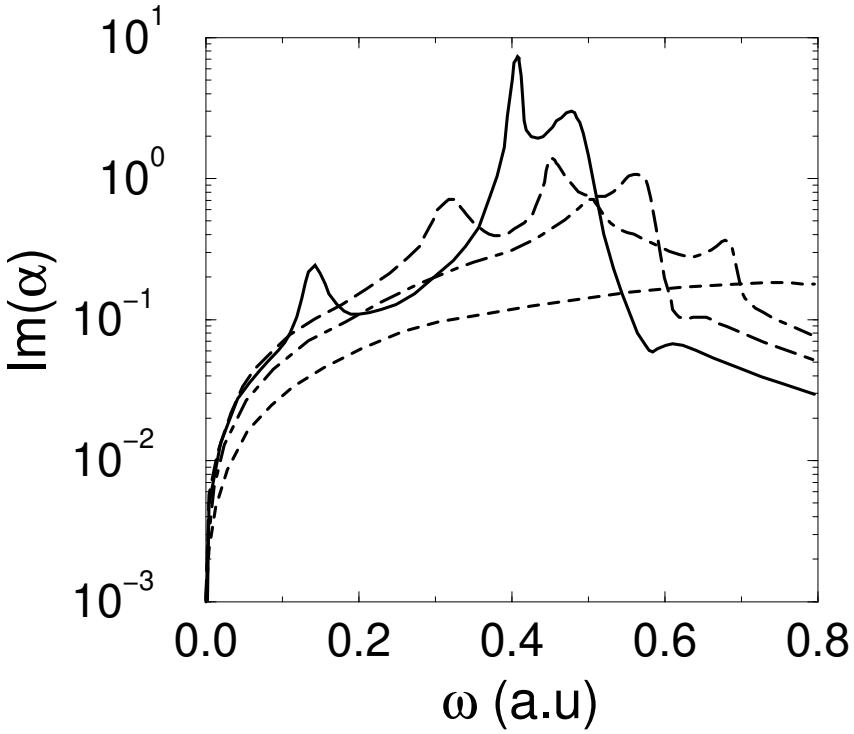

Figure 4.12: ω dependence of the imaginary part of the α_q coefficient for four different q-values, obtained as in Fig. 4.11. The values of q are 0.1 a.u. (solid line), 0.3 a.u. (dashed line), 0.5 a.u. (dot-dashed line) and 0.8 a.u. (short-dashed line).

one can define an average value of the energy of the excited system (perturbed by $Q(q)$) from any moment pair m_p and m_{p-2} by the relation

$$E = \left(\frac{m_p}{m_{p-2}} \right)^{1/2}, \tag{4.22}$$

or equivalently $\omega(q)$.

It has been demonstrated [30, 89] that m_1 and m_3 can be obtained from the expressions

$$m_1 = \frac{1}{2} \langle \phi | \left[Q^\dagger, [H, Q] \right] | \phi \rangle \tag{4.23}$$

and

$$m_3 = \frac{1}{2} \langle \phi | \left[\left[Q^\dagger, H \right], [H, [H, Q]] \right] | \phi \rangle, \tag{4.24}$$

where only two ingredients are necessary; the Hamiltonian H of the system and its ground state. m_1 and m_3 can be obtained with RPA precision from Lang-Kohn calculations involving GS expectation values. However, instead of this an analytical approximation for the self-consistent GS electron density is used

$$n(z) = \frac{n_0}{e^{z/\delta} + 1}, \tag{4.25}$$

and an improved Thomas-Fermi-von Weizsäcker functional for the kinetic energy density,

$$\tau = \frac{3}{10} (3\pi^2)^{2/3} n^{5/3} + \frac{1}{8} \beta \frac{n'^2}{n}, \tag{4.26}$$

where β is the Weizsäcker coefficient, and n' denotes the z-derivative. δ in Eq. 4.25 is adjusted to each metal (further discussion of this point is made below).

Following the same approach used previously in the case of metallic clusters [34], the jellium model is used to describe the neutralizing positive background. The metal occupies the negative part of the z-axis and $z = 0$ is the position of the positive jellium edge. The Hamiltonian consists of a kinetic term (T) and a direct Coulomb term (C) which includes electron-electron and electron-jellium interactions. The jellium-jellium interaction is a constant term and has no contribution to the expectation values.

It can be shown [34] that for external operators Q which satisfy the Laplace equation, $\Delta Q = 0$, there is a vanishing contribution to m_3 from those terms in the Hamiltonian that depend only on the electronic density n. This is the case for the Q operator used in our calculation (see Eq. 4.27), as is the case for operators which generate only surface

excitations. For this reason, within a local model for exchange and correlation interactions, there is no contribution to m_3 from these effects [34, 77]. Nonetheless, Liebsch [62] has proved in a self-consistent calculation, which includes exchange and correlation, that their effects are important and lower the momentum dispersion relation of surface plasmons.

The appropriate operator for the semi-infinite medium presented here is

$$Q = \sum_j e^{i\vec{q}\vec{\rho}_j} e^{qz_j}. \tag{4.27}$$

Inserting this operator in Eqs. 4.23 and 4.24, the following expressions are obtained

$$m_1 = Aq^2 \int_{-\infty}^{\infty} dz e^{2qz} n(z), \tag{4.28}$$

where A is the normalization area on the XY plane,

$$\begin{aligned} m_3(C) = \quad & 2\pi A q^2 \int_{-\infty}^{\infty} dz n n_j e^{2qz} \\ & + 2\pi A q^3 \int_{-\infty}^{\infty} dz n e^{2qz} \\ & \times \left(\int_z^{\infty} dz' \tilde{n} - \int_{-\infty}^{z} dz' \tilde{n} \right), \end{aligned} \tag{4.29}$$

$\tilde{n} = n - n_j$ and $n_j = n_0 \Theta(-z)$ is the jellium particle density ($\Theta(z)$ is the step function), and

$$\begin{aligned} m_3(T) = \quad & \frac{4}{5}(3\pi^2)^{2/3} A q^4 \int_{-\infty}^{\infty} dz n^{5/3} e^{2qz} \\ & + \frac{1}{3}\beta A q^4 \int_{-\infty}^{\infty} dz \frac{n'^2}{n} e^{2qz}, \end{aligned} \tag{4.30}$$

where $\beta = 1/2$ [34] and where n' denotes the z-derivative.

Even through a simple analytical expression for the electronic GS, $n(z)$, is used, the dispersion relation $\omega(q) = (m_3/m_1)^{1/2}$ must be obtained numerically. However, there are two quiet instructive limits that yield compact analytical expressions.

Firstly, to obtain the dispersion relation for small momentum transfer, only the Coulomb contribution to m_3 is considered (the kinetic part has higher order q-contributions). Substituting Eq. 4.25 into Eqs. 4.28 and 4.29, the following relationships are obtained

$$m_1 = \pi A n_0 q^2 \delta \csc(2\pi q \delta) \tag{4.31}$$

and

$$m_3 = 2\pi A n_0^2 q^2 \left[\pi \delta \csc(2\pi q \delta) - \delta \ln(2)\right] \tag{4.32}$$

which produces a linear dispersion relation for small values of q given by

$$\omega(q) = \frac{\omega_p}{\sqrt{2}} \left[1 - q\delta \ln(2)\right], \tag{4.33}$$

similar to the one obtained by Feibelman [17] from an RPA calculation of the response function. In Feibelman's expression the linear coefficient is given by the centroid of the induced charge relative to the positive jellium edge, calculated at $\omega = \omega_p/\sqrt{2}$. In the calculation presented here the linear coefficient characterizes the GS electronic density. This relation will be used later (in the case of Na and K) to fix the δ parameter to the experimental dispersion slope near $q = 0$.

Another useful limit is obtained by using a step particle density:

$$n(z) = n_0 \Theta(-z). \tag{4.34}$$

In this case, the dispersion relation adopts the form:

$$\omega^2(q) = \frac{1}{2}\omega_p^2 + \frac{4}{5}k_F^2 q^2 \tag{4.35}$$

or, for small q-values:

$$\omega(q) = \frac{\omega_p}{\sqrt{2}} + \frac{4}{5\sqrt{2}}\frac{k_F^2}{\omega_p}q^2 - \frac{8}{25\sqrt{2}}\frac{k_F^4}{\omega_p^3}q^4 + \cdots, \tag{4.36}$$

where a negative q-coefficient is missing because no electronic diffuseness is considered. A positive linear q-coefficient due to the kinetic contribution was also found to be missing. However, in the case when a one-step hydrodynamical calculation is performed, a positive linear q-coefficient appears. In this latter case the surface dispersion relation

$$\omega = \omega_p/\sqrt{2} + \frac{1}{2}\sqrt{3/5}k_F q \tag{4.37}$$

is obtained [90]. The linear q-coefficient comes from the so-called pressure term, that is, resistance against compression which, in the hydrodynamical approximation, produces a force proportional to $\vec{\nabla} n$. In the SR approach this same effect is part of the kinetic contribution (the first-term on the right-hand side of Eq. 4.26, from Pauli repulsion) and instead produces the q^2 and q^4 terms in Eq. 4.36. The total kinetic contribution (the last term on the right-hand side of Eq. 4.35) does not yield, within this one-step approximation, a free electron-like term of the type $q^4/4$ similar to that in the bulk dispersion relation (see Eq. 4.19).

The analytical electronic density function used in the SR calculation was taken from Ref. [91]. In this reference (see Fig. 1 therein) an excellent agreement between the profile obtained by Eq. 4.25 and a Lang-Kohn calculation is shown for Al. The best fit is obtained for $\delta = 0.6585$ a.u. The width t of the double-step used in the dielectric function calculations has been adjusted in such a way that the surface layer extends from z_1 where $n(z_1) = 0.9n_0$ to z_2 where $n(z_2) = 0.1n_0$. The electronic density within the layer is $0.5n_0$.

In Fig. 4.13 the SR results for the aluminium dispersion relation are shown using Eqs. 4.22 and 4.28 - 4.30 for the smooth profile given by Eq. 4.25 (full line 1) and for the single step function of Eq. 4.34 (full line 2). For comparison, the results obtained using in Eq. 4.9 and Eq. 4.3 the RPA dielectric function of Eq. 4.18 (short dashed line) and the LM dielectric function (long dashed line) are shown. As indicated, the δ parameter used in Eq. 4.25 is $\delta = 0.6585$ a.u. and the overlayer is characterized by $r_s = 2.61$ a.u. and $t = 2.9$ a.u. The damping parameter is $\gamma = \omega_p/50$.

From Fig. 4.13 the crucial role played by the electronic profile is seen as it produces not only a different slope for small values of q (the density diffuseness is at the origin of the negative slope), but also a completely different behavior for large values of q.

The main difference between the RPA (dielectric approximation) and the SR calculation for large values of q comes from the excitation average inherent to the last procedure: for increasing values of q, the plasmon energy is mixed up with electron-hole excitations of increasing energy and the different weight of the E_l term in m_3 and m_1 (see Eq. 4.21) produces a decrease of the energy E in Eq. 4.22 [38].

4.4 Results and discussion

SR calculations for some nearly free electron-like metals have been carried out for which experimental data are available, such as Al ($r_s = 2.07$ a.u.) [69], Na ($r_s = 3.93$ a.u.) and K ($r_s = 4.86$ a.u.) [18].

In Fig. 4.14 the ω_1 (now called SR) and LM curves of Fig. 4.13 are compared with experimental values. For this high density material, the best agreement with experimental data is obtained from the LM approximation. The RPA dielectric calculation has a much steeper slope and a larger value of t (approximately equal to 7 a.u.) must be used if one wants to reproduce experimental data.

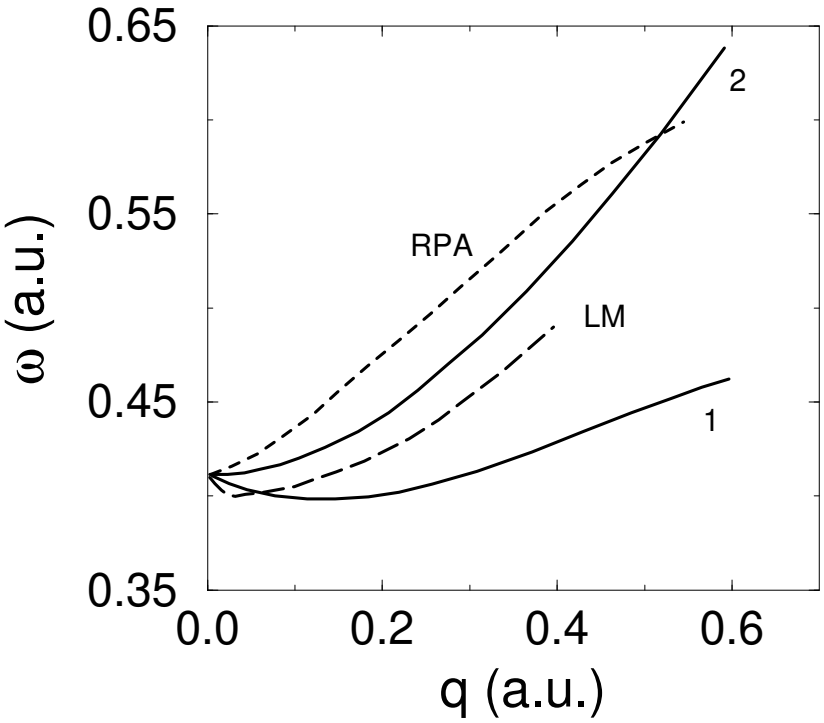

Figure 4.13: SR surface plasmon dispersion relation for Al calculated by substitution of Eq. 4.25 (full line 1) and Eq. 4.34 (full line 2) into Eqs. 4.28 - 4.30 and 4.22. The results obtained from Eqs. 4.9 and 4.3 for the RPA (Eq. 4.18) and the Linhard-Mermin dielectric function are also shown. $\delta = 0.6585$ a.u. in Eq. 4.25. A double step of thickness $t = 2.9$ a.u. is used in the last two cases, and the same electronic densities as in Fig. 4.1 for the bulk and the overlayer are used.

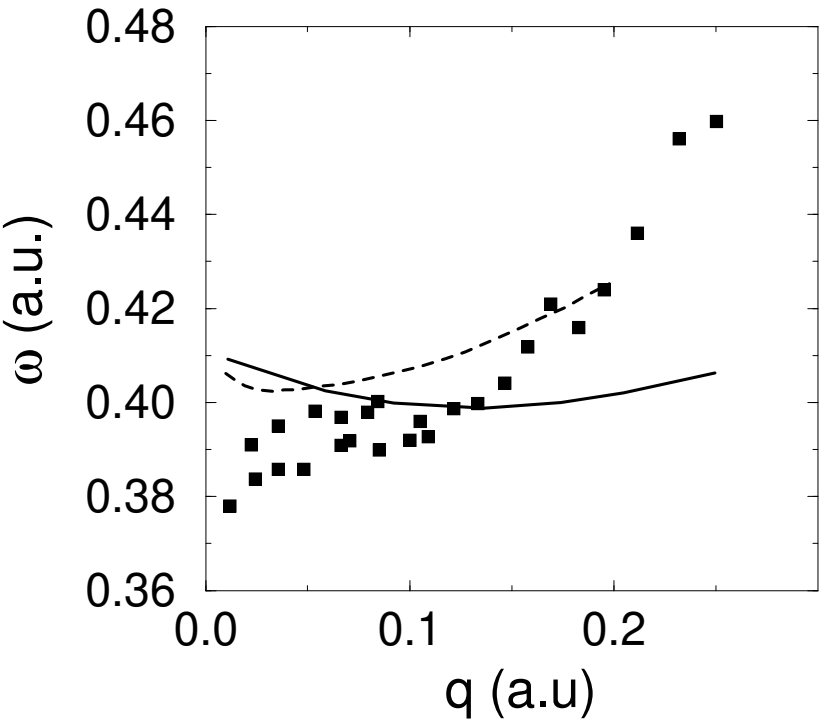

Figure 4.14: Comparison between the curves 1 (solid line) and LM (dashed line) from Fig. 4.13 and experimental data (points) for Al from Ref. [69] is shown.

In Figs. 4.15 and 4.16, results for Na and K are shown. Two parameters have been adjusted to the experimental values. The δ parameter of Eq. 4.33 is now obtained from the linear term in the polynomial fitted to the experimental data given in Ref. [18]. The obtained values are $\delta = 1.06$ a.u. for Na and $\delta = 1.05$ a.u. for K. The second parameter is the surface plasmon energy at $q = 0$. This latter correction produces a constant shift of the curves towards lower energies. The surface plasmon energy $\omega_p/\sqrt{2}$, which is equal to 0.157 a.u. for Na (0.1143 a.u. for K) is then lowered down to the experimental value 0.147 a.u. (0.1007 a.u. for K). The latter correction is equivalent [34] to the use of an effective electronic mass (m^*) which introduces band effects and reduces the collective mode energies. Considering that the dispersion relation at $q = 0$ corrected by band effects takes the form

$$\omega^2 = \frac{\omega_p^2}{2m^*} \tag{4.38}$$

effective masses of $m^*(Na) = 1.14$ and $m^*(K) = 1.28$ are obtained

In the case of aluminium, no effective mass type correction was performed as the extrapolation to $q = 0$ of the experimental data was not as clear as in the Na or K cases. The reason is that the radiative nature of the surface modes is much more apparent in the aluminium case. The decrease of the frequency for long wavelength modes reflects retardation effects and the correct dispersion relation for small q-values is that of the light-line given by $\omega = cq$ (c is the speed of light).

To aid comparison, the LM dielectric results and the local density approximation (LDA) response calculation reported in Ref. [19] are given. This latter calculation was obtained by Liebsch [62] from a time-dependent local density approximation assuming a jellium model for the positive background and including self-consistently exchange and correlation effects. The bars in the figure indicate the uncertainty of these results.

In the LM calculation, the electronic step width is taken to be the surface width of the smooth density (Eq. 4.25), defined as $t = z_2 - z_1$ where $n(z_2) = 0.05n_0$ and $n(z_1) = 0.095n_0$. The criterion to define the surface width is different from that used for Al, because for Na and K the negative slope at the origin is much larger, thus a more significant part of the surface region participates in the response, a fact related to the lower electron gas density (the length scale is larger). Nonetheless, the disagreement with experimental data for large q-values is significant.

The SCIB model is an attempt to derive a phenomenological specular reflection model of

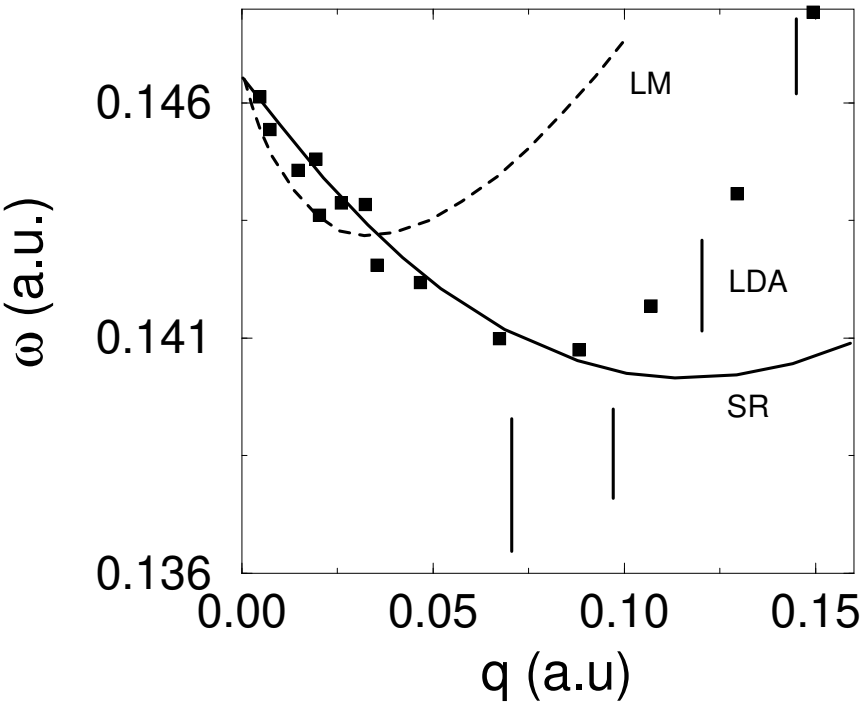

Figure 4.15: SR and LM surface plasmon dispersion relation for Na compared with experimental data (points) from Ref. [18]. The vertical lines denote the results of the LDA calculation from Ref. [19]. The parameters used in the SR calculation are: $\delta = 1.06$ a.u. and $\omega(q = 0) = 0.147$ a.u. The overlayer for the LM calculation is defined by: $r_s = 4.95$ a.u. and $t = 4.34$ a.u.

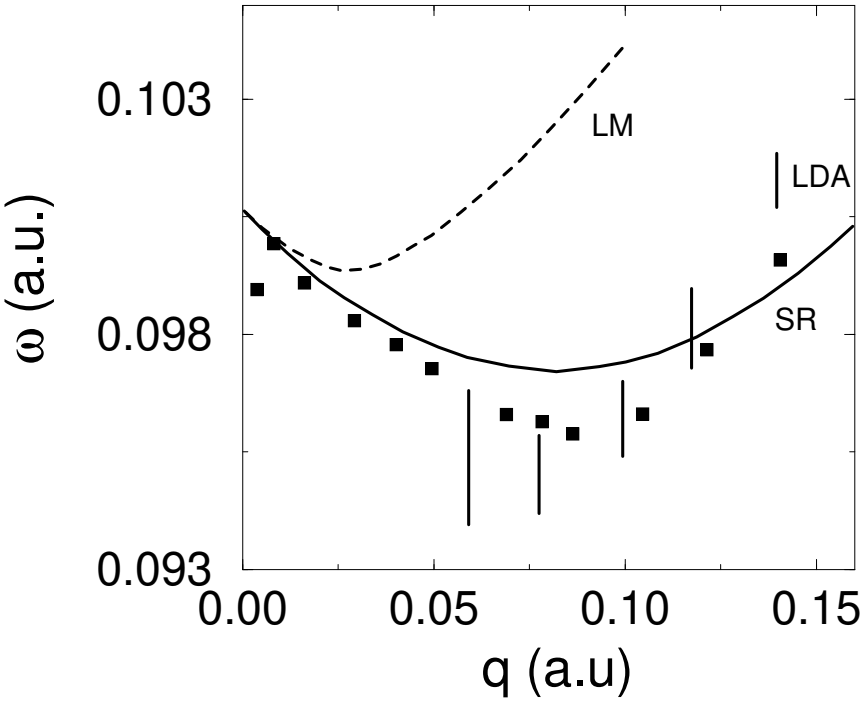

Figure 4.16: The same as in Fig. 4.15 for K. $\delta = 1.05$ a.u., $\omega(q = 0) = 0.1007$ a.u., $r_s = 6.12$ a.u. and $t = 4.29$ a.u.

the surface and although it incorporates quantum effects contained in the Linhard dielectric function and in the boundary conditions [3], it forces the use of a poor approximation to the smooth decrease of the electronic density at the surface. For increasing values of q, the part of the material that contributes to the response becomes increasingly concentrated at the surface, where the electronic density is lower than that of the bulk, thus lowering the surface plasmon energy. This tendency competes with the increasing importance of the kinetic contribution which tends to increase the plasmon energy. For high density metals such as Al, the kinetic contribution to the energy of the eigenmodes is the most important contribution and a poor model for the electronic profile does not produce such undesirable deviations in the dispersion relation as in the case of lower electron density metals such as Na or K.

The discrepancy between experimental data and the SR calculation is smaller than 6% for Al, 5% for Na and 2% for K (notice the different scales in the last two cases) up to $q = 0.2$, 0.15 and 0.15 a.u., respectively. The inclusion of exchange and correlation effects in the LDA calculation increases the negative linear coefficient.

4.5 Concluding remarks

An explicit expression for the q- and ω-dependent α_q coefficient for plane surfaces within a double step model has been obtained, which is valid for general non-local dielectric functions. This approximation has been compared to the SR calculation for metals. The LM approximation is well suited for use in low energy probe spectroscopies and high density metals. The critical role played by the step suggests that the use of a more realistic electronic profile is necessary within the dielectric formalism, especially for low density metals.

The SR calculation of the dispersion relation can handle realistic electronic profiles and allows one to include exchange and correlation effects in the calculation at two different levels: one is through the electronic GS profile and the other is through the Hamiltonian. The use of a more general external operator Q which does not satisfy the Laplace equation would provide non-zero exchange and correlation contributions even for local models of the interactions and would probably produce a much richer spectrum of collective excitations.

From the study of the analytical and numerical results it can be concluded that the dispersion relation is determined by the Coulombic interaction for low q-values and by the

kinetic contribution for large momenta where the electron-hole contribution to the response function increases its importance compared to that of the collective modes. A consequence of this is that for dense metals such as Al, for which the important part of the electronic energy is the kinetic contribution, the electronic profile at the surface plays a minor role and the dispersion relation is not very sensible to the density profile. On the other hand, for low metallic densities, the Coulombic interaction is the dominant part and the dispersion relation is strongly dependent on the GS electronic density

Chapter 5

Multipole surface-plasmon modes on simple metals

The average multipole surface-plasmon energy for simple-metals, as well as that of ordinary surface and bulk plasmons, is obtained using energy-weighted moments of the electronic response to sufficiently general external perturbations. A local approximation of exchange and correlation effects is used within a jellium model. Band-structure effects are incorporated through an effective electronic mass. Taking advantage of the transparency of the method, we analyze under what circumstances such modes might be observable. It is shown that due to an interplay between Coulomb and kinetic energies, the multipole modes become unobservable for increasing values of the transferred momentum (q) parallel to the surface. The value of q at which the multipole mode becomes unobservable is much smaller than the cutoff value for Landau damping. The effect of the electronic surface diffuseness is also analyzed. We compare our results with previous density-functional calculations and with recent experimental data for Na, K, and Cs.

5.1 Introduction

Despite the great amount of theoretical effort invested in the characterization and understanding of multipole plasmon modes on metal surfaces [2, 16, 49, 62, 64, 65, 66, 92], and the existence of some indirect experimental signs in surface photo-emission from Al (Ref. [4]) and photo-yield data form alkali metals [63], direct experimental evidence has not been

reported until recently in inelastic reflection electron scattering on smooth films of Na, K, and Cs [19, 26]. Up to now, no experimental observation has been reported of the existence of these modes from energy-loss spectroscopy on high-density metals such as aluminium and still some uncertainties concerning their nature and properties are unsolved.

Multipole plasmon modes are associated with electronic-density fluctuations that are peaked at the surface region and have decreasing oscillating amplitude towards the interior of the metal. The integral of the electronic density perpendicular to the surface is zero [26, 62]. Although these modes have a surface origin, they carry momentum both in the normal as well as in the parallel directions, making them optically active in contrast to ordinary surface plasmons, which have a monopole character. The frequency of the multipole mode lies, for a fixed value of the momentum q parallel to the surface, between the bulk and the monopole plasmon values. At $q = 0$, both experimental data and theoretical calculations [26] intersect at approximately $0.8\omega_p$. This value of ω is between the bulk and the surface values (ω_p and $\omega_p/\sqrt{2} = 0.71\omega_p$, respectively).

For small q values, the slope of the dispersion relation is positive as a consequence of the induced electronic charge distribution. the centroid of the induced electronic charge, defined as

$$d(\omega) = \frac{\int dz z \delta n(z,\omega)}{\int dz \delta n(z,\omega)}, \tag{5.1}$$

where the induced charge δn is, in general, a complex function [26], lies in the interior of the metal in contrast to the case of the centroid of ordinary surface modes, which lies outside and has a negative slope. As was discussed by Feibelman [2] and Tsuei et al. [19] in the long-wavelength limit, the energy of the mode depends on the average ground-state (g.s.) electronic density seen by the electrostatic potential created by the induced charge. The induced potential is peaked at the centroid position and as q increases becomes more localized in the region of the centroid, thus making the slope of the dispersion relation positive because of the increase of the average electronic density. There is no known analytical expression for the dispersion relation in the low-q limit.

The first theoretical predictions were developed within the hydrodynamical approximation [16, 49], which turned out to be able to obtain the new modes if a surface electronic structure, which mimicked the electronic-surface diffuseness, was assumed. Such modes disappear if a sharp metal-vacuum interface is assumed. Dobson and Harris [66] confirmed

the existence of additional surface-plasmon modes on a bare jellium surface within a microscopic calculation and emphasized the use of a correctly self-consistent zero-order surface electron-density profile. Feibelman [2] and later Liebsch [62] obtained the response of the surface characterized by the centroid of the charge induced by time-dependent arbitrary external fields. The imaginary part of this frequency-dependent centroid function develops a resonant structure at about $0.8\omega_p$, which is due to the multipole normal mode. Within a time-dependent density-functional approach (TDLDA), Tsuei et al. [26] obtained a good agreement with experimental data. In their calculation they emphasize the consistent treatment of the electron-electron interaction in the g.s. and in the dynamical response to an external perturbation.

The aim of the work presented in this Chapter is to investigate some properties of the collective multipole excitations that have not been handled in previous studies, taking advantage of the facilities of the sum-rule (SR) method used. The SR provides a useful approximation of the average excitation energies of fermion systems confined to different geometries. It has produced a wealth of information about the nature of collective modes in metallic systems [32, 34, 37, 39, 76, 77, 93]. Exchange and correlation can be easily incorporated within a local-density approximation and band effects can be included in a jellium model through an effective electronic mass. We pay special attention to the different contributions to the energy and address the question of under what circumstances such modes might be observable.

In the calculation we closely follow some previous works [34, 39] and will only remark on the new points included in the present case. This Chapter is organized as follows. In Sec. 5.2, the SR calculation is performed and compared with previous formulations carried out on different systems using the same technique. In Sec. 5.3, results are compared with experimental data and previous theoretical calculations, and in Sec. 5.4, we present some concluding remarks.

5.2 General equations

The SR approximation used in this work provides a method of obtaining the average excitation of a system in response to a given external operator, and it is especially useful when the system develops a dominantly collective response. SR's are energy moments of

the strength function (also called the response function) $S(E)$ defined as

$$S(E) = \sum_l \delta(E - E_l)|\langle l|Q|0\rangle|^2, \tag{5.2}$$

where the sum extends over all excited states. Q is the perturbing operator, E_l, $|l>$, and $|0>$ are the excitation energies, excited state, and the g.s. of the system, respectively. If by definition, the p-sum rule reads

$$m_p = \int E^p S(E) dE = \sum_l E_l^p |\langle l|Q|0\rangle|^2, \tag{5.3}$$

the average value of the excitation energy and the variance σ^2 are given by

$$\bar{E} = \frac{m_1}{m_0}, \tag{5.4}$$

$$\sigma^2 = \frac{m_2}{m_0} - \left(\frac{m_1}{m_0}\right)^2. \tag{5.5}$$

Among these moments, the ones with $p = -1$, 1, and 3 play an important role in the application of SR's to the study of collective resonance states of the system. They can be used to estimate $\bar{E}$ and σ^2. Defining $E_p = (m_p/m_{p-2})^{1/2}$, it has been shown [30] that

$$E_1 \leq \bar{E} \leq E_3, \tag{5.6}$$

$$\sigma^2 \leq (E_3^2 - E_1^2)/4. \tag{5.7}$$

If the external operator Q has the appropriate symmetry and couples to the normal modes of the system, then the response saturates by a single mode and most of the strength is in a narrow energy region. Under such conditions, as is the case for some resonant collective states, E_1 and E_3 are close together and both are good estimates of $\bar{E}$. We will concentrate on E_3 (the upper bound to the energy) from which good results have been obtained in previous works [34, 39, 77]. The dispersion relation will be obtained from

$$E_3 = \left(\frac{m_3}{m_1}\right)^{1/2} \tag{5.8}$$

Manipulation of Eq. 5.3 for $p = 1$ and 3 leads [30, 89] to simplified expressions that depend only on the Hamiltonian of the system, its g.s., and the external operator. These are given by

$$m_1 = \frac{1}{2}\langle 0|[Q^\dagger, [H, Q]]|0\rangle, \tag{5.9}$$

and

$$m_3 = \frac{1}{2}\langle 0|[[Q^\dagger, H], [H, [H, Q]]]|0\rangle, \tag{5.10}$$

where $Q^\dagger$ denotes the Hermitian conjugate operator. The linear-energy moment m_1 is easily calculated from Eq. 5.9 when Q depends only on position. The cubic moment is easier to obtain by scaling the g.s. $|0\rangle$. Defining the scaled function as

$$|\eta\rangle = e^{\eta[H,Q]}|0\rangle, \tag{5.11}$$

we get

$$m_3 = \frac{1}{2}\frac{\partial^2}{\partial\eta^2}\langle\eta|H|\eta\rangle|_{\eta=0}. \tag{5.12}$$

We define the scaled particle and kinetic-energy densities (we use atomic units throughout)

$$n_\eta = \langle\eta|\hat{n}|\eta\rangle = n + \eta n_1 + \eta^2 n_2 + \cdots, \tag{5.13}$$

$$\sigma_\eta = \langle\eta|\hat{\sigma}|\eta\rangle = \sigma + \eta\sigma_1 + \eta^2\sigma_2 + \cdots, \tag{5.14}$$

where

$$\hat{n} = \sum_i \delta(\vec{r} - \vec{r}_i), \tag{5.15}$$

$$\hat{\sigma} = \sum_i \overleftarrow{\nabla}_i\, \delta(\vec{r} - \vec{r}_i)\vec{\nabla}_i, \tag{5.16}$$

and

$$n = \langle 0|\hat{n}|0\rangle, \tag{5.17}$$

$$n_1 = \langle 0|[\hat{n}, [H, Q]]|0\rangle, \tag{5.18}$$

$$n_2 = \langle 0|[[\hat{n}, [H, Q]], [H, Q]]|0\rangle, \tag{5.19}$$

with similar expressions for σ, σ_1, and σ_2. Notice that our particle and kinetic-energy densities are defined as

$$n = \sum_i |\phi_i|^2, \tag{5.20}$$

$$\sigma = \sum_i |\vec{\nabla}\phi|^2. \tag{5.21}$$

Expanding the expectation value of the Hamiltonian in powers of η, Eq. 5.12 provides a straightforward but cumbersome evaluation of m_3.

For $\vec{r}$-dependent operators Q it has been shown [45] that σ_1 does not contribute to m_3 and that

$$n_1 = -\nabla_i(nu_i), \tag{5.22}$$

$$n_2 = -\frac{1}{2}\nabla_i(n_1 u_i), \tag{5.23}$$

$$\begin{aligned}\sigma_2 = \quad & \frac{1}{3}\sigma\{-u_k(\nabla_k\nabla_i u_i) + (\nabla_j u_i)[\nabla_i u_j + \nabla_j u_i]\} \\ & + \frac{1}{4}(\nabla_i\nabla_j u_j)[\nabla_i\nabla_k(nu_k)] \\ & + \frac{1}{4}(\nabla_i n)(\nabla_j\nabla_k u_k)[\nabla_i u_j + \nabla_j u_i],\end{aligned} \tag{5.24}$$

where ∇_i means the Cartesian i-coordinate derivative, a sum over repeated indices is understood and

$$\vec{u} = \vec{\nabla}Q. \tag{5.25}$$

We refer the interested reader to Ref. [34] and references therein for further details.

The most accurate application of the method consists in the use of the self-consistent g.s. calculated from the same Hamiltonian H as that used in the determination of m_1 and m_3 in Eqs. 5.9 and 5.12. Instead, we use different analytical approximations of the g.s. We will show in the next section that the sensitivity of the results on the choice of the g.s. is extremely low.

The jellium model is used to describe the neutralizing positive background. The metal occupies the negative part of the z-axis and $z = 0$ is the position of the positive jellium edge. The Hamiltonian consists of a kinetic term (T), a direct Coulomb term (C), which includes electron-electron and electron-jellium interactions, as well as both an exchange (ex) and correlation (cor) term.

For the exchange and correlation energy densities, Slater- and Wigner-type local expressions are used,

$$e(ex) = -\frac{3}{4}\left(\frac{3}{\pi}\right)^{1/3} n^{4/3} \tag{5.26}$$

$$e(cor) = -\frac{a(4\pi n/3)^{1/3} n}{b(4\pi n/3)^{1/3} + 1}, \tag{5.27}$$

respectively, where n is the electron-density operator, $a = 0.44$, and $b = 7.8$. The use of other state-of-the-art representations of the local correlation energy, such as those of Refs. [94] and [95], does not change the numerical results by more than a few percent

[93]. We stress that a different treatment has been followed with the kinetic term. The kinetic contribution to m_1 and m_3 has been evaluated using the one-body kinetic-energy operator of Eq. 5.16 in Eq. 5.12, which finally yields an expression that depends on the g.s. electronic and kinetic-energy densities (see Eq. 5.24). For this last density, the improved Thomas-Fermi-von Weizsäcker functional given by

$$\tau = \frac{3}{10}(3\pi^2)^{2/3} n^{5/3} + \frac{\beta}{8}\frac{n'^2}{n} \tag{5.28}$$

is used, where β is the von Weizsäcker coefficient (taken equal to 1/2) and n' denotes the z derivative. As a consequence, the kinetic contribution contains non-locality in contrast to the exchange and correlation terms that are purely local.

Once the Hamiltonian is fixed, the key part of the method lies in the election of an appropriate external operator Q; it must not mix nor miss the eigenmodes of the system. In previous works using the same method and the same Hamiltonian in the study of the normal modes of metallic spheres, two different operators where used. The first, $Q_s^{sph} = r^l Y_{l0}(\theta, \phi)$ [32], where $Y_{l0}(\theta, \phi)$ is the spherical harmonic function, provided the mean energy of the surface-plasmon excitations characterized by the well-defined quantum number l and the dispersion relation (energy versus radius of the sphere). The dispersion relation obtained agreed with previous calculations and with experimental data. A second operator, $Q_b^{sph} = j_l(rq_r)Y_{l0}(\theta, \phi)$ [34], where j_l is the spherical Bessel function, added a new parameter q_r (momentum along the radial direction). This operator allowed the possibility of excitation of modes throughout the volume of the sphere. The induced density is peaked at the surface region but has decreasing amplitude oscillation towards the interior of the sphere. The spectrum turns out to be much richer than in the case of the first operator and for each l value, an extra index is necessary to specify the eigenmode. Due to the finite size of the sphere, the q_r momentum is quantized and only for some q_r values, related to the radius R of the sphere, the response has a resonant behavior, which yields an oscillatory structure to the energy of the system as a function of q_r (see Fig. 5 in Ref. [34]).

Recently, the plane metallic surface has been examined using this same approximation [38, 39]. The operator used to generate surface plasmons is $Q_s = e^{i\vec{q}\vec{\rho}} e^{qz}$, where $\vec{r} = (\vec{\rho}, z)$. The well-defined quantum number is the momentum q parallel to the surface and the exponentially decreasing behavior inside the metal guarantees the convergence of the space integrals in the calculation.

For potassium the agreement with experimental data is quite good, comparable with other self-consistent theoretical calculations [26]. However, for Na this agreement diminishes for large q values.

The operator Q_{mp} capable of generating the multipole surface-plasma modes must fulfill several conditions. One of these conditions is that it must depend on an extra parameter (τ), momentum of a standing wave in the z direction. Furthermore, to generate extended modes in the volume with a non-negligible probability, the external operator must be peaked within the metal. The function chosen is

$$Q_{mp} = e^{i\vec{q}\vec{\rho}} e^{-q^2 z^2} \cos(\tau z). \tag{5.29}$$

The q component of the Fourier transform of the potential created by a point charge moving parallel to the surface at $z = 0$ would be $Q = (1/2\pi q) e^{i\vec{q}\vec{\rho}} e^{-q|z|}$.

A quiet common criticism of this procedure is that one loses the physical meaning of the Q operator. The answer to this objection is that, in general, the energies of the normal modes of the system do not depend on the way one excites them. The main problem arises from the possible mixture of modes caused by Q. However, if the response is dominated by a collective mode, the structure of $S(E)$ in Eq. 5.2 has only one peak, the summation in Eq. 5.3 has only one term, and the contribution of Q to E_3 in Eq. 5.8 is completely eliminated. This is the case in the low-q-value region of the spectrum, but it is only approximate for increasing values q. Other operators, which were easier to manage analytically, were tested, but either they did not show a sensitive resonant behavior of the energy as a function of τ, as we expected, or they did not correctly reproduce the limits for low q and τ values.

Using Eqs. 5.26-5.28 and 5.29 into Eqs. 5.9 and 5.12 yields integral expressions on the g.s. electronic density $n(z)$ along the z axis. The expressions for m_1 and m_3 are given in the Appendix. An effective electronic mass has been included to incorporate band effects.

Two different analytical approximations are used for $n(z)$; the first, a double-step function centered at $z = 0$,

$$n_S(z) = \frac{n_0}{2}\left[\theta\left(-z - \frac{d}{2}\right) + \theta\left(-z + \frac{d}{2}\right)\right], \tag{5.30}$$

where $n_0 = 3/4\pi r_s^3$ (where r_s is the bulk one-electron radius), $\theta(x)$ is the step function, and d is the width of the electronic-profile step of density $n_0/2$. The second is an analytical

approximation of the Lang-Kohn calculation given by

$$n_{LK}(z) = \frac{n_0}{e^{z/\delta} + 1} \tag{5.31}$$

The double step is taken to be the surface width of the smooth density (Eq. 5.31), defined as $d = z_2 - z_1$ where $n(z_2) = 0.1n_0$, and $n(z_1) = 0.9n_0$ [39].

The effective electron mass used in the calculations and the δ parameter, which determines the softness of the electronic profile (Eq. 5.31), are taken from the fit of the polynomial approximation to the experimental data given in Ref. [26] for the surface monopole modes and the analytical expression obtained using Q_s in the low-q limit, which is given by [39]

$$\omega(q) = \frac{\omega_p}{\sqrt{2m^*}}[1 - q\delta \ln(2)]. \tag{5.32}$$

Numerical calculation of the space integrals is carried out along a longitude centered at $z = 0$ and bounded by z values that satisfy the condition

$$e^{-2q^2z^2} \leq 10^{-10}, \tag{5.33}$$

for each q value. This exponential comes from the Q_{mp} function and appears in all the z integrals. Analytical expressions for the energy moments in the low-q limit could not be obtained, even for the double-step case. We could only infer that the first non-vanishing q-dependent term in the expansion of the dispersion relation $\omega(q)$ is proportional to q^2.

If $q = d = 0$ is considered, the bulk plasma energy ω_p is recovered in the limit $\tau \to 0$. The values used in the calculations are summarized in Table 5.1. The last column of Table 5.1 is the experimental value of the monopole surface plasmon ($q = 0$) used in the normalization of the experimental data given in Ref. [26].

In the case of Al, no polynomial approximation is given in Ref. [26]. To obtain numerical results from the use of Eq. 5.31, a trial value of $\delta = 1.6$ a.u. was used. No effective-mass-type correction was performed.

5.3 Results and discussion

We have applied the method described in the preceding section to free-electron-like plane surfaces. The first point in question is related to the value of the τ parameter that must be used, once q is fixed, in order to calculate the dispersion relation $\omega(q)$.

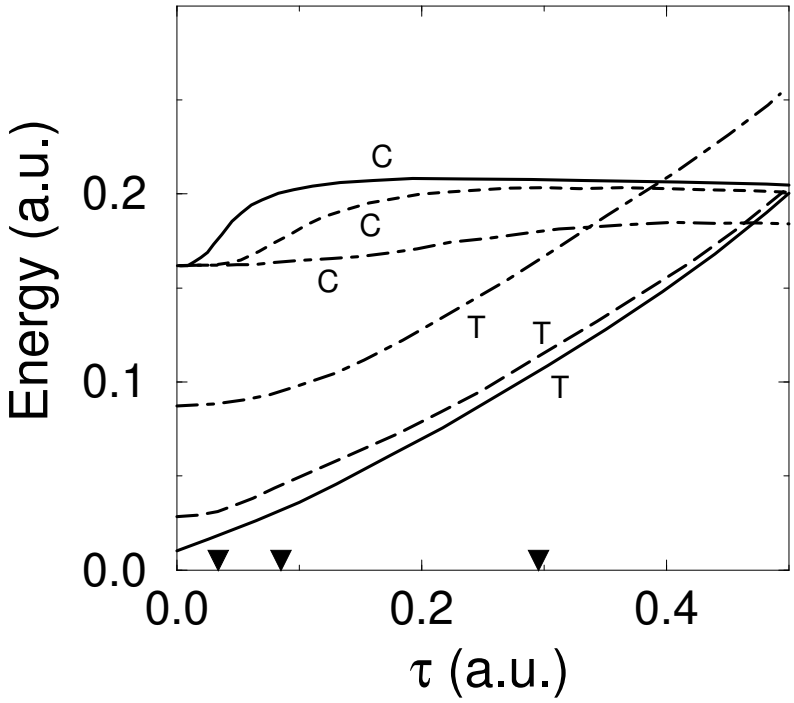

Figure 5.1: τ dependence of the Coulomb (C) and kinetic (T) contributions to the excitation energy for Na. Curves labeled C are $\sqrt{m_3(C)/m_1}$ and those labeled T are $\sqrt{m_3(T)/m_1}$. Three different values of q are considered: 0.02 a.u. (solid line), 0.05 a.u. (dashed line) and 0.15 a.u. (dot-dashed line). The triangles below indicate the place of largest slope in each case. They correspond, from left to right, to the solid, dashed and dot-dashed lines. Eq. 5.30 is used for the electronic profile.

metal	Al	Na	K	Cs
r_s	2.07	3.93	4.86	5.62
d		4.34		
δ	1.6	1.06	0.95	0.6
m^*	1	1.14	1.3	1.58
$\omega_{sp}(exp)$ eV	10.3	3.99	2.73	1.99

Table 5.1: Physical parameters used in the calculations. δ and m^* for Na, K, and Cs are obtained from the fitting of our model (Eq. 5.32) for surface plasmon and the polynomial approximation to the experimental data given in Ref. [26]. The δ and m^* values for Al are trial values. d is the width of the electronic step (see text). The experimental surface-plasmon frequencies used in the normalization of the data reported in Ref. [26] are also given.

Figure 5.1 shows the contribution to the energy of the Coulomb ($\sqrt{m_3(C)/m_1}$) and kinetic ($\sqrt{m_3(T)/m_1}$) terms for Na at three different q values, as functions of the τ parameter. Whereas the kinetic contribution has a monotonic increasing behavior, the Coulomb term develops an abrupt increase for τ approximately equal to $2q$ (marked below by arrows). Though not apparent on the scale represented in Fig. 5.1, the Coulomb term shows an oscillatory behavior along the τ axis that resembles the structure obtained for the excitation energy of a metallic sphere as a function of q_r [34]. In this last case, the peaks of the oscillatory behavior of the energy function correspond with the q_r-quantized values that describe the bulk modes of the system. In the planar case, the first τ derivative of the total energy gives a much more accurate evaluation of the resonant values of τ, as can be seen in Fig. 5.9 (for $q = 0.05$ a.u.), which will be commented on below (in addition to Na, results for Al, K, and Cs are also shown). This q-dependent resonant value is the one chosen in the determination of the energy of the modes. In Fig. 5.1, a double-step density is considered (Eq. 5.30), whereas in Fig. 5.9 a soft profile is used (Eq. 5.31). Within the accuracy of our numerical calculations, the resonant value of τ does not depend on the electronic profile for these low q values, as is pointed out below.

As q increases, the resonant behavior becomes less and less apparent, as the Coulomb

contribution is flatter and the kinetic term is shifted towards larger values, thus making the structure of the total energy less pronounced and in turn the modes less observable. This behavior agrees with experimental results that show that the multipole modes become unobservable for values of q much smaller that the Landau damping cutoff value given approximately by $q_c = \omega_p/v_F = 0.90\sqrt{r_s}$ ($q_c = 0.45$ a.u. for Na, v_F is the Fermi velocity). In a TDLDA calculation of the dispersion relation of the multipole modes given in Ref. [26], the error bars become larger for increasing values of q (see Figs. 6-8 therein) showing an increase in damping, in agreement with our results.

To give an idea of the sensitivity of the resonant τ value on the width of the step, two different values of d are chosen to study the behavior of the Coulomb contribution. Figure 5.2 shows that the value of τ that makes the most abrupt variation of the energy is the same for both values of d (the position of the arrow is the same in both cases). Even for $d = 0$ (a one-step electronic profile), the Coulomb term would show an abrupt increase in τ and so a multipole mode, contrary to the result obtained by Bennett [16] who found within a hydrodynamical calculation that multipole modes are strongly dependent on the electronic profile, and appear only for a certain value of the decay length at the surface.

Figure 5.3 shows all the different contributions to the energy in order to study the relative importance of the exchange and correlation interactions within the local model used (Eqs. 5.26 and 5.27). For $\tau = 0.1$ a.u., the exchange term is about 13% of the Coulombic plus the kinetic contributions, whereas the correlation term is only about 4%. Both terms are negative (the values presented in Fig. 5.3 are $-\sqrt{|m_3(ex)/m_1|}$ and $-\sqrt{|m_3(cor)/m_1|}$, respectively) and tend to lower the slope of the dispersion relation in a similar way as was previously reported for bulk plasmons (see Ref. [93]). If nonlocal effects are considered in the exchange term, its contribution to the Coulombic part decreases but still produces a lower slope [96]. The inclusion of exchange and correlation makes the Coulomb interaction weaker, the electrons freer, and decreases the necessary energy to create a plasma oscillation. Eq. 5.31 is used for the electronic profile.

To study the dependence of our results on the metallic density, in Fig. 5.4 a comparison between the dressed Coulomb ($\sqrt{[m_3(C) + m_3(ex) + m_3(cor)]/m_1}$) and kinetic contributions for Al, Na, K, and Cs for a fixed value of $q = 0.05$ a.u. is shown. The dressed Coulomb contribution of Al lies off the scale (it is about 0.45 a.u.) and crosses the kinetic

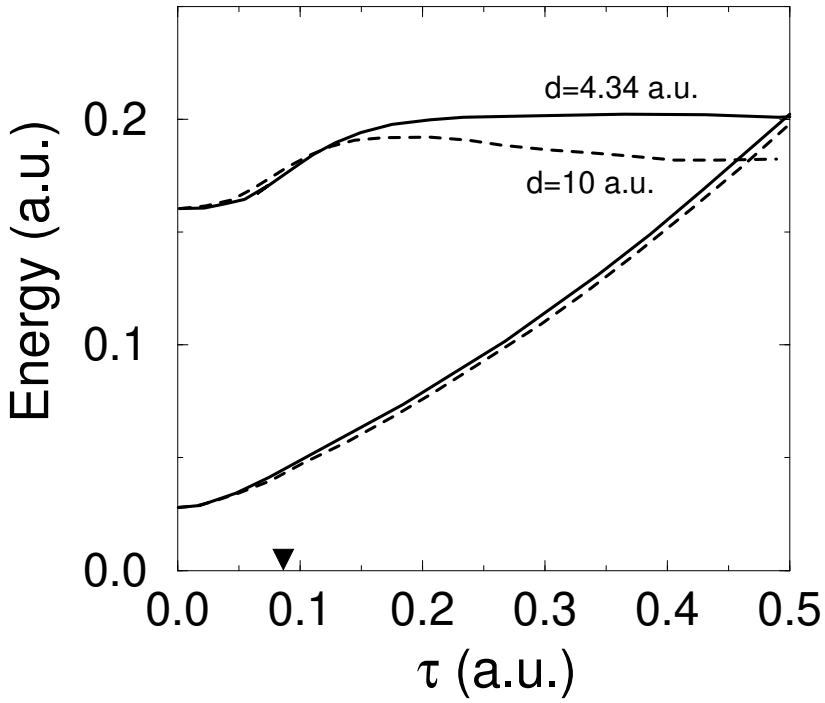

Figure 5.2: Same as Fig. 5.1 for $q = 0.05$ a.u. for two different values of the double-step width. The triangle below indicates the position of the largest slope for both cases.

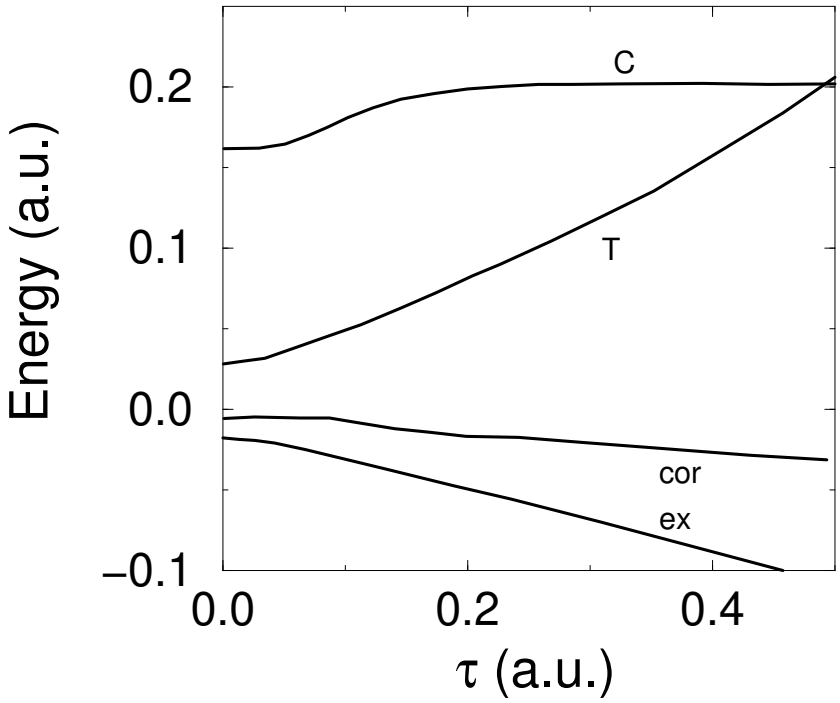

Figure 5.3: Same as Fig. 5.1 for the Coulomb and kinetic contributions to the excitation energy, together with the exchange ($-\sqrt{|m_3(ex)/m_1|}$) and correlation ($-\sqrt{|m_3(cor)/m_1|}$) terms as functions of τ. q has a value of 0.05 a.u. Eq. 5.31 is used for the electronic profile.

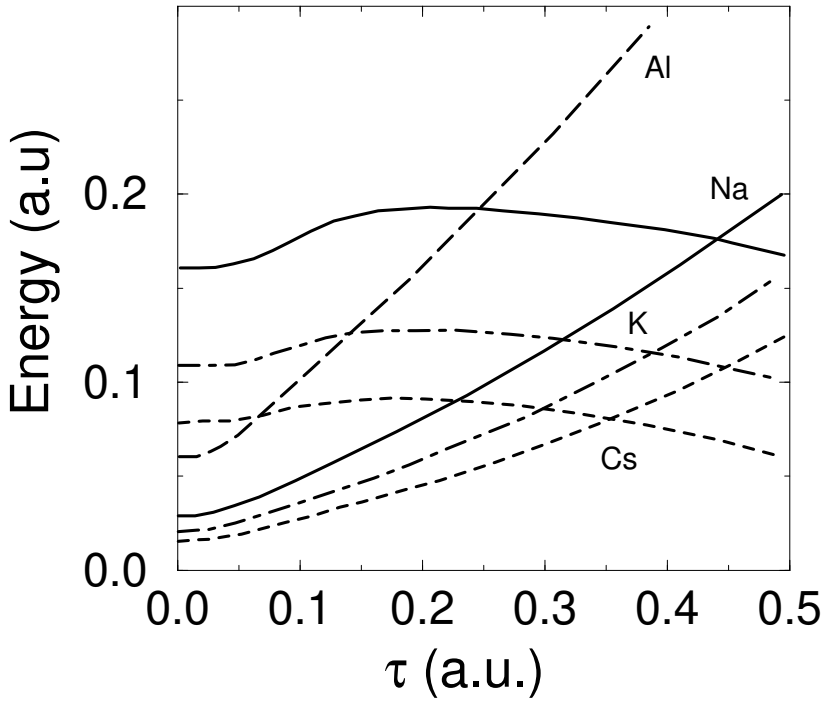

Figure 5.4: Dressed Coulomb ($\sqrt{[m_3(C) + m_3(ex) + m_3(cor)]/m_1}$) and kinetic (the same as in Fig. 5.1) contributions to the excitation energy as functions of τ for four different metals. The Coulombic term for Al is off the scale and crossed the kinetic branch for τ larger than 0.5 a.u. The arrow below indicates the position of the largest slope, the same in all cases. Again, $q = 0.05$ a.u.

branch for τ larger than 0.5 a.u. It is clear from the figure that the structure of the total energy is washed out as r_s is increased, as the cross point of the Coulombic and kinetic branches decreases, and the Coulomb contribution becomes flatter. This behavior again agrees with the tendency shown in the electron-loss spectra given in Ref. [26] (see Fig. 5 therein). The peak of the multipole mode is much less apparent in the Cs case than it is in the Na or K. The transition from a collective to a single electron-hole excitation is related to the increasing contribution of the kinetic energy to m_3 and so to the position of the cross point of the Coulomb and kinetic branches, which decreases for higher r_s values. However, according to the above, Fig. 5.4 would predict the observability of multipole modes in Al, in contrast to experiments. This point will be discussed in the last section.

Figure 5.5 represents the dispersion relation for Na within a calculation that excludes exchange and correlation interactions and its aim is to compare the results obtained from the use of Eq. 5.30 (full line) and Eq. 5.31 (crosses). We also added the experimental data taken for Ref. [26]. As was previously pointed out, there is a negligible dependence of the results on the details of the electronic profile for these values of q.

Figures 5.6-5.8 collect the full calculation (including exchange and correlation terms and using Eq. 5.31 for the electronic profile) of the dispersion relation for Na, K, and Cs (full curves). The best fit with experimental data takes place for K as was previously the case for monopolar surface modes [39]. The TDLDA results reported in Ref. [26] are also given. The bars in the figure indicate the uncertainty of these results. The extrapolation to $q = 0$ of our numerical calculation gives a value of

$$\omega = \frac{\omega_p}{\sqrt{m^*}} a, \tag{5.34}$$

where m^* is the effective electronic mass and $a = 0.84$ is independent of the metal, in excellent agreement with experimental findings.

As one moves from Na to Cs, the TDLDA results become better than the SR results. The reason lies in the nature of the SR method in which an average evaluation of the response function is implicit. As r_s increases, the electron-hole contribution to the average becomes more important as a consequence of the relative increase of the kinetic term as was discussed previously (see Fig. 5.4). The presence of electron-hole excitations lowers the average energy. Due to the energy factors in the SR (see Eqs. 5.3 and 5.8), the high energy collective state continues to exhaust the m_3 SR also at relatively high q, but not the

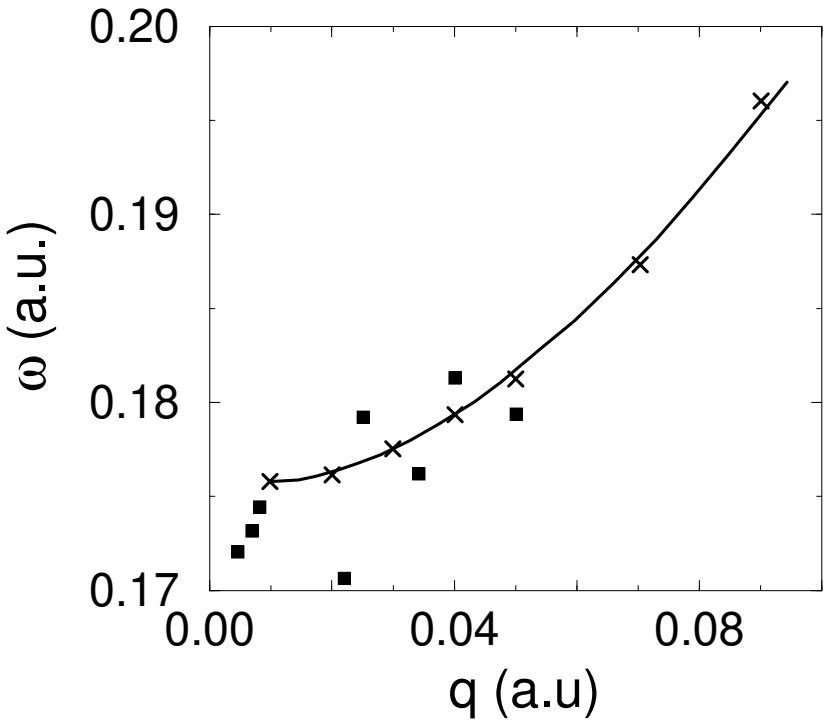

Figure 5.5: Dispersion relation of multipole modes for Na. The solid line is obtained using a double-step profile (Eq. 5.30) and the crosses using the soft profile (Eq. 5.31). Exchange and correlation interactions are not included. Experimental data taken from Ref. [26] are also given (squares).

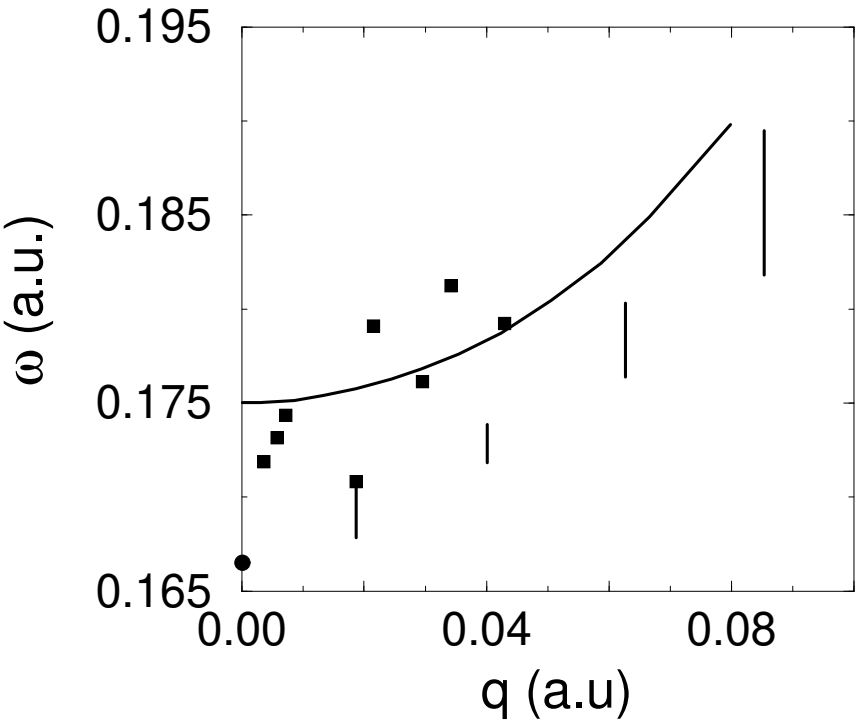

Figure 5.6: Dispersion relation of the multipole plasmon modes for Na including exchange and correlation effects and using Eq. 5.31 for the electronic profile. Experimental data from Ref. [26] is included (squares). The vertical lines denote the results of the TDLDA calculation from Ref. [26]. The dot at $q = 0$ is the extrapolated plasma frequency in the TDLDA calculation.

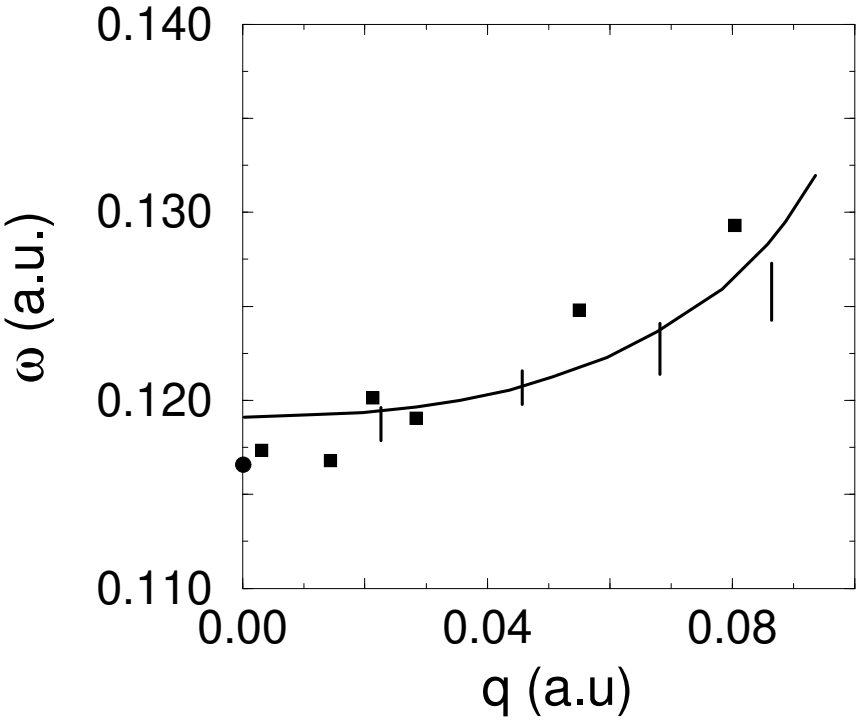

Figure 5.7: Same as Fig. 5.6 for K.

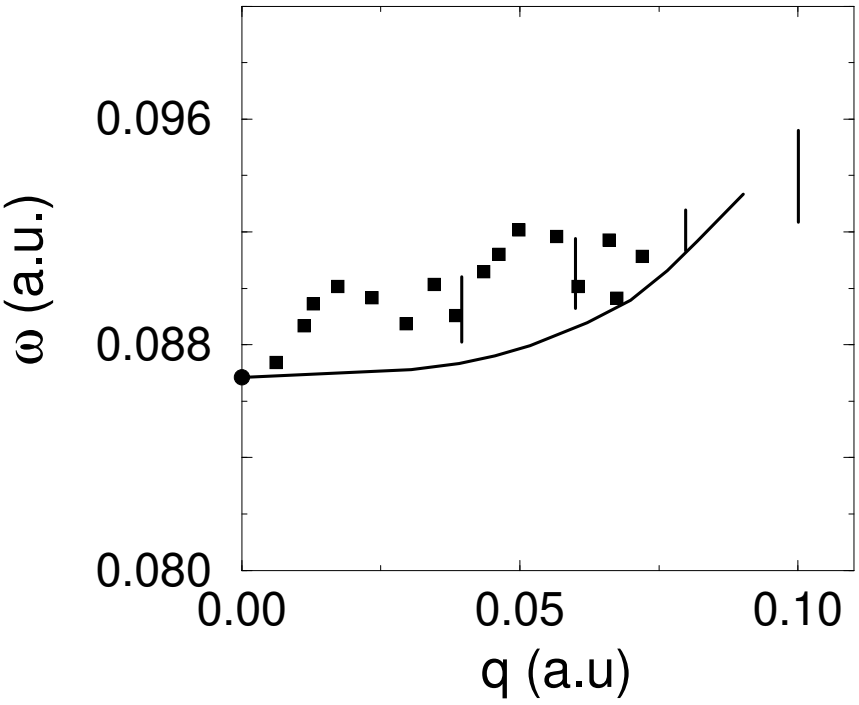

Figure 5.8: Same as Fig. 5.6 for Cs.

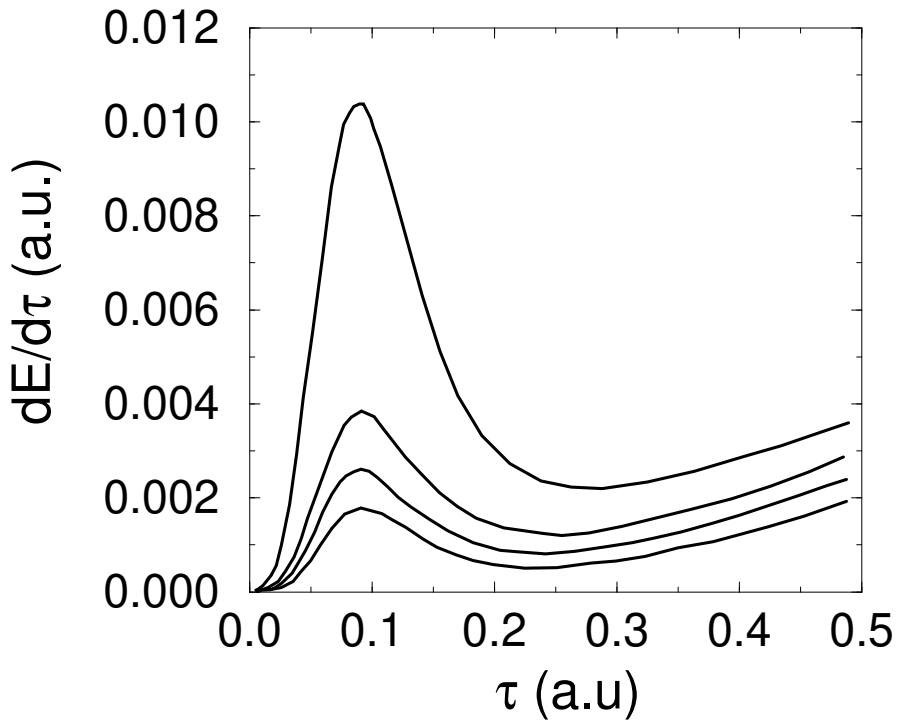

Figure 5.9: First τ derivative of the excitation energy for four different metals as a function of τ. From top to bottom: Al, Na, K and Cs. Exchange and correlation terms are included and a soft electronic profile is considered (Eq. 5.21).

m_1 SR, which begins to take contributions from single-particle excited states and then E_3 becomes lower than the TDLDA value.

Finally, Fig. 5.9 shows the first τ derivative of the total energy which develops a pronounced peak for $\tau = 2q$, nearly independent of the metal. Contrary to the findings of some previous works [16, 97, 98] that suggest that the multipole mode is a trapped standing wave inside the surface layer and therefore strongly dependent on the width of the surface region as a consequence of the matching condition, τ (and its associated wavelength $\lambda = 2\pi/\tau$) is mainly determined by the localization of the operator Q_{mp} around $z = 0$ determined by q in the exponential $e^{-q^2z^2}$. There are some arguments that support this observation. One is

related to the behavior of the electronic-density fluctuation related to a multipole mode. In Ref. [26], the density distribution for $r_s = 5$ a.u. and $q = 0.06$ a.u. extends over a distance of about 16 a.u. on the z axis, while for this value of r_s the width of the surface region would be about 4 a.u. The other argument refers to a consequence of sum-rule calculations in that a relationship is established between the operator Q and the electronic-density fluctuation, which is, to first order in Q, given by Eq. 5.22,

$$n_1(\vec{r}) = -\vec{\nabla}(n\vec{\nabla}Q), \tag{5.35}$$

where n is the g.s. density. This relation gives to the n_1 function the same exponential dependence on z, that is to say, the plasma oscillation is localized in a region determined by q. There is, however, a residual dependence of τ on the metal that augments as q increases, thus making the localization region and the surface width comparable. The matching condition on τ determined by the width of the surface would give a constant value of τ for all q momenta and within a SR calculation, it would produce a negative slope of the dispersion relation.

There are more resonant peaks for larger values of τ for a fixed q. However, they lie in the unobservable region due to the high value of the kinetic-energy contribution. Actually, the experimental values correspond to the first quantized value of τ (the one in Fig. 5.9). It is due to this quantization on the momentum along the z direction that makes it possible to obtain the dispersion relation of the multipole modes from inelastic- electron-scattering experiments in the reflection mode of Ref. [26] as there is no momentum conservation in the z direction.

5.4 Concluding remarks

An alternative study which clarifies some aspects of multipole collective modes in metal surfaces is presented. The interplay between Coulomb and kinetic energies allows us to predict under what circumstances these modes might be observable. The Coulomb contribution develops resonant behavior for discrete values of the z-direction momentum. This resonant structure is washed out by the kinetic contribution for increasing q values smaller than the Landau damping cutoff. For a fixed q, only the first quantized mode turns out to be observable. The resonant z-direction momentum is approximately equal to $2q$ for low

q values and is increasingly dependent on the surface profile as its associated wavelength becomes comparable to the surface size. Exchange and correlation effects reduce the slope of the dispersion relation due to the weakening of the Coulomb interaction.

The fact that in the case of Al experimental data do not show multipole modes means that further modifications to our calculations must be made in order to account for the probability of excitation of these modes. In Refs. [2] and [62] the imaginary part of the centroid function $d(\omega)$ directly related to the probability is obtained. This function develops a resonant structure at the multipole frequency, which decreases for denser metals. This tendency competes with the increasing resonant structure shown in Fig. 5.9. Considering that a simple metal in our model is characterized by three parameters r_s, δ, and m^*, everything tends to suggest that the softening of the electronic profile at the surface produces an effective strong damping mechanism that extinguishes the mode.

Chapter 6

Plasmons in simple-metal slabs: a semi-classical approach

Collective excitations in simple metal systems can be described successfully in terms of a local one-body excitation operator Q. For the plasmon modes of a simple-metal slab, plane wave expansions of Q are calculated using a variational procedure, equivalent to a restricted RPA calculation. The dispersion relation and the density fluctuation for each mode are found in the sudden approximation using the proper Q operator and the RPA sum-rule formalism. The contribution of the exchange and correlation energy is estimated using a local density functional. The positive background is described within a jellium model while the ground-state electronic density is approximated by a double step profile. The response of the slab to a q-dependent external operator is analyzed. The density fluctuation of the plasmon modes above the plasma frequency form standing waves across the slab. The spectra below the plasma frequency is qualitatively different to that of local optics calculations, due to the appearance of two multipole plasmon modes that shift down the origin of the ω_+ plasmon. The dependence of the results on the width of the slab, on the density of the simple-metal and on the surface diffuseness is discussed. Throughout, the difference with previous RPA and TDLDA calculations is stressed.

6.1 Introduction.

There are several ways in which the dispersion relation of the plasmon modes in systems with translational invariance can be measured. The first experiments on simple metal slabs used a dielectric substrate to support the metal film and measured the light transmittance [99] or the photo-electric yield [9]. More recently, molecular-beam epitaxy has been applied to grow thin metallic layers between two insulators [100] or $Al_xGa_{1-x}As$ heterostructures simulating a positive jellium background [101]. Also electron energy loss spectroscopy (EELS) has been used to study adsorbed simple-metal layers on an aluminium substrate [27].

The spectrum of a simple-metal slab has two distinct parts: the plasmon modes that lie above ω_p, corresponding to standing waves across the slab, and the surface plasmon modes, with lower frequencies. Among the surface modes of a slab, the ω_- and the ω_+ modes give rise to the ordinary surface plasmon when the width of the slab becomes large. Also, one should expect to find in a slab surface modes that are equivalent to the multipole plasmon mode of a surface. The first successful attempts to study the collective modes of a simple metal slab were made employing macroscopical Maxwell equations together with a Drude dielectric function [102] and an hydrodynamical model [90]. More recently some theoretical calculations have been done using the random-phase approximation (RPA) [100, 103, 104, 105, 106] and the time-dependent local density approximation (TDLDA) [21, 22, 23, 107]. These microscopical approaches overcome most of the difficulties presented by classical models [2]. The ω_- and the ω_+ plasmons are studied thoroughly in all this references but the results do not differ too much from the hydrodynamical model ones [108]. Only some of them discuss the existence of additional multipole plasmon modes. Liebsch [23], in a calculation of the plasmon modes of a simple-metal overlayer on an aluminium substrate, finds a multipole plasmon that hybridizes with the ω_+ plasmon. Schaich and Dobson [21] also obtain a peak in the response function at frequencies between ω_p and $\omega_p/\sqrt{2}$ but they do not conclude whether the cause is a collective mode or is due to intersubband excitations, although in a previous work [22] Dobson suggests the existence of two multipole plasmons and gives its dispersion relations.

A multipole plasmon mode has been detected in simple-metal clean surfaces using EELS [19]. Its dispersion relation has a positive slope when the momentum k parallel to the surface is zero while the frequency at this point is $0.8\omega_p$. This value agrees with theoretical

calculations [19, 40]. Multipole plasmon modes are associated with electronic-density fluctuations that are peaked at the surface region and have decreasing oscillating amplitude towards the interior of the metal. It can be shown [62] that the integral of the electronic density perpendicular to the surface is zero. Unlike ordinary surface plasmons, they are optically active because their frequency is different from 0 in the small momentum limit and, hence, its dispersion relation crosses the one of light. The common lore states that multipole plasmons are the bulk modes of the selvedge region, which is not very sensitive to the thickness of the slab. One expects that at least some of these properties, well established for simple-metal surfaces, should be valid for slabs.

The aim of this work is to show that with the RPA sum-rule formalism (SR) it is possible to obtain the full spectrum of collective excitations of a simple-metal slab, even the rarely studied multipole plasmon modes, without the heavy numerical computation that is involved in a self-consistent calculation. This formalism is able to produce useful results for different geometries [37, 38, 76, 93]. In particular, a good agreement has been obtained between experimental data and the dispersion relation of surface plasmons [39] and multipole plasmons [40] on a plane simple-metal surface. It has some advantages over other methods. The different contributions to the energy of each mode can be analyzed on its own and semi-classical approximations for the kinetic energy are easily implemented. It can incorporate electronic exchange and correlation interactions using a local density approximation. Within the SR formalism it is not difficult to employ realistic electronic profiles. In fact the results have RPA precision as long as a self-consistent ground-state electronic profile is used [43], although only an average of the response function can be obtained.

Usually, when working within the SR method, it is assumed that for every collective mode there exists a local one-body observable that excites that mode without mixing it with others. In order to obtain useful results an appropriate excitation operator Q must be found and the system must have well-defined collective modes. Otherwise it would not be possible to get any valuable information from the averaged response function. There is not a unique way to find such an operator. Sometimes the properties of a given operator Q determine the kind of mode that it excites. For example, an operator that fulfills Laplace's equation can only excite monopole surface modes [39]. A restricted variation of Q on a parameter

[40] can be useful if a sufficiently general form of Q is employed. In RPA calculations an excitation operator Q can be found for each mode but although it will be an observable, in general it is not a local operator. To approximate Q as a local operator is called local-RPA [36] and has been applied successfully to liquid helium [109], nuclei [110] and metal clusters [37]. We use local-RPA to find a proper Q operator as a momentum expansion.

Instead of a self-consistent electronic profile, a double step profile is used to describe the ground-state. This leads to a simplification of the calculations which can be performed analytically without a great loss of precision because it has been shown [40] that there is little quantitative difference between the results from any of the two models.

6.2 Application of local RPA to a metal slab

In this section we first give a short review of the method as it was stated in [36] (see this reference for more details). Then we expatiate on the particularities that we have had to devise to adapt it to our problem, the most important being the choice of the form of the functions that give rise to the sought-after excitation operators.

Both local and full RPA demand as a starting point a description of the ground state of the system at issue. Within the quasi-bosonic approximation this description is usually furnished by working out the Hartree-Fock approximation to the ground state state $|\phi_0\rangle$. This approximation is acceptable as long as one assumes that correlations are small. Once the Hartree-Fock problem is solved, the essence of the method is to build the excitation operators as linear combinations of one-particle–one-hole operators, and determine the coefficients of the expansion by solving the equation of motion

$$\langle\phi_0|\left[C_m,[H,C_n^\dagger]\right]|\phi_0\rangle = \delta_{nm}\hbar\omega_m, \tag{6.1}$$

where $C_n^\dagger$ and C_m are the creation and the annihilation operators. These operators fulfill the well known orthonormality relations

$$[C_n, C_m^\dagger] = \delta_{nm}. \tag{6.2}$$

An alternative description of RPA can be made based upon the operator

$$Q_n = \frac{C_n^\dagger + C_n}{\sqrt{2}}. \tag{6.3}$$

Eq. 6.1 becomes

$$\Big[H,[H,Q_n]_{ph}\Big]_{ph} = (\hbar\omega_n)^2\, Q_n. \tag{6.4}$$

The ph symbol means that the operator is projected onto the linear space spanned by one-particle–one-hole states.

The operators Q_n have a clear physical meaning. Within the framework of Quantum Mechanics the operator Q_n represents the physical process that excites only the n-mode when applied over the ground state. This follows from definition 6.3 and the properties of the creation and annihilation operators.

Local RPA assumes that the operator Q_n is a local one-body operator. This means that it can be expanded in terms of a function f_n as follows,

$$Q_n = \sum_{i=1}^{N} f_n(\hat{r}_i)\,, \tag{6.5}$$

where N is the number of electrons and $\hat{r}_i = (x_i\,, y_i\,, z_i)$ is the position operator of the i-th particle.

In order to determine f_n we expand it in a series that we shall choose taking advantage of the particular problem we are facing at.

We will focus on the problem of a gas of electrons in a simple metal slab of very large area A and thickness d. If the gas is made of N electrons, then the operator of total momentum q_{tot} of the gas will be;

$$\hat{q}_{tot} = \sum_{i=1}^{N} \hat{q}_i \tag{6.6}$$

We will assume the slab to be parallel to the XY plane and consequently write any vector as $\vec{q} = (\vec{k}, p)$, $\vec{k}$ being the 2 dimensional vector that lives in the $x-y$ plane and p is the projection along the z axis. Translation invariance in the x and y axis leads to the conservation law;

$$\Big[H, \hat{k}_{tot}\Big] = 0 \tag{6.7}$$

So, the eigenvalues k of operator $\hat{k}$ are good quantum numbers for our system. As k is a true quantum number of the problem, we may advance that each Q_n operator has a well defined k, in other words, it has the form

$$Q_n = \sum_{j=1}^{N} e^{ik\hat{R}_j}\phi_n(\hat{z_j}), \tag{6.8}$$

where $\vec{R}$ stands for the 2 dimensional vector (x, y). This observation suggests that we relabel Q_n as $Q_{k,n}$ in the sequel.

As for the f_n functions, which we haste to relabel in accordance with the previous discussion, we may write

$$f_{k,n}(R, z) = \exp(ikR)\phi_n(z). \tag{6.9}$$

Any realistic electronic profile vanishes for distances far enough from the boundaries of the slab. We can think the gas of electrons to live in a linear box of size L. We must take L to be larger than d as there are electrons wandering outside the slab, but provided L is large enough, physical results are L-independent. Nevertheless the value of L must not be larger than necessary because this would increase the number of terms needed in the expansion. It should be emphasized that the exact value of L is not critical as long as these conditions are fulfilled.

Now we have a physically motivated choice for the basis which generates ϕ_n; we take ϕ_n to be expanded in terms of a Fourier basis

$$\phi_n(z) = \sum_l a_n^l e^{ip_l z}, \tag{6.10}$$

with $p_l = \frac{2\pi l}{L}$. Equivalently, we may expand the $Q_{k,n}$ operators

$$Q_{k,n} = \sum_l a_n^l Q_{k,p_l}, \tag{6.11}$$

with

$$Q_{k,p_l} = \sum_{j=1}^{N} \exp(ik\hat{R}_j) \exp(ip_l \hat{z}_j). \tag{6.12}$$

In this way, we have expanded the operators Q_n in a complete series where every term represents a plane wave with a well defined momentum.

We adopted this approach as it is the one that yields the simpler equations. It is not so easily applicable in the case of infinite or semi-infinite systems, as L has to be sent to ∞ and the system of equations is no longer discrete. The formalism leads then, from Eq. 6.4, to a fourth-order differential equation for Q [36].

The completeness of the series is a requirement that can be overlooked if we are interested in obtaining just a part of the spectrum. Anyway, a non-complete series should be used only if there are clear physical arguments that fix the form that the operators Q_n should

have. As we are trying to obtain a number M of modes, not limited by the mathematical form of the series, in our case the use of an expansion as general as possible is compulsory.

By construction, the Q_n operators will have a period L. This is done just for mathematical convenience. We have truncated the previous Fourier series Eq. 6.10 or Eq. 6.11 making sure that the terms not considered do not affect the energy of the modes that we are going to study. This can be done checking the convergence of the results as the number of terms is increased. a_n^p are coefficients that can be obtained by minimizing the energy functional [36]. Written in terms of the Fourier coefficients Eq. 6.4 reads [36]

$$\left[\mathcal{K}_{\alpha\beta} - (\hbar\omega_n)^2\mathcal{B}_{\alpha\beta}\right] a_n^\alpha = 0, \tag{6.13}$$

$\mathcal{K}_{\alpha\beta}$ and $\mathcal{B}_{\alpha\beta}$ being respectively;

$$\mathcal{B}_{\alpha\beta} = \langle\Phi_0|\left[Q_\alpha,[H,Q_\beta]\right]|\Phi_0\rangle, \tag{6.14}$$

$$\mathcal{K}_{\alpha\beta} = \langle\Phi_0|\left[\left[Q_\alpha,H\right],[H,[H,Q_\beta]]\right]|\Phi_0\rangle. \tag{6.15}$$

H is the Hamiltonian of the system and $|\Phi_0\rangle$ the (Hartree-Fock) ground state. Needless to say that the sum-rule approach

$$m_1 \equiv \sum_n \hbar\omega_n|\langle n|Q|\Phi_0\rangle|^2 = \frac{1}{2}\langle\Phi_0|\left[Q,[H,Q]\right]|\Phi_0\rangle, \tag{6.16}$$

$$m_3 \equiv \sum_n (\hbar\omega_n)^3|\langle n|Q|\Phi_0\rangle|^2 = \frac{1}{2}\langle\Phi_0|\left[\left[Q,H\right],[H,[H,Q]]\right]|\Phi_0\rangle, \tag{6.17}$$

$$E_3 = \sqrt{\frac{m_3}{m_1}}, \tag{6.18}$$

is a particular case of Eq. 6.13 because if we could find a series expansion such that every term would couple to a different eigenmode, Eq. 6.13 would be separated into a set of equations like Eq. 6.18, one for each term of the series. It can be shown [30] that E_3 is an upper bound to the energy of the mode excited by Q.

Once equation 6.13 is solved, it should be checked that the operators C_n and $C_n^\dagger$ fulfill relation 6.2, or, what is the same, that the array

$$B_{nm} \equiv \mathcal{B}_{\alpha\beta}a_n^\alpha a_m^\beta \tag{6.19}$$

is diagonal.

Solving equation 6.13 for a fixed value of k does not only deliver the optimal operator Q but also the dispersion relations of the collective excitations $\omega_n(k)$. We calculate the dispersion relation in an equivalent, but more transparent way. As the Hamiltonian

$$\begin{aligned} H &= \int dr \left[\frac{\hbar^2}{2m_e}\tau(r) + \frac{n(r)}{2}\left(e^2 \int dr' \frac{n(r')}{|r-r'|} + 2v_j(r) \right) \right] \\ &\equiv H_k + H_c. \end{aligned} \tag{6.20}$$

contains a kinetic and a Coulomb term, we can evaluate separately the contribution of each part of the Hamiltonian to the m_3 sum-rule. When the Q operator used is that obtained in solving Eq. 6.13, the eigenvalues of this equation are, by construction, the E_3 energy obtained from Eq. 6.18 taking into account all the contributions to m_3. If E_3 is calculated using only a contribution to m_3, the quantity obtained gives an idea of the relative importance of that term in the total energy. The inclusion of an exchange and correlation term when solving Eq. 6.13 is done in a perturbative way, as explained later on.

Another important magnitude in the sum-rule formalism is the sudden approximation to the density fluctuation given by

$$n_1(Q) = -\hbar\vec{\nabla}\left[n\vec{\nabla}Q \right]. \tag{6.21}$$

It is the first-order contribution to the density fluctuation of the $|\eta\rangle$ state described in the appendix and usually gives a reliable description of the properties of the eigenstates of the system. It can be employed to calculate a semi-classical approximation of the transition probabilities of any given external excitation operator Q_{ext} using

$$|\langle n|Q_{ext}|\Phi_0\rangle|^2 = \frac{\hbar}{2\omega_n B_{nn}} \left| \int dr Q_{ext} n_1(Q_n) \right|^2. \tag{6.22}$$

It can be proved using Eq. 6.19 that for any operator that belongs to the space spanned by the Fourier basis, the sum rules m_1 and m_3 are evaluated exactly inserting these probabilities in the definitions given by Eqs. 6.16 and 6.17. As an easy exercise, we could replace Q_{ext} by any solution Q_m and build the spectrum of the system when it is excited by this operator. The spectrum or strength function is defined as

$$S(\omega) \equiv \sum_n \delta(E_n - \hbar\omega)|\langle n|Q_{ext}|\Phi_0\rangle|^2. \tag{6.23}$$

The result turns out to be a Dirac delta. This demonstrates that the response obtained from Eq. 6.22 for any excitation operator takes into account only the excitation of infinite-

life plasmons. This is just a characteristic of the RPA. Nevertheless, we will use it later to analyze the response of the slab to a particular operator.

The key part of the calculation is to choose the number M of terms of the Q expansion. This is done, for a given momentum k parallel to the surface, examining the energy of the modes in front of M. It is also checked that the results corresponding to the modes studied diagonalize the array given in Eq. 6.19. The value of M necessary to attain convergence depends on a great number of physical factors. As the main assumption of Local RPA is the existence of well defined collective excitations, we should expect the convergence to be difficult or even impossible in all those situations where a severe damping of the plasmon modes is expected.

From a quantitative point of view, the Coulomb contribution to $\mathcal{K}$ is the responsible for the appearance of real solutions in Eq. 6.13. The kinetic term has a monotonic behavior along rows and lines and only modifies the basic structure of $\mathcal{K}$ given by the Coulomb term. Moreover, if the magnitude of the kinetic contribution becomes comparable to that of the Coulomb one, the solutions become unreliable because the Coulomb contribution is washed out by the kinetic one.

A physical picture can serve to connect this mathematical behavior with the damping of the plasmon modes. Within the jellium model, the damping is due only to the Landau mechanism, in which a plasmon decays into a particle-hole excitation. This process is only probable when the kinetic contribution to the energy is comparable to the total energy of the collective mode. This kinetic contribution to the total energy is provided by the own superposed particle-hole excitations that form the collective mode.

The relative importance of the Coulomb contribution against the kinetic one increases with the electronic density. For this reason in high-density metals like aluminium convergence will need lower values of M than in low-density metals like cesium. Also when the momentum k approaches the Landau cutoff value, given approximately by $q_c = \omega_p/v_F$, convergence is impaired. The surface diffuseness also plays its role because an increasing diffuseness tends to lower the Coulomb contribution to the energy. All these trends, that are related to the damping of the modes, are present in our calculations.

The size of the system is also an important factor, as the bigger the system, the more terms we need to reach a certain accuracy. In fact, for large values of M adding more

terms to the series does not improve the precision of the results because, although the Q_n operators may be calculated with a greater precision, new high energy modes have to be orthogonalized together with the others. This sets an upper bound on the size of the slabs that can be treated within this method. In the case of sodium the results are reliable for slabs of $60a.u.$, taking $M = 75$, whereas if the width is $100a.u.$, a few modes, like the ω_+, do not converge even for $M = 101$.

At this point we just need to solve equation 6.13 and we will do so by expressing $\mathcal{K}_{\alpha\beta}$ and $\mathcal{B}_{\alpha\beta}$ in terms of the local density $n(r)$ and the kinetic-energy density $\tau(r)$ (due to the symmetry discussed so far the only dependence of this quantities is on the z axis)

$$n(r) = \sum_i |\phi(r)|^2, \qquad \tau(r) = \sum_i |\nabla\phi(r)|^2, \tag{6.24}$$

To compute the kinetic term the most direct approach consists in taking the kinetic energy of a free gas of electrons;

$$\tau = an(r)^{5/3}. \tag{6.25}$$

The Coulomb part contains the Coulomb interaction between electrons (of charge e) and the interaction with the jellium through a potential $v(r)$. An estimation of the exchange and correlation energy is made using the following Slater- and Wigner-type expressions

$$\epsilon_{ex} = -\frac{3}{4}an(r)^{1/3} - b\frac{n(r)^{1/3}}{cn(r)^{1/3} + d}, \tag{6.26}$$

with $a = \sqrt{3/\pi}$,$b = .44$,$c = 7.8$ and $d = a/2$. Although this term is not included in the Hamiltonian when computing Q, a contribution to the m_3 sum-rule is calculated just as if it were another part of Eq. 6.20 and added to the other contributions. So the final values of the dispersion relation are slightly different to the ones obtained in Eq. 6.13. In this way the exchange and correlation interactions are included in the results. The main drawback is that the self-consistency of the calculation is lost to a certain extent but this is acceptable because exchange and correlation do not play a crucial role in the existence of the collective excitations in an electron gas, at least for not too thin slabs.

The details necessary to solve equation 6.13 are postponed to the appendix as they become rather technical and do not contain any new physics.

n_b(metal)	$2.69 \cdot 10^{-2}$(Al)	$3.93 \cdot 10^{-3}$(Na)			$2.08 \cdot 10^{-3}$(K)	$8.84 \cdot 10^{-3}$
d	25	18	25	40	25	25
δ	1.61	2.13	2.17	2.21	2.46	1.92
L	35	28	35	50	35	35
M	39	35	39	59	41	39

Table 6.1: Unless stated otherwise, these are the parameters used to modelize slabs of different widths and metals. Other quantities involved in the calculation, although not through the characterization of the ground state, are also included.

6.3 Results and discussion

We applied the method described in the preceding section to simple metal slabs. A double step electronic profile is used as a description of the ground state

$$n(z) = \frac{n_b}{2}\left[\theta(z+\frac{d+\delta}{2}) + \theta(z+\frac{d-\delta}{2}) - \theta(z-\frac{d+\delta}{2}) - \theta(z-\frac{d-\delta}{2})\right]. \qquad (6.27)$$

The length of the step δ has been adjusted in all the cases by a minimal squares procedure to an improved Thomas-Fermi electronic profile [111] calculated for each system. The height of the step is taken to be half of the bulk electronic density. Some Thomas-Fermi profiles are plotted in Figure 6.1, together with their corresponding double-step profiles. The values that characterize the density profile (from now on, atomic units are used throughout) are collected in Table 6.1 together with other parameters chosen for the calculation.

Figure 6.2 represents the dispersion relation of the plasmon modes below ω_p for a typical system. The lower mode is the ω_- mode. It begins at $\omega = 0$ for $k = 0$ and tends to the surface plasmon frequency $\omega_p/\sqrt{2}$ as k tends to infinite. This behavior is completely in agreement with Local Optics [102], not like the next mode, which we identify as the ω_+ mode of Local Optics because of its behavior in the short wavelength limit. In our calculation it has a frequency of approximately $\omega = 0.8\omega_p$ for $k = 0$ when according to Local Optics, and most RPA and TDLDA calculations (even taking into account the diffusivity of the density profile), it should tend to $\omega = \omega_p$ for a small k. For large values of k it becomes degenerate with the ω_- mode. There is another mode whose frequency tends to $0.8\omega_p$ for low k. We call it the even multipolar mode and it behaves very similarly to multipolar

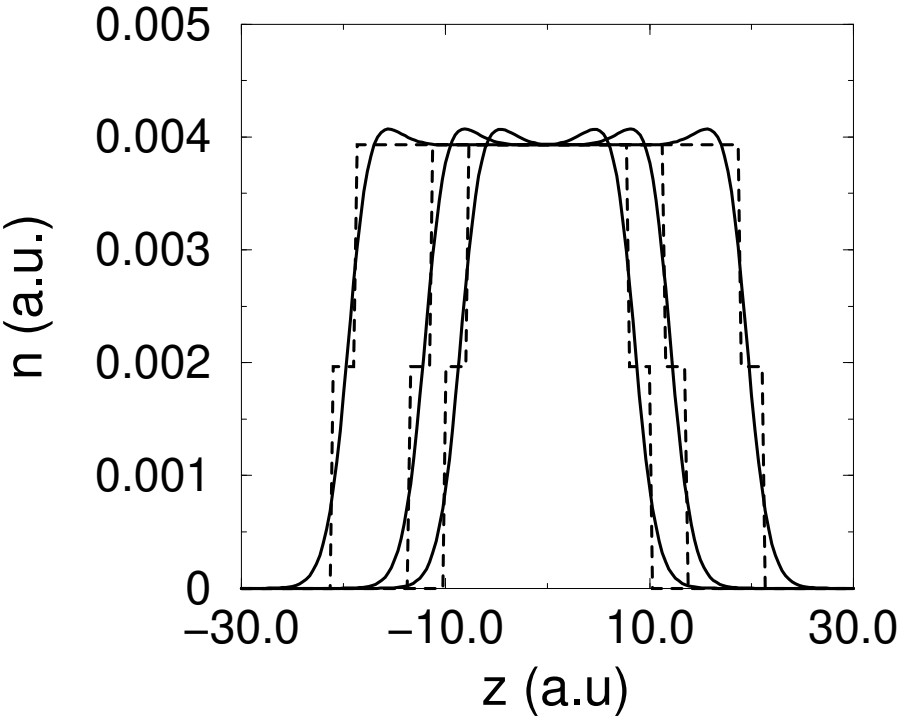

Figure 6.1: Ground state electronic density profile for several sodium slabs of $d = 18a_0$, $d = 25a_0$ and $d = 40a_0$ (where a_0 is the Bohr radius). The solid lines are the Thomas-Fermi profiles. The dashed lines represent the double-step profiles adjusted from them.

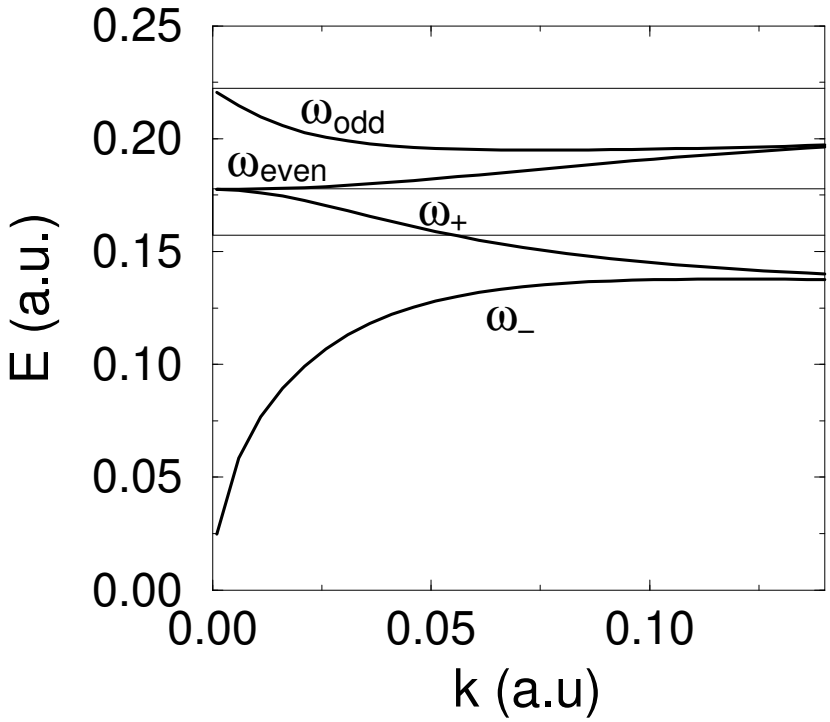

Figure 6.2: Dispersion relation of the plasmon modes below the plasma frequency in a sodium slab ($d = 25a_0$) From bottom to top can be seen the ω_-, ω_+,even multipole and odd multipole modes. Thin lines represent, from bottom to top, $\omega_p/\sqrt{2}$, $0.8\omega_p$ and ω_p.

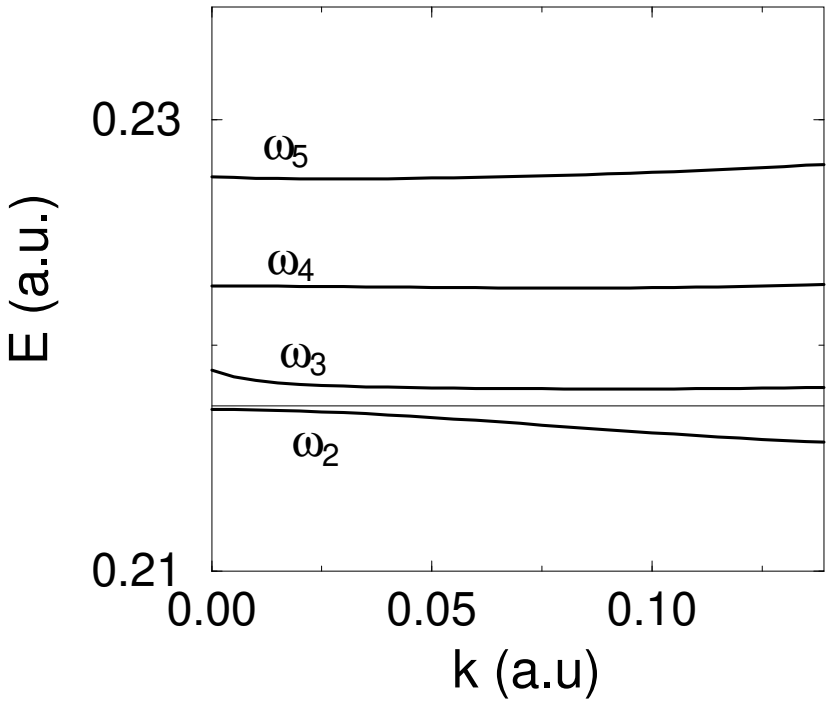

Figure 6.3: Dispersion relation of the four lowest bulk plasmon resonances in the same case as Fig. 6.2. The thin line represents the plasma frequency.

modes in surfaces of semi-infinite systems. Its dispersion relation has a positive slope when $k = 0$ and tends to the same value, $0.8\omega_p$, as in the semi-infinite case. In our calculation it becomes degenerate for large k with a mode that we call the odd multipolar mode. This last mode has its origin at the plasma frequency ω_p. The reason for the shift down of the origin of the ω_+ mode can be stated as follows: two new modes that are not usually present in other works appear and modify the classical origins of the remaining modes. Although this scheme is not the common one in semi-classical or fully quantum-mechanical calculations of collective excitations in metal slabs, it is the same found in some TDLDA results [22] and a similar behavior has been reported for plasmons in a simple-metal overlayer [23].

Figure 6.3 displays the dispersion relation of the first four bulk resonances. These

dispersion relations are qualitatively similar to those obtained by discretization of the z component of the momentum in a bulk plasmon dispersion relation but the slopes are flatter than those obtained with other methods, even classical, like the Boltzmann model [9]. This discrepancy must be attributed to the lack of terms in the kinetic energy functional given by Eq. 6.25 taking into account the gradient of the electronic density. The discretization of the bulk resonances is due to the finite size of the slab in the z axis because as bulk resonances are standing waves their associated wavelength must fulfill a matching condition that only allows the existence of a discrete set of modes. We would like to remark that the relative positions of the origins of the upper bulk modes, well above the scale on Fig. 6.3, should not be given a quantitative meaning. A comparison with simple models, like the one of Ref. [9], shows that this result becomes worse as we consider higher resonances.

Further insight can be gained looking at the sudden approximation of the density fluctuation for each mode. Each one of the four discontinuities in the ground-state electronic profile produces an avoidable discontinuity in the density fluctuation. In those points the first derivative of the density fluctuation is also discontinue. A more realistic profile should be used to obtain quantitatively correct results but as the double-step model includes the most important physical aspects, such as diffuseness, qualitative information like symmetry and number of nodes is reliable. Anyway, this simple model allows to calculate the arrays $\mathcal{K}$ and $\mathcal{B}$ analytically. The computational effort required to implement a soft density profile would be much greater, since a numerical calculation of these arrays should be done for each point of the dispersion relation.

The density fluctuation of the ω_- and the ω_+ modes is shown in Fig. 6.4. The symmetry and the number of nodes of this modes are the same as those of the even multipole and the odd multipole respectively, in Fig. 6.5. The density fluctuation of these modes is concentrated at the surface and the main difference between them is that in the multipole modes the density fluctuation is not constant in the middle of the slab. This result, that seems to contradict the paradigm according to which multipole plasmons are bulk resonances of the selvedge region, will be discussed later on. It is observed that the decreasing oscillating amplitude that multipole plasmons show in a semi-infinite medium is not found in our calculation for thin slabs, but we would expect to find it for widths larger than the ones that have been considered in this work. Also, the integral along the z-axis of the density

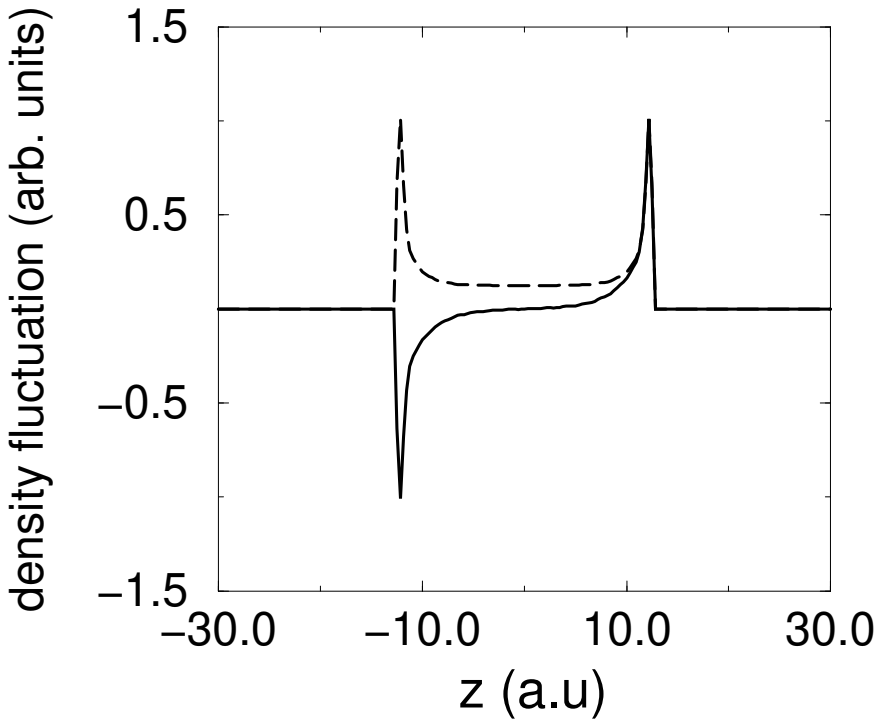

Figure 6.4: Sudden approximation to the density fluctuation calculated as explained in the text for a sodium slab ($d = 40a_0$). The dashed line represents the ω_- mode while the solid line is the ω_+ mode.

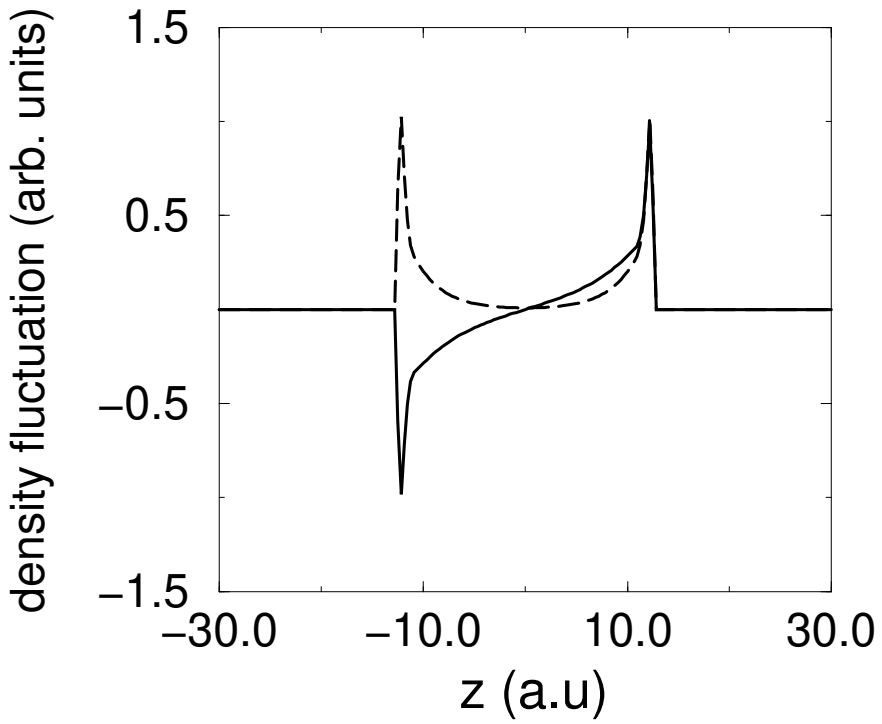

Figure 6.5: The dashed line represents the density fluctuation of the even multipole mode in the same case as Fig. 6.4. The solid line is the odd multipole mode.

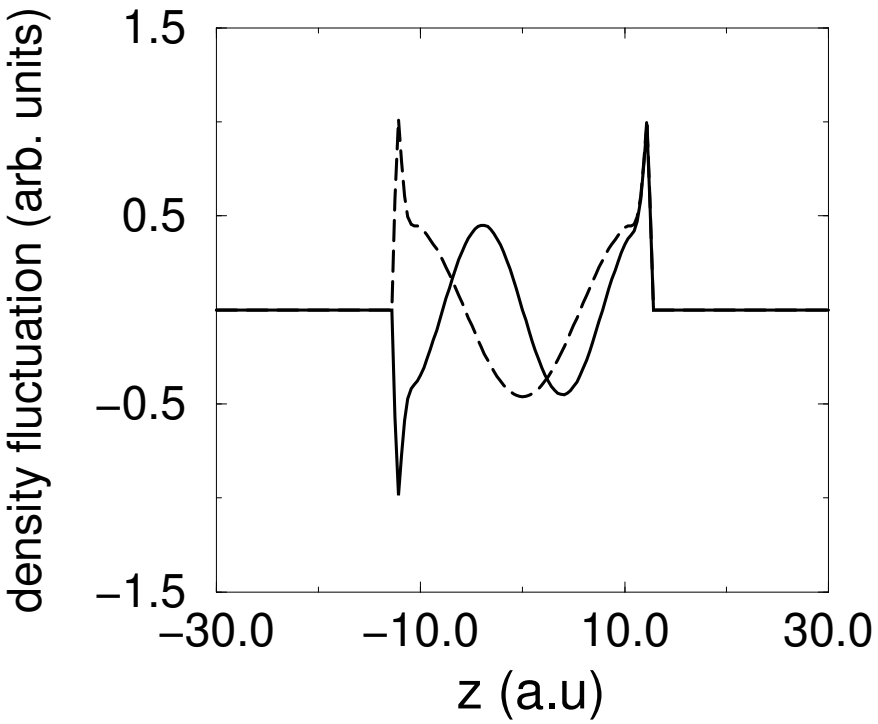

Figure 6.6: Density fluctuation of the two lowest bulk plasmon resonances for the same system as Fig. 6.4. The dashed line represents the lowest resonance and the solid line represents the next resonance.

fluctuation is different from zero. Lets recall that in a semi-infinite system this integral tends to 0. The density fluctuation of the bulk resonances is represented in Figs. 6.6 and 6.7. The first resonance has two nodes and presents the typical profile of a standing wave across the slab. In fact, we can label a resonance with its number of nodes as every resonance has one more node than the one which lies beneath it.

Taking advantage of the transparency of the method, the contributions of the kinetic and the Coulomb parts of the Hamiltonian to the dispersion relation are represented in Fig. 6.8. The ratio between the Coulomb and the kinetic energy differs for each mode. The ω_- mode has a negligible kinetic energy in front of the Coulomb contribution while they

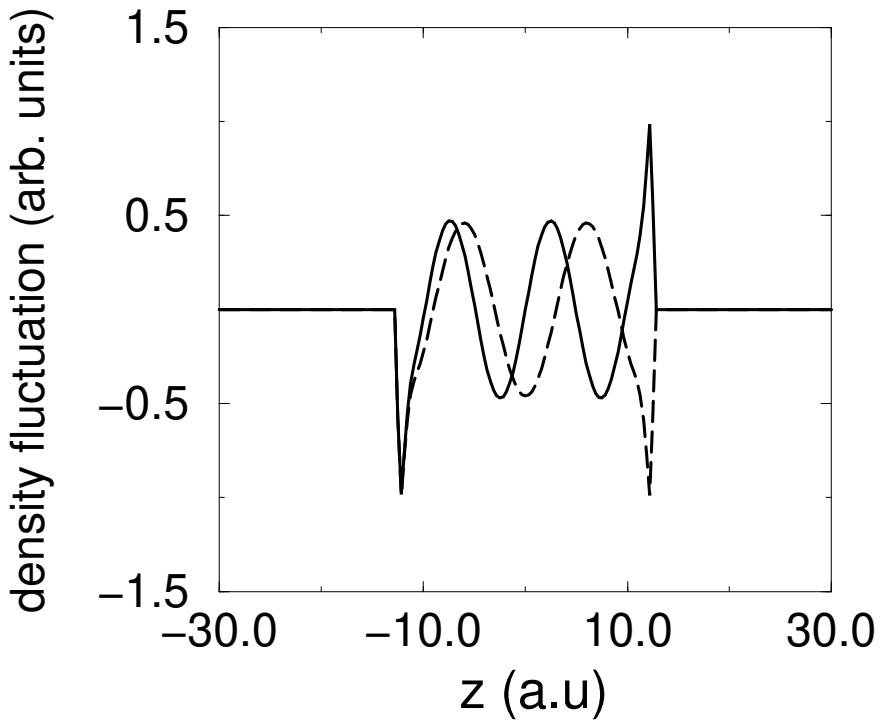

Figure 6.7: The dashed line is the third bulk resonance with lowest energy and the solid line is the fourth. Calculation for the same system as previous cases.

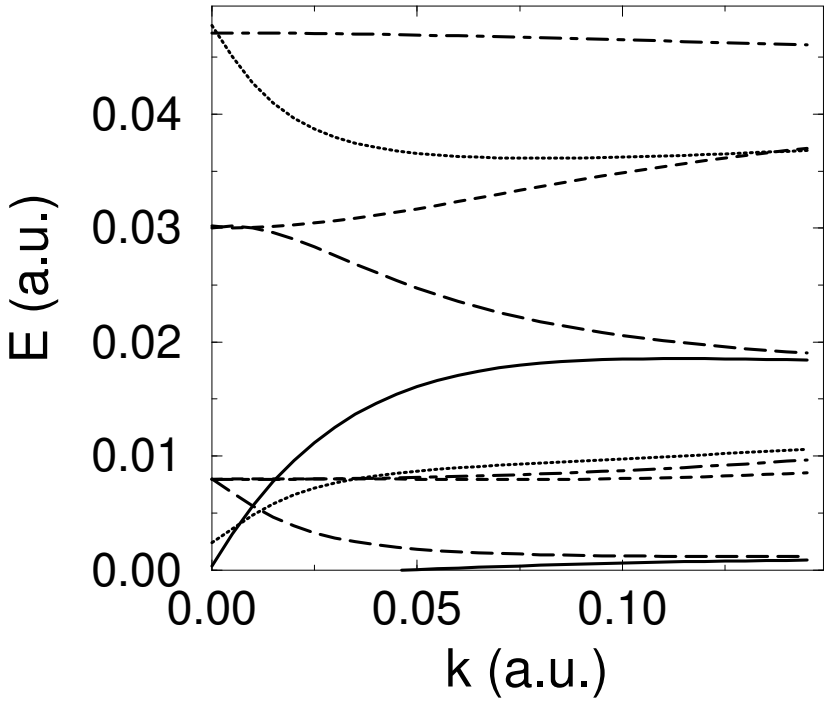

Figure 6.8: The energy contributions of the same mode are plotted in the same type of line. The upper one is the Coulomb contribution and the lower one is the kinetic contribution. The solid line corresponds to the ω_- mode, the long-dashed to the $\omega+$ mode, the short-dashed to the even multipole mode, the dotted line to the odd multipole mode and the dot-dashed line corresponds to the lowest bulk resonance. The calculations are made for the same case as Fig. 6.2.

are comparable in the ω_+ mode, in the region where they are far from being degenerate. In fact, the ω_+ mode has kinetic contribution even at $k = 0$, unlike the ω_- mode. As explained earlier, damping is significant when the kinetic contribution becomes important, so we can predict that this mode will not be so cleanly observed as the ω_-. As a direct consequence of the large kinetic contribution is that we can expect the ω_+ mode to have a notoriously bad convergence, as it really happens in our calculation. This also happens in TDLDA calculations [21], that show how peaks in the excitation spectra are noticeably wider for the ω_+ mode than for the ω_-. In the case of the multipole plasmons, the kinetic contribution is smaller than the Coulomb but significant, in the small wavelength limit, where both modes do degenerate. In this region their features should be similar to those of the multipole plasmon in the semi-infinite medium, which is known to be severely damped even for values of k below the Landau cutoff [26]. In the large wavelength limit their behavior is completely opposite: the damping of the even multipole increases slightly and tends to be the same as that of the ω_+ plasmon. Instead, the odd multipole plasmon increases its Coulomb contribution and, according to our results, is scarcely damped in the low-k region —even less that the first bulk resonance. The discussion of the relative importance of the contributions for large k would require a more accurate kinetic functional as the one used tends to underestimate its magnitude in this limit.

The dependence of the dispersion relation on the width d of the slab can be seen in Figs. 6.9 and 6.10. The ω_- and the ω_+ modes tend to degenerate when $k >> d^{-1}$ and the same is true for the even and the odd multipole modes. This is due to the fact that the symmetry of the mode is not relevant when the density fluctuation of two modes is concentrated on each one of the two faces of the slab and these are enough apart in comparison with the wavelength of the mode. Obviously, the thicker the slab, the smaller the value of k at which both plasmon modes do degenerate. The ω_- and the ω_+ modes degenerate at an energy close to $\omega_p/\sqrt{2}$. In the semi-infinite medium limit their dispersion relations will join at $k = 0$ and they will form the well known surface plasmon. The even and the odd multipole modes will also join in a unique multipole plasmon mode [40] for extremely large slabs. In Fig. 6.10 it can be seen that the dispersion relation of the odd plasmon mode is much more affected by the change of the width of the slab than that of the even multipole mode, so the dispersion relation of the multipole mode in a semi-infinite medium will be closer to that

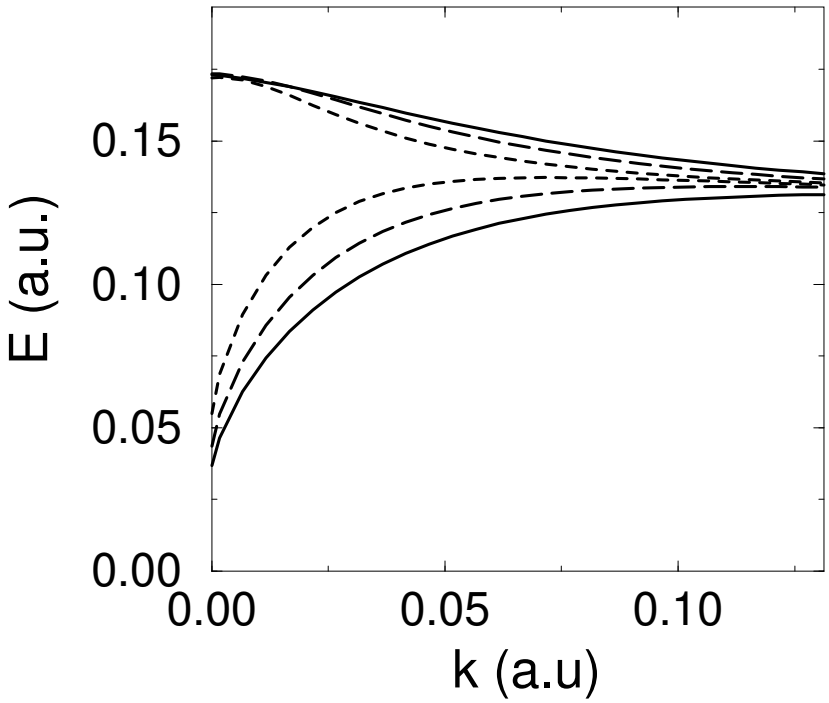

Figure 6.9: Dispersion relation of the ω_- and the ω_+ modes for a sodium slabs of different widths. The solid line represents a width $18a_0$, the long-dashed line stands for $25a_0$ and the short-dashed line is the result for $40a_0$.

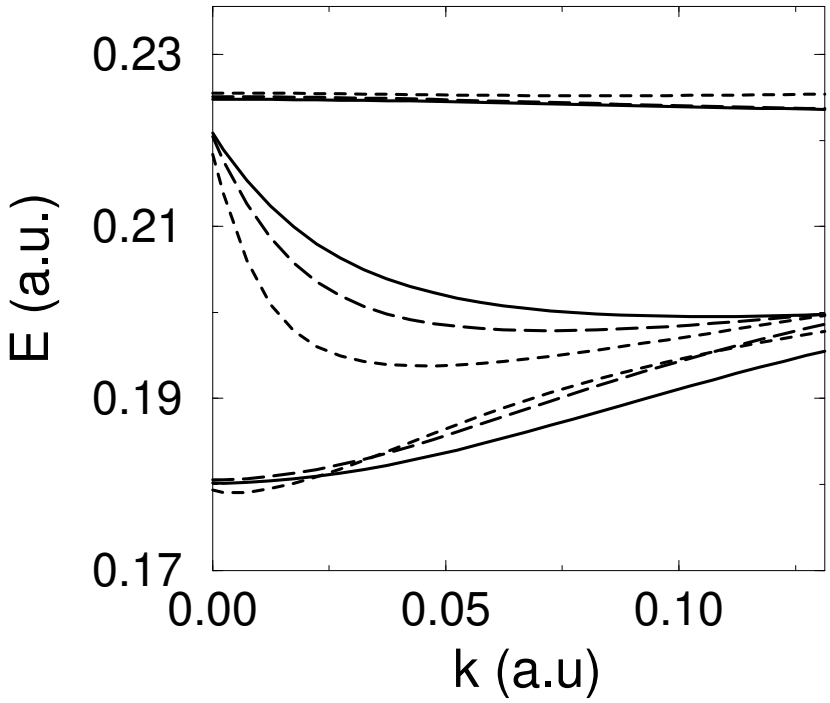

Figure 6.10: Same as Fig. 6.9 but with the even and the odd multipole plasmon modes.

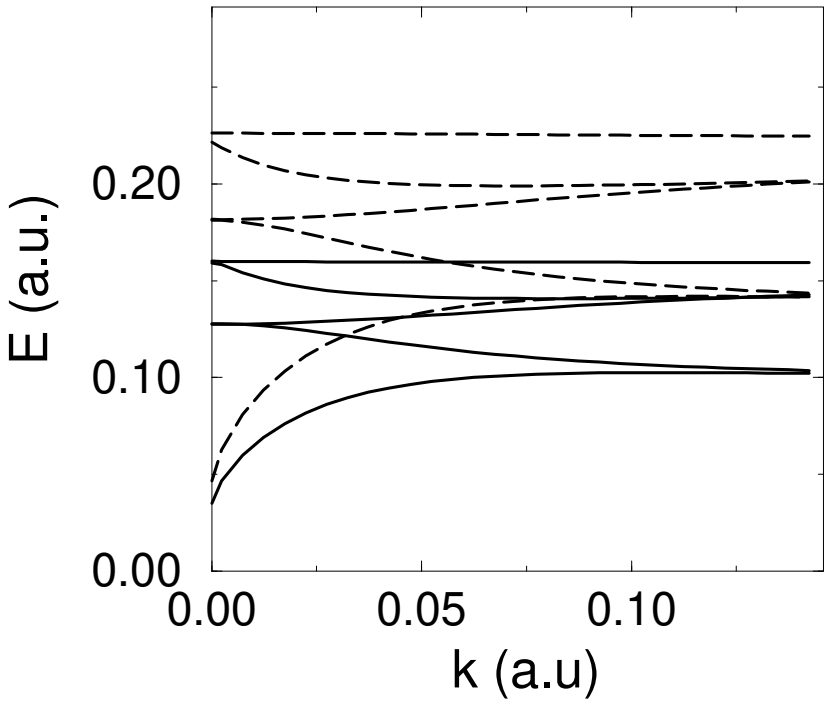

Figure 6.11: Dispersion relation of the plasmon modes of two slabs of different metals and the same width ($d = 25a_0$). The solid line corresponds to a potassium slab. The dashed line is used for the sodium slab.

of this last mode.

In Fig. 6.11 the dispersion relations of two slabs with a different electronic density are plotted. The sodium slab has a greater electronic density and the energy of its modes is higher than those of the potassium slab. Surface modes degenerate for lower values of k and larger values of M are needed in slabs of this last metal.

In a high-density metal plasmon modes have higher energies. Both the kinetic and the Coulomb contribution are greater but as the kinetic functional has a $n_b^{5/3}$ dependence and the Coulomb contribution is proportional to n_b^2, the importance of the Coulomb contribution grows as $n_b^{1/3}$. The value of the bulk density also influences the dispersion relation of the

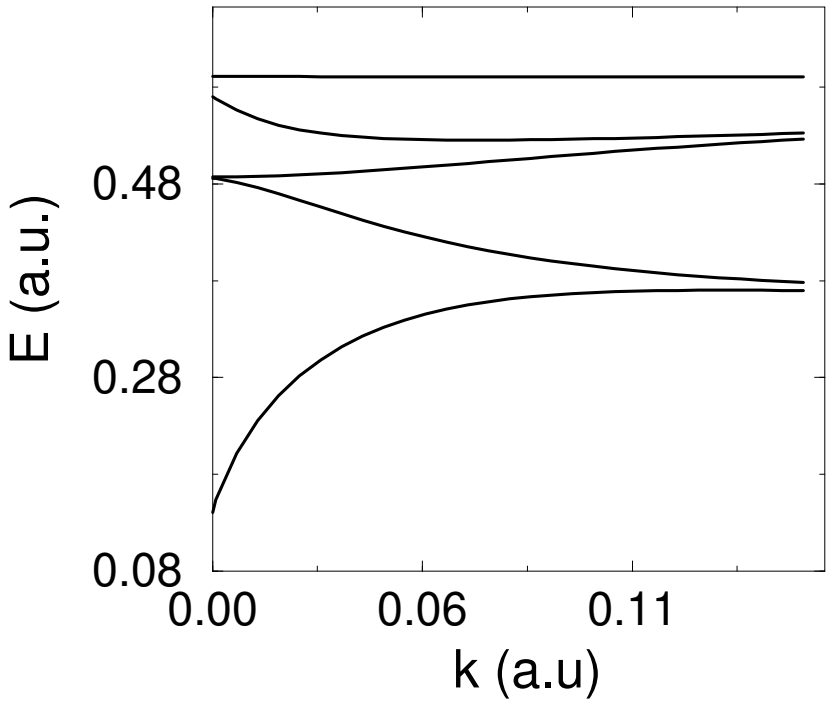

Figure 6.12: Dispersion relation of the plasmon modes of an aluminium slab. The width is $25a_0$.

plasmons, in an indirect way, through the diffuseness of the electronic profile, that depends mainly on this magnitude. As discussed earlier, these two factors have an important effect on the convergence of the expansion series. A plot of the plasmon modes for an aluminium slab is displayed in Fig. 6.12. Besides the rise of the energies of the modes we can notice a greater gap between the origin of the odd multipole mode and the first bulk resonance. This is not due directly to the higher electronic density but to the steeper slope of the electronic profile as will be seen soon.

In order to distinguish the effects due to the change of electronic density and those caused by a different diffuseness of the profile, we studied three systems where we changed only the length of the intermediate step, keeping the bulk density constant. Results are

represented in Fig. 6.13. If the length of the step is reduced, the origins of the ω_+ and of the even multipole tend to rise, they are no longer at $0.8\omega_p$, and a gap appears between them. It is clear that the origin $0.8\omega_p$ depends strongly on the diffuseness of the surface and can be used as a test on how realistic an electronic profile is. The odd multipole and the first bulk resonance also have higher energies for $k = 0$ and the gap between their origins also increases. The slopes of the dispersion relations of the even and the odd multipole modes suffer a significant change and are closer than before. Finally, for a system with no diffuseness, the origin of the ω_+ mode has risen up to ω_p and the two dispersion relations of the multipole modes are in the same place as the first and second bulk resonances in the previous systems. The result of the reduction of the diffuseness is that even and odd multipole modes merge into the first two bulk resonances.

Although these results correspond to unphysical values of the diffuseness, they show that the accepted paradigm about multipole plasmons is incomplete. Multipole plasmons are commonly considered standing waves in the selvedge region but calculations of their density fluctuation [26, 40], in the case of the semi-infinite medium, reveal that they are extended over a wider region. A similar situation appears in TDLDA calculations of slabs [22]. In Fig. 6.5 it can be seen that the density fluctuation varies over the whole length of the slab, in contrast with that of the ω_- and $\omega+$ that does not change outside the surface of the slab. This makes possible a smooth variation, as the diffuseness is reduced, from these profiles to those presented in Fig. 6.6, which correspond to the first two bulk resonances.

The operator $e^{ikR}e^{|k|z}$ can be used to represent the Fourier component of the electric potential due to a point charge placed outside the slab that couples to the plasmons whose momentum parallel to the surface is k. Therefore, it can be used to model the interaction of the system with a classical electron, although this approach has some limitations. The Hamiltonian given by Eq. 6.20 corresponds to a free system. Sum rules assume that the ground state of this free system is perturbed by the external operator but do not include the effects due to the response of the system induced by this operator. As a consequence, the following discussion must be restricted to the large wavelength limit or, in other words, for low values of the transfered momentum.

In Fig. 6.14 it can be seen the contribution of each one of the surface modes and the eight lowest bulk resonances to the m_1 sum-rule of the previous operator, according to Eq.

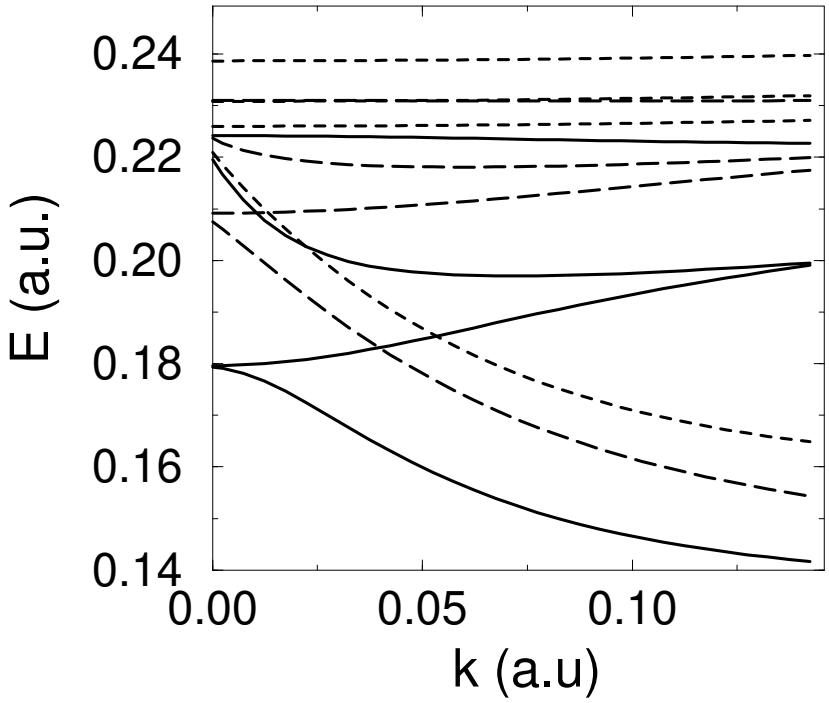

Figure 6.13: Dispersion relation of the four modes with lowest energy calculated with different δ parameters. The width of the slab is $18a_0$ and it is made of sodium. The periodicity of the Q operator is taken to be $L = 28$. The solid line represents the modes with an intermediate step set to the realistic value $\delta = 2.13a_0$. The long-dashed lines are calculated with $\delta = 1a_0$ while while short-dashed lines stand for a system with $\delta = 0$. The number of terms M considered in each case is 35, 35 and 25 respectively.

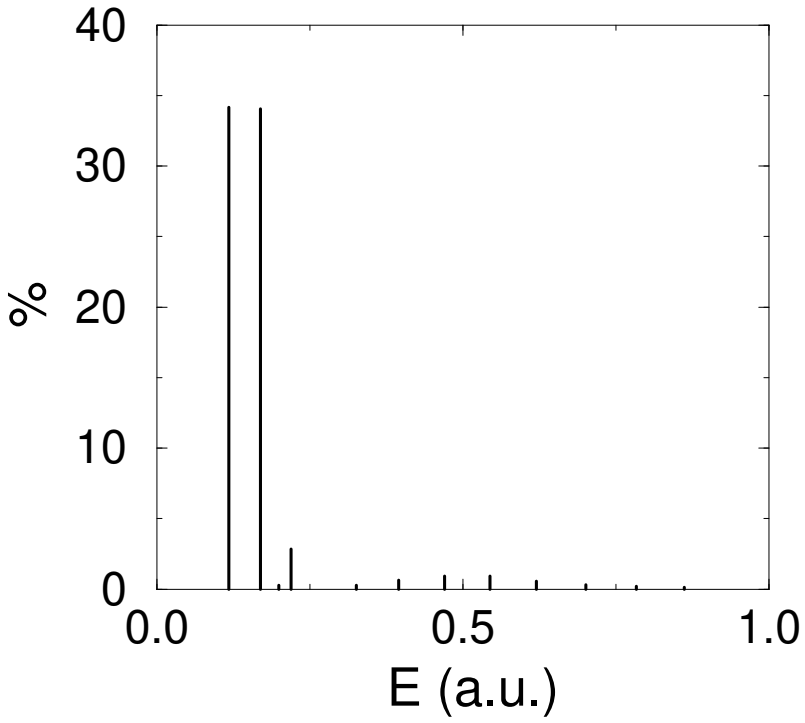

Figure 6.14: Contribution to the m_1 sum-rule of the external operator specified in the text. The width of the sodium slab is $d = 18a_0$ and the momentum is $k = 0.05a.u.$

6.22. The m_1 contribution to the sum-rule is used instead of the strength function as it gives a better insight of the transition probability for a set of discrete excited states. A sharp peak in the strength function will be revealed by a dominant contribution to the m_1 sum-rule

Clearly the major contribution comes from the surface modes ω_- and ω_+, while the two multipole modes can hardly be seen. The results from the upper modes must be taken with caution as the peak lies in the region were the orthogonalization of the modes is not complete.

A mode will be observable if it has a distinct peak in the strength function given by Eq. 6.23. The existence of such a peak for a certain mode depends on three factors: the lifetime of the mode, the physical process that is used to excite the mode and the presence of larger nearby peaks. The response calculated from Eq. 6.22 corresponds to plasmons with an infinite lifetime, but the other two factors are included in the response and can be discussed. The observability of the two multipole plasmons in experiments that involve excitation from external charges will be difficult, in part because the transition probability will be small, but the main reason is that the peaks of the ω_- and ω_+, much more prominent according to its contribution to m_1, will nearly wash out the peaks of the even and odd multipole modes. This difficulty can be overcome using optical methods, like photo-emission, to detect multipole modes in an indirect way. As surface plasmons are not optically active, the peak of the multipole modes would stand alone and, therefore, their effects would be visible.

Finally, in Fig. 6.15 a comparison between our calculation and some previous works is presented. The main difference between Local RPA and TDLDA as compared with an hydrodynamical calculation [90] and a local optics calculation [102] is the presence of two additional modes, but this is due to the fact that no surface diffuseness has been introduced in the last two calculations. Although it has not been included in the figure, when the diffuseness is set to zero, the local RPA results overlaps perfectly with the local optics dispersion relation. The hydrodynamical model calculation presents a much steeper slope of the dispersion relation since a kinetic contribution proportional to the gradient of the electronic density is included.

The local RPA and the TDLDA results show a good qualitative agreement, but in the

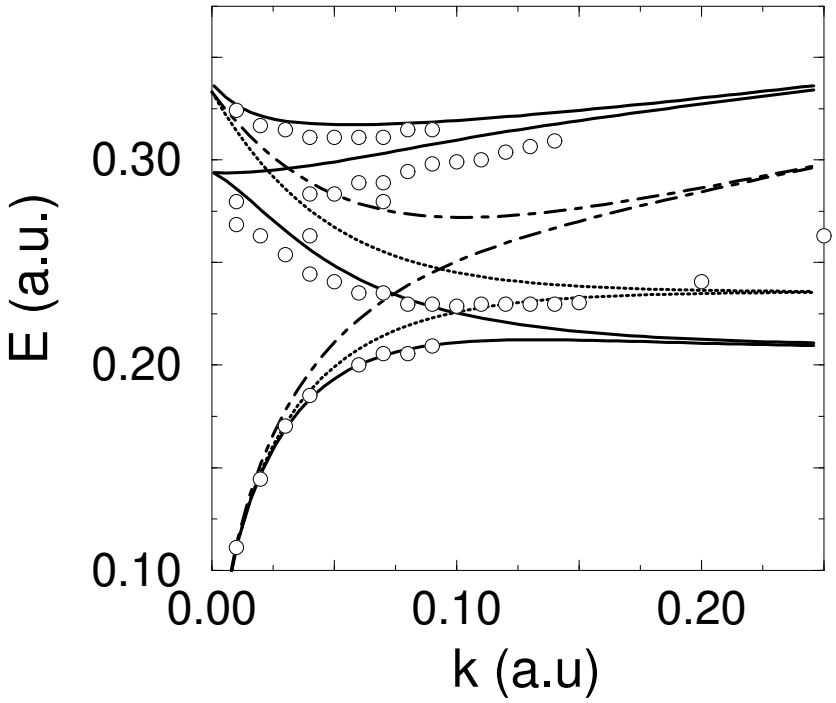

Figure 6.15: Comparison between the dispersion relations obtained by several methods for a generic simple-metal (see the last column of the table for its characteristics). The solid line represents the local RPA curve, but without any estimation of the exchange and correlation energy to allow a better comparison with classical methods. The dotted line stands for local optics and the dashed line for the hydrodynamical model. The circles are TDLDA results.

short wavelength limit the more accurate treatment of the kinetic energy in the TDLDA approach yields larger values for the energy and a quadratic shape of the dispersion relation. Also, the origin of the even multipole plasmon mode seems to lie at a slightly lower energy. This is due to the differences in the ground state used in each calculation.

6.4 Summary and conclusions

We have succeeded in developing a semi-classical calculation that includes as solutions the even and the odd multipole modes, which are not usually considered in related calculations. In the semi-infinite medium they are brought together into the by now well studied multipole plasmon mode. These multipole modes modify the classical origin of the ω_+ mode and are closely dependent on the diffuseness of the electronic profile. Their origin is shifted upwards when the diffuseness is reduced and they become bulk modes when it is set to zero. The study of the m_1 sum-rule of an external operator that stands for the electric potential of a point charge reveals that multipole plasmon modes are not excited by this operator, although a conclusive statement about this issue would a require a calculation including the response of the system induced by an approaching charge. The present work does not address the question whether with a more realistic model for the electronic profile the multipole plasmon modes would continue to be well-defined collective excitations. It is true that the softening of the profile could induce some damping in these modes but the great similarity between the selvedge region of the semi-infinite medium and that of a slab indicates that their properties should not be very different. In fact, some TDLDA calculations [22] support the existence of multipole plasmon modes in slabs.

The ω_- plasmon is far more observable for intermediate values of k than the ω_+ plasmon. This can be stated either examining the convergence of the results on the number of terms of the expansion series, or taking into account the relative contribution of the Coulomb and the kinetic energies. The bulk resonances closer to ω_p are also realistically described. The Thomas-Fermi density functional gives a too flat slope of the kinetic energy. The exchange and correlation contribution lowers the energy for large values of k.

Local RPA is an economic method for finding the excitation operator Q whenever well-defined collective excitations are expected. The size of the system determines, among other factors, the number of terms needed in the expansion series. If a strong damping acts on

the plasmon modes due to high diffuseness of the electronic profile, low electronic density or whatever other cause, convergence can be difficult to reach or even non-existent at all. Anyway it can be a useful method to complement more involved self-consistent calculations and, more important, to connect their results with those of macroscopic or hydrodynamical calculations.

Chapter 7

Conclusions and future developments

7.1 Conclusions

Local one-body operators have been used to study plasmon modes in simple-metal systems with plane symmetry. The formalisms employed can be derived from the RPA and semi-classical approximations have been made to simplify some calculations. The main conclusions of this work can be summarized as follows.

7.1.1 Ordinary surface plasmon modes

The results of a sum-rule approach have been compared with the ones of a calculation based on general non-local dielectric functions. For this reason, an explicit expression of the coefficient $\alpha_q(\omega)$ has been derived within a double-step model and has been applied using an RPA and a Linhard-Mermin dielectric functions. The critical role played by the step suggests that the use of a more realistic electronic profile is necessary within the dielectric formalism, especially for low density metals.

The operator that has been used in the sum-rule calculation is able to give a good agreement with experimental data. The best results are obtained for low-density metals like sodium or potassium. For high-density metals, like aluminium, a Linhard-Mermin dielectric treatment is more adequate.

A simple analytical approximation has been used to modelize the electronic density

profile. The comparison of sum-rule results with experimental data has been used to obtain appropriate parameters for sodium and potassium. These parameters can be useful in future spectroscopic applications.

In the case of ordinary surface plasmon modes, the dispersion relation is dominated by the Coulomb interaction for low values of the momentum parallel to the surface k. Instead, the main contribution for large momenta comes from the kinetic term.

For dense metals, such as aluminium, the electronic profile at the surface plays a minor role and the dispersion relation is not very sensible to the density profile. The contribution of the kinetic term is more significant than for low metallic densities. In this last case, the Coulomb interaction is the dominant part and the dispersion relation is strongly dependent on the electronic density.

7.1.2 Multipole surface plasmon modes

In order to excite multipole plasmons, the external excitation operator has to depend on an additional parameter. The operator that has been employed yields results close to experimental data. This extra parameter τ can be interpreted as the momentum in the z-direction of a standing wave.

Predictions about the observability of multipole plasmons can be made paying attention to the interplay between kinetic and Coulomb energies. The Coulomb contribution develops resonant behavior for a given value of k at discrete values of τ. Only the multipole mode that corresponds to the lowest of these discretized values of τ turns out to be observable. The remaining resonances are masked by the kinetic contribution.

This resonant structure is washed out by the kinetic contribution for increasing k values, even if they are smaller than the Landau damping cutoff.

Exchange and correlation effects reduce the slope of the dispersion due to the weakening of the Coulomb interaction.

It has not been possible to find an analytical relation between k and τ although for low k-values τ is approximately twice as k. For large k-values τ depends on the surface profile. This happens when the associated wavelength of k becomes comparable to the surface size.

Our approach is not able to explain on its own why multipole modes are not visible in aluminium but everything tends to suggest that the softening of the electronic profile at

the surface produces an effective strong damping mechanism that extinguishes the mode.

7.1.3 Plasmon modes of a slab

The operator considered, that has been calculated variationally, is able to excite the whole spectrum of a metal slab, including two multipole modes, for the electronic profile considered. The appearance of these modes in the spectrum modifies the classical origin of the ω_+ plasmon. Bulk resonances are also realistically described.

Multipole plasmons in a slab are closely dependent on the diffuseness of the electronic profile. For realistic values of the diffuseness the origin of their dispersion relation is placed at $0.8\omega_p$ and it becomes closer to ω_p as the diffuseness is reduced. Also the shape of the dispersion curve becomes more similar to those of the bulk resonances when the diffuseness has lower values.

A soft electronic profile would be needed to obtain a satisfactory density fluctuation. It would be also useful to discuss the observability of the multipole modes.

The ω_- plasmon is far more observable for intermediate values of k than the ω_+ plasmon. This conclusion follows from the convergence of the results on the number of terms of the expansion series and from the relative contribution of the Coulomb and the kinetic energies.

The Thomas-Fermi functional that has been used gives a too flat slope of the kinetic energy. The exchange and correlation contribution lowers the energy for large values of k.

The number of terms needed in the expansion series depends, among other factors, on the size of the slab. As a rule of thumb, more terms are needed in those situations where a strong damping is expected, like low electronic density or high diffuseness of the electronic profile.

7.2 Future developments

From our point of view, this work can be continued along many promising lines. In the following we comment briefly some of the most remarkable.

In the slab calculation, the quantum treatment of the kinetic term should be kept further, following the same scheme as in the semi-infinite surface calculations. The dispersion relation would then show a correct behavior for large k. Also a realistic density profile should be introduced in order to obtain reliable density fluctuations.

For some systems it can be easy to infer the form that the external excitation operator should have but for many others this is a difficult task. In these cases the variational local RPA method can be used to obtain the whole spectrum of collective excitations. An interesting system of this kind is a simple metal overlayer over a substrate because experimental data is already available [27]. Also the parabolic quantum well should be investigated and results compared with experimental ones [101]. A more speculative possibility is the search of new multipole modes with a higher order multipolarity in multilayer systems [13].

There have been several recent models used to calculate the effect of the bulk band structure on the surface plasmon dispersion [24, 25]. Their implementation instead of the jellium model would allow to treat transition metals within the sum rule approach. As a consequence interesting phenomena could be investigated with this formalism, like the anisotropic dispersion in silver crystals [112].

Finally, a theoretical effort should be made to understand better some features of the variational local RPA method [36], mainly those concerned with the error produced by taking a finite series.

Appendix A

Atomic units, effective mass and dielectric constant

A.1 Dimensionality of equations in atomic units

Let m be the electron mass and ϵ_0 the dielectric constant of the vacuum. Any equation can be expressed in atomic units by

$$\hbar = m = \frac{e^2}{4\pi\epsilon_0} = 1 \tag{A.1}$$

The opposite is not so easy. Some work is required to express an equation that is given in atomic units in any other units. The more general type of energy functional, that is likely to be found in an equation, has the form

$$E[n, z, k], \tag{A.2}$$

where all these quantities are in atomic units. To regain the constants that we set to 1, we rewrite the functional as

$$hE[na^3, \frac{z}{a}, ka]. \tag{A.3}$$

The constants a and h are combinations of elementary constants

$$a = \frac{\hbar^2 4\pi\epsilon_0}{me^2}, \tag{A.4}$$

$$h = \frac{e^2}{4\pi\epsilon_0 a}. \tag{A.5}$$

The generalization to functionals with another dimensionality is straightforward.

A.2 Effective mass and dielectric constant

An effective mass and a dielectric constant can be implemented in two different ways. In the first one, the functional A.2 has to be modified

$$\frac{m^*}{\epsilon/\epsilon_0} E[n\frac{(\epsilon/\epsilon_0)^3}{(m^*)^3}, z\frac{m^*}{\epsilon/\epsilon_0}, k\frac{\epsilon/\epsilon_0}{m^*}]. \tag{A.6}$$

In this expression $m^* = m_{eff}/m$. If we want express this functional in terms of the elementary constants, we only have to follow the procedure described previously.

A second way leaves the equations written in atomic units unmodified

$$\hbar = m^* = \frac{e^2}{4\pi\epsilon} = 1. \tag{A.7}$$

Instead, the definitions of a and h are changed

$$a = \frac{\hbar^2 4\pi\epsilon}{m_{eff}e^2}, \tag{A.8}$$

$$h = \frac{e^2}{4\pi\epsilon a}. \tag{A.9}$$

If any calculation is done with the functional in atomic units, the parameters should be given in the system defined by A.7. Often they are tabulated in the units defined by A.1. A conversion should be made in this case

$$n_b^* = n_b\frac{(\epsilon/\epsilon_0)^3}{(m^*)^3}, \tag{A.10}$$

$$d^* = d\frac{m^*}{\epsilon/\epsilon_0}, \tag{A.11}$$

$$k_f^* = k_f\frac{\epsilon/\epsilon_0}{m^*}. \tag{A.12}$$

The parameters with an asterix are the one to be used.

Appendix B

Sum rules of the operator given by $q = e^{i\vec{k}\vec{R}} e^{k^2 z^2} cos(\tau z)$

The expressions are given per unit area XY and are valid for an arbitrary electronic density $n(z)$. From a dimensional analysis, we have incorporated the effective electronic mass m^* (See Appendix A) to the energy expression $\sqrt{m_3/m_1}$ and have assigned it to the m_3 term. We obtain

$$m_1 = \int_{-\infty}^{\infty} dz\, e^{-2k^2z^2}\{n(z)[k^2+\tau^2+4k^4z^2][\cos(2\tau z)+1] + n'(z)\tau\sin(2\tau z)\}, \tag{B.1}$$

$$\begin{aligned}
m_3(T) = {} & \frac{1}{3m^{*2}}\int_{-\infty}^{\infty} dz\, \sigma(z)\, e^{-2k^2z^2}\{8k^2\tau\sin(2\tau z)[a_{11}z + a_{13}z^3] + \\
& \cos(2\tau z)[a_{20} + a_{22}z^2 + a_{24}z^4] + a_{30} + a_{32}z^2 + a_{34}z^4\} \\
& + \frac{1}{4m^{*2}}\int_{-\infty}^{\infty} dz\, n(z)\, e^{-2k^2z^2}\{4k^2\tau\sin(2\tau z)[b_{11}z + b_{13}z^3 + b_{15}z^5] \\
& + \cos(2\tau z)[b_{20} + b_{22}z^2 + b_{24}z^4 + b_{26}z^6] + b_{30} + b_{32}z^2 + b_{34}z^4 + b_{36}z^6\} \\
& + \frac{1}{4m^{*2}}\int_{-\infty}^{\infty} dz\, n'(z)\, e^{-2q^2z^2}\{\sin(2\tau z)[c_{10} + c_{12}z^2 + c_{14}z^4] \\
& + \cos(2\tau z)[c_{21}z + c_{23}z^3 + c_{25}z^5] + c_{31}z + c_{33}z^3 + c_{35}z^5\},
\end{aligned} \tag{B.2}$$

$$\begin{aligned}
& m_3(C) = \frac{2\pi}{m^*}\int_{-\infty}^{\infty} dz\, n(z)\, e^{-2k^2z^2}\{\tau\sin(2\tau z)[k^2+\tau^2-12k^4z^2] \\
& +2k^2\cos(2\tau z)[(k^2+3\tau^2)z - 4k^4z^3] + 2k^2[(k^2-\tau^2)z - 4k^4z^3]\} \\
& \int_{-\infty}^{\infty} dz'\,[n(z) - n_j(z)]sgn(z'-z) \\
& + \frac{4\pi}{m^*}\int_{-\infty}^{\infty} dz\, n(z)n_j(z)\, e^{-2k^2z^2}\{4k^2\tau z\sin(2\tau z) + [4k^4z^2 - \tau^2]\cos(2\tau z) + 4k^4z^2 + \tau^2\}
\end{aligned}$$

$$+\frac{4\pi k}{m^*}\int_{-\infty}^{\infty}dz\ \int_{-\infty}^{z}dz'\ n(z)n(z')\,e^{-k^2(z^2+z'^2)}e^{-k(z-z')}\{2\tau k\sin[\tau(z-z')]$$
$$[k(z-z')+1]-2\tau k^2\sin[\tau(z+z')](z+z')+\cos[\tau(z-z')]$$
$$[k^2-\tau^2-4k^4zz'+2k^3(z-z')+\cos[\tau(z+z')]$$
$$[k^2+\tau^2-4k^4zz'+2k^3(z-z')]\} \tag{B.3}$$

$$m_3(ex+cor)=\frac{1}{3m^*}\int_{-\infty}^{\infty}dz\,e^{-2k^2z^2}\left[-\left(\frac{3}{\pi}\right)^{1/3}n^{1/3}(z)+c\frac{gn^{2/3}(z)+2n^{1/3}(z)}{(gn^{1/3}+1)^3}\right]$$
$$(\cos(2\tau z)\{2k^2n'(z)[3(k^2+\tau^2)z-4k^4z^3]$$
$$+n(z)[(3k^2+\tau^2)^2-24k^4(k^2+\tau^2)z^2+16k^8z^4]\}$$
$$+\sin(2\tau z)\{\tau n'(z)[3k^2+\tau^2-12k^4z^2]$$
$$+8k^2\tau n(z)[-(3k^2+\tau^2)z+4k^4z^3]\}-2k^2n'(z)$$
$$[(-3k^2+\tau^2)z+4k^4z^3]+n(z)[(3k^2+\tau^2)^2$$
$$+8k^4z^2(-3k^2+\tau^2)+16k^8z^4]), \tag{B.4}$$

where

$$\sigma(z)=\frac{3}{5}(3\pi^2)^{2/3}n^{5/3}(z)+\frac{\beta}{4}\frac{n'^2(z)}{n(z)}, \tag{B.5}$$

$$a_{11}=k^2-\tau^2, \tag{B.6}$$

$$a_{13}=4k^4, \tag{B.7}$$

$$a_{20}=13k^4-2k^2\tau^2+\tau^4, \tag{B.8}$$

$$a_{22}=8k^4(k^2-3\tau^2), \tag{B.9}$$

$$a_{24}=16k^8, \tag{B.10}$$

$$a_{30}=13k^4+20k^2\tau^2+3\tau^4, \tag{B.11}$$

$$a_{32}=8k^4(k^2+2\tau^2), \tag{B.12}$$

$$a_{34}=16k^8, \tag{B.13}$$

$$b_{11}=43k^4+26k^2\tau^2+3\tau^4, \tag{B.14}$$

$$b_{13}=-8k^4(13k^2+5\tau^2), \tag{B.15}$$

$$b_{15}=48k^8 \tag{B.16}$$

$$b_{20}=9k^6-43k^4\tau^2-13k^2\tau^4-\tau^6, \tag{B.17}$$

$$b_{22} = 4k^4(43k^4 + 78k^2\tau^2 + 15\tau^4), \tag{B.18}$$

$$b_{24} = -16k^8(13k^2 + 15\tau^2), \tag{B.19}$$

$$b_{26} = 64k^{12}, \tag{B.20}$$

$$b_{30} = 9k^6 + 55k^4\tau^2 + 15k^2\tau^4 + \tau^6, \tag{B.21}$$

$$b_{32} = 4k^4(43k^4 + 2k^2\tau^2 + 3\tau^4), \tag{B.22}$$

$$b_{34} = -16k^8(13k^2 - 3\tau^2), \tag{B.23}$$

$$b_{36} = 64k^{12}, \tag{B.24}$$

$$c_{10} = -2\tau^5 - 26k^4\tau - 12k^2\tau^3, \tag{B.25}$$

$$c_{12} = 114k^6\tau + 80k^4\tau^3, \tag{B.26}$$

$$c_{14} = -160k^8\tau, \tag{B.27}$$

$$c_{21} = -52k^6 - 72k^4\tau^2 - 20k^2\tau^4, \tag{B.28}$$

$$c_{23} = 96k^8 + 160k^6\tau^2, \tag{B.29}$$

$$c_{25} = -64k^{10}, \tag{B.30}$$

$$c_{31} = -52k^6 - 32k^4\tau^2 - 12k^2\tau^4, \tag{B.31}$$

$$c_{33} = 96k^8 - 64k^6, \tag{B.32}$$

$$c_{35} = -64k^{10}, \tag{B.33}$$

$$c = -\frac{0.88}{3}\left(\frac{4\pi}{3}\right)^{1/3}, \tag{B.34}$$

$$g = \frac{7.8}{m^*}\left(\frac{4\pi}{3}\right)^{1/3}, \tag{B.35}$$

$$n_j(z) = n_b\theta(-z). \tag{B.36}$$

Appendix C

Evaluation of mixed sum-rules

In this appendix we will present the formulae which were used in the solution of Eq. 6.13.

The first object to compute, that is $\mathcal{B}$, is a straightforward calculation;

$$\mathcal{B}_{(k,p),(k',p')} = A(k^2 + pp') \int dz \exp\left(-i(p-p')z\right) n(z) \tag{C.1}$$

To compute $\mathcal{K}_{\alpha\beta}$ we start by considering;

$$\begin{aligned}
\mathcal{M}_{\alpha\beta} &\equiv \mathcal{M}_{\alpha\beta}{}^{k} + \mathcal{M}_{\alpha\beta}{}^{ex} + \mathcal{M}_{\alpha\beta}{}^{c} \\
&= \langle\Phi_0| \exp\eta\left([Q_\alpha, H]\right) \exp\left(\eta'\left[Q_\beta, H\right]\right) \left(H_k + H_{ex} + H_c\right) \times \\
&\quad \exp\left(-\eta'\left[Q_\beta, H\right]\right) \exp\left(-\eta\left[Q_\alpha, H\right]\right) |\Phi_0\rangle \\
&\equiv \langle\eta\eta'|H_k + H_{ex} + H_c|\eta\eta'\rangle
\end{aligned} \tag{C.2}$$

The previous object is useful as it is connected to the one we are interested in through formulae;

$$\mathcal{K}_{\alpha\beta} = \left(\frac{\partial^2}{\partial\eta\partial\eta'}\mathcal{M}_{\alpha\beta}\right)_{\eta=0,\eta'=0} \tag{C.3}$$

At this point we have reduced the problem of calculating the expressions in Eq. 6.15 to the evaluation of expressions such as $\langle\eta\eta'|F(n)|\eta\eta'\rangle$ which are still quite intractable. Some approximations are needed to go any further. We will approximate terms like this one as

$$\langle\eta\eta'|F(n)|\eta\eta'\rangle = F(\langle\eta\eta'|n|\eta\eta'\rangle) + ... \tag{C.4}$$

and keep just the first term.

The rest of the computation is straightforward but lengthy. We arrive at

$$\begin{aligned}
\mathcal{K}^{c}_{(k,p),(k,p')} &= 4\pi App' \int dz n(z)^2 \exp(-i(p-p')z) \\
&+2\pi A \int dz dz' n(z) n(z') \exp(-i(p-p')z) \exp(-|z-z'|k) \times \\
&\left(k^3 - pp'k + i(p+p')k^2 sgn(z-z')\right) \\
&-4\pi App' \int dz \left(n(z) - n_j(z')\right) n(z) \exp(-i(p-p')z) \\
&-2i\pi A \left(pp' + k^2\right) p' \int dz dz' \left(n(z) - n_j(z')\right) n(z) \exp(-iz(p-p')z) sgn(z-z')
\end{aligned} \tag{C.5}$$

The exchange term is easily computed with the result;

$$\begin{aligned}
\mathcal{K}^{ex}_{(k,p),(k,p')} &= A(k^2+p^2)(k^2+p'^2) \int dz n(z)^2 \frac{\partial^2 \epsilon_x(n)}{\partial n(z)^2} \\
&-(k^2+p'^2)p(p-p') \int dz \exp(-i(p-p')z) \left(n(z)\frac{\partial \epsilon_x(n)}{\partial n(z)} - \epsilon_x(n)\right)
\end{aligned} \tag{C.6}$$

The kinetic part does not show up any further complication as compared to the exchange term since where one reads ϵ_{ex} one substitutes $\tau(n)$ and the rest is exactly the same.

Bibliography

[1] D. Pines, Rev. Mod. Phys. **28**, 184 (1956).

[2] P. J. Feibelman, Prog. Surf. Sci. **12**, 287 (1982) and references therein.

[3] F. Forstmann and R. Gerhardts, Metal Optics Near the Plasma Frequency, in: Advances in Solid State Physics, Volume XXII, 291, J. Treusch (ed.), Vieweg, Braunschweig (1982) and references therein.

[4] H. J. Levinson, E. W. Plummer and P. J. Feibelman, Phys. Rev. Lett. **43**, 952 (1979).

[5] J. M. Elson and R. H. Ritchie, Phys. Rev. B **4**, 4129 (1971).

[6] J. G. Endriz and W. E. Spicer, Phys. Rev. B **4**, 4144 (1971).

[7] M. S. Chung, T. A. Callcott, E. Kretschmann and E. T. Arakawa, Surf. Sci. **91**, 245 (1980).

[8] R. Berndt, J. K. Gimzewski and P. Johansson, Phys. Rev. Lett. **67**, 3796 (1991).

[9] M. Anderegg, B. Feuerbacher and B. Fitton, Phys. Rev. Lett. **27**, 1565 (1971).

[10] R. Ray and G. D. Mahan, Phys. Lett. A **42**, 306 (1972).

[11] A. Sunjic, G. Toulouse and A. A. Lucas, Solid State Commun. **11**, 1629 (1972).

[12] R. H. Ritchie, Phys. Lett. A **38**, 189 (1972).

[13] E. W. Plummer, K. D. Tsuei and B. O. Kim, Nucl. Instr. and Meth. in Phys. Res. B **96**, 448 (1995).

[14] R. H. Ritchie, Phys. Rev. **106**, 874 (1957).

[15] C. J. Powell and J. B. Swan, Phys. Rev. **115**, 869 (1959).

[16] A. J. Bennett, Phys. Rev. B **1**, 203 (1970).

[17] P. J. Feibelman, Phys Rev. Lett. **30**, 975 (1973); ibid. B **9**, 5077 (1974); ibid. B **12**, 1319 (1975).

[18] K. D. Tsuei, E. W. Plummer and P. J. Feibelman, Phys. Rev. Lett. **63**, 2256 (1989).

[19] K. D. Tsuei, E. W. Plummer, A. Liebsch, K. Kempa and P. Bakshi, Phys. Rev. Lett. **64**, 44 (1990).

[20] M. Brack, Rev. Mod. Phys. **65**, 677 (1993) and references therein.

[21] W. L. Schaich and J. F. Dobson, Phys. Rev. B **49**, 14700 (1994).

[22] J. F. Dobson, Phys. Rev. B **46**, 10163 (1992).

[23] A. Liebsch, Phys. Rev. Lett. **67**, 2858 (1991).

[24] A. Liebsch, Phys. Rev. Lett. **71**, 145 (1993).

[25] P. J. Feibelman, Surf. Sci. **282**, 129 (1993).

[26] K. D. Tsuei, E. W. Plummer, A. Liebsch, E. Pehlke, K. Kempa and P. Bakshi, Surf. Sci. **247**, 302 (1991).

[27] J. A. Gaspar, A. G. Eguiluz, K. D. Tsuei and E. W. Plummer, Phys. Rev. Lett. **67**, 2854 (1991).

[28] T. Aruga, H. Tochihara and Y. Murata, Phys. Rev. Lett. **53**, 372 (1984).

[29] M. Rocca, Surf. Sci. Rep. **22**, 1 (1995) and references therein.

[30] O. Bohigas, A. M. Lane and J. Martorell, Phys. Rep. **51**, 267 (1979).

[31] W. Ekardt, Phys. Rev. B **32**, 7659 (1985).

[32] Ll. Serra, F. Garcias, M. Barranco, J. Navarro, C. Balbás and A. Mañanes, Phys. Rev. B **39**, 8247 (1989).

[33] Ll. Serra, F. Garcias, M. Barranco, J. Navarro, C. Balbás, A. Rubio and A. Mañanes, J. Phys. Condens. Matter **1**, 10391 (1989).

[34] Ll. Serra, F. Garcias, M. Barranco, N. Barberán and J. Navarro, Phys. Rev. B **41**, 3434 (1990).

[35] E. Lipparini and S. Stringari, Z. Phys. D **18**, 193 (1991).

[36] P. G. Reinhard, M. Brack and O. Genzken, Phys. Rev. A **41**, 5568 (1990).

[37] M. Brack, Phys. Rev. B **39**, 3533 (1989).

[38] E. Lipparini and F. Pederiva, Z. Phys. D **22**, 553 (1992).

[39] N. Barberán, J. Sellarès and J. Bausells, Surf. Sci. **292**, 159 (1993).

[40] J. Sellarès and N. Barberán, Phys. Rev. B **50**, 1879 (1994).

[41] A. Kiejna and J. Peisert, Surf. Sci **320**, 355 (1994).

[42] S. Leseduarte, J. Sellarès and A. Travesset, Surf. Sci. **384**, 1 (1997).

[43] D. J. Thouless, Nuc. Phys. **22**, 78 (1961).

[44] P. Ring and P. Schuck, The nuclear many-body problem, Springer-Verlag (1980) and references therein.

[45] J. Navarro and M. Barranco, Nuc. Phys. A **505**, 173 (1989).

[46] E. A. Stern and R. A. Ferrell, Phys. Rev. **120**, 130 (1960).

[47] P. J. Feibelman, Phys. Rev. B **3**, 220 (1971).

[48] B. N. J. Persson and E. Zaremba, Phys. Rev. B **30**, 5669 (1984).

[49] J. Harris and A. Griffin, Can. J. Phys. **48**, 2592 (1970); Phys. Lett. A **34**, 51 (1971).

[50] F. Flores and F. Garcia-Moliner, Solid State Commun. **11**, 1295 (1972).

[51] D. E. Beck and V. Celli, Phys. Rev. Lett. **28**, 1124 (1972).

[52] D. E. Beck, Phys. Rev. B **4**, 1555 (1971).

[53] K. Kempa and W. L. Schaich, Phys. Rev. B **32**, 8375 (1985).

[54] H. Raether, in: Surface Plasmons, Vol. 111 of Springer Tracts in Modern Physics (Springer, Berlin, 1988).

[55] H. Raether, in: Excitation of Plasmons and Interband Transitions by Electrons, Vol 88 of Springer Tracts in Modern Physics (Springer, Berlin, 1980).

[56] C. Kunz, Z. Phys. **196**, 311 (1966).

[57] T. Kloos and H. Raether, Phys. Lett. A **44**, 157 (1973).

[58] C. B. Duke, L. Peitronero, J. O. Porteus and J. F. Wendelken, Phys. Rev. B **12**, 4059 (1975).

[59] P. J. Feibelman, Phys. Rev. B **9**, 5077 (1974).

[60] R. Contini and J. M. Layet, Solid State Commun. **64**, 1179 (1987).

[61] J. M. Layet, R. Contini, J. Devrien and H. Luth, Surf. Sci. **168**, 142 (1986).

[62] A. Liebsch, Phys. Rev. B **36**, 7378 (1987).

[63] J. Monin and G. A. Boutry, Phys. Rev. B **9**, 1309 (1974).

[64] A. Eguiluz and J. J. Quinn, Phys. Lett. **53**A, 151 (1973).

[65] J. E. Inglesfield and E. Wikborg, J. Phys. C **6**, L158 (1973).

[66] J. F. Dobson and G. H. Harris, J. Phys. C **21**, L729 (1988).

[67] H. W. Werner and R. P. H. Garten, Rep. Prog. Phys. **47**, 221 (1984); J. E. Inglesfield and B. W. Holland, in: The Chemical Physics of Solid Surfaces and Heterogeneous Catalysis., Vol. 1, Eds. D. A. King and D. P. Woodruff (Elsevier, Amsterdam, 1981).

[68] G. Mukhopadhyay and S. Lundqvist, Solid State Commun. **25**, 881 (1978).

[69] K. J. Krane and H. Raether, Phys. Rev. Lett. **37**, 1355 (1976).

[70] A. D. Boardman, B. V. Paranjape and R. Teshima, Surf. Sci. **49**, 275 (1975).

[71] G. Barton, Rep. Prog. Phys. **42**, 65 (1979).

[72] R. R. Gerhardts, in: Spatial Dispersion in Solids and Plasmas, Vol. 1, Ed. P. Halevy (Elsevier, Amsterdam, 1992).

[73] B. I. Lundqvist, Phys. Kondens. Mat. **6**, 206 (1967).

[74] J. Lindhard, K. Dan. Vidensk. Selsk. Mat. Fys. Medd. **28**, 1 (1954); N. D. Mermin, Phys. Rev. B **1**, 2362 (1970).

[75] A. A. Lushnikov and A. J. Simonov, Z. Phys. **270**, 17 (1974).

[76] G. Bertsch and W. Ekardt, Phys. Rev. B **32**, 7659 (1985).

[77] Ll. Serra, F. Garcias, J. Navarro, N. Barberán, M. Barranco and M. Pí, Phys. Rev. B **46**, 9369 (1992).

[78] B. B. Dasgupta and R. Fuchs, Phys. Rev. B **24**, 554 (1981).

[79] G. Mukhopadhyay and S. Lundqvist, Phys. Scr. **17**, 69 (1978).

[80] R. Rojas, F. Claro and R. Fuchs, Phys. Rev. B **37**, 6799 (1988).

[81] M. W. Cole, Rev. Mod. Phys. **46**, 451 (1974) (After Eq. 5).

[82] K. L. Kliewer, Phys. Rev. B **14**, 1412 (1976).

[83] P. J. Feibelman, Phys. Rev. Lett. **34**, 1092 (1975).

[84] R. H. Ritchie and A. L. Marusak, Surf. Sci. **4**, 243 (1966).

[85] F. Forstmann and H. Stenschke, Phys. Rev. B **17**, 1489 (1978).

[86] D. L. Johnson and P. R. Rimbey, Phys. Rev. B **14**, 2398 (1976).

[87] B. I. Lundqvist, Phys. Status Solidi **32**, 273 (1969).

[88] R. Fuchs and F. Claro, Phys. Rev. B **35**, 3722 (1987).

[89] E. Lipparini and S. Stringari, Phys. Rep. **175**, 103 (1989).

[90] R. H. Ritchie, Prog. Theor. Phys. **29**, 607 (1963).

[91] A. P. Brown, A. B. Walker and R. N. West, J. Phys. F **17**, 2491 (1987).

[92] B. B. Dasgupta, Z. Phys. B **29**, 245 (1978).

[93] Ll. Serra, F. Garcias, M. Barranco, N. Barberán and J. Navarro, Phys. Rev. B **44**, 1492 (1991).

[94] S. H. Vosko, L. Wilk and M. Nusair, Can. J. Phys. **58**, 1200 (1980).

[95] J. P. Perdew and A. Zunger, Phys. Rev. B **23**, 5048 (1981).

[96] J. Providencia Jr. and N. Barberán, Phys. Rev. B **45**, 6935 (1992).

[97] C. Schwartz and W. L. Schaich, Phys. Rev. B **26**, 7008 (1982).

[98] C. Schwartz and W. L. Schaich, Phys. Rev. B **30**, 1059 (1984).

[99] I. Lindau and P. O. Nilsson, Phys. Lett. **31A**, 352 (1970); I. Lindau and P. O. Nilsson, Phys. Scripta **3**, 87 (1971).

[100] W. H. Backes, F. M. Peeters, F. Brosens and J. T. Devreese, Phys. Rev. B **45**, 8437 (1992).

[101] P. R. Pinsukanjana, E. G. Gwinn, J. F. Dobson, E. L. Yuh, N. G. Asmar, M. Sundaram and A. C. Gossard, Phys. Rev. B **46**, 7284 (1992).

[102] R. A. Ferrell, Phys. Rev. **111**, 1214 (1958).

[103] S. D. Sarma, Phys. Rev. B **29**, 2334 (1984).

[104] W. G. Teich and G. Mahler, Phys. Stat. Sol. B **138**, 607 (1986).

[105] J. K. Jain and S. D. Sarma, Phys. Rev. B **36**, 5949 (1987).

[106] W. L. Schaich and A. H. MacDonald, Solid State Commun. **83**, 779 (1992).

[107] R. Fuchs and W. Ekardt, J. Phys. Condens. Matter **1**, 4081 (1989).

[108] K. Dharamvir, B. Singla, K. N. Pathak and V. V. Paranjake, Phys. Rev. B **48**, 12330 (1993).

[109] C. C. Chang and M. Cohen, Phys. Rev. B **11**, 1059 (1975).

[110] P. Gleissl, M. Brack, J. Meyer and P. Quentin, Ann. Phys. (N.Y.) **197**, 205 (1990).

[111] N. Barberán and M. Pí, Phys. Rev. B **51**, 7329 (1995).

[112] M. Rocca, M. Lazzarino and U. Valbusa, Phys. Rev. Lett. **69**, 2122 (1992).